Chair of Processing of Composites and Design for Recycling

Doctoral Thesis

On the Potential of Epoxy Binder Rovings in Automated Dry Fiber Filament Winding

Dipl.-Ing. Stefan Neunkirchen

July 2024

MONTANUNIVERSITÄT LEOBEN
www.unileoben.ac.at

AFFIDAVIT

I declare on oath that I wrote this thesis independently, did not use any sources and aids other than those specified, have fully and truthfully reported the use of generative methods and models of artificial intelligence, and did not otherwise use any other unauthorized aids.

I declare that I have read, understood and complied with the "Good Scientific Practice" of the Montanuniversität Leoben.

Furthermore, I declare that the electronic and printed versions of the submitted thesis are identical in form and content.

Date 15.07.2024

_____

Signature Author
Stefan Neunkirchen

Dedicated to the memory of Prof. Ralf Schledjewski

ACKNOWLEDGEMENT

Working on a thesis this long, a couple of people influenced it to whom I want to show my gratitude:

First and foremost, I want to thank the late Prof. Dr.-Ing. Ralf Schledjewski for giving me the opportunity to write this thesis and for believing in its finalization. His way of constantly challenging but also encouraging made me (and I think the whole group) grow not only in academia but also as a person. He is sorely missed.

I am also extremely grateful to assoc. Prof. Dr.mont. Ewald Fauster for stepping in during these difficult times and for supporting the last steps of this thesis. Moreover, he provided valuable lessons in automation and programming over the years. Many thanks to Prof. Dr.-Ing. Peter Mitschang and his colleagues at Leibniz-Institut für Verbundwerkstoffe GmbH for the mentorship and good cooperation. Special thanks to Dr.mont Neha Yadav for proofreading. I am also thankful to Lukas Haiden and the Institute of Materials Science and Testing of Polymers for helping me with the digital microscope. I'd like to acknowledge the funding agencies and company partners who worked with me on many interesting projects and also partially financed my work at the LVV.

Since the list of every single one would be too long, I want to thank **all** my colleagues (scientific/administrative/technical) and all the students with whom I had the pleasure to work within the last six years. Thank you for the always good and humorous atmosphere at the workplace!

Finally, I want to thank my parents, my siblings, and especially Melanie and Nils. They all showed a lot of support and patience with me working on this thesis.

ABSTRACT

Filament winding has been a well-established process in the manufacturing of composite parts for decades. In recent years it has gained increased attention due to the demand for gas transport and storage systems, especially hydrogen. Apart from automation and monitoring, which are essential for every modern-day manufacturing process, new design methods as well as process modifications and variations are now the focus of research. One such process variation is dry (fiber) filament winding, where, unlike the established wet and prepreg winding processes, unimpregnated fibers are used. The usage of dry, untwisted fiber bundles, so-called rovings, comes with certain challenges but also opportunities. On the one hand, the process speed can be increased, and the potential for automation rises. Whereas, on the other hand, an additional subsequent process step is required to impregnate the reinforcing structure. This can lead to increasing production time and cost. The main challenge of the winding process itself is the different behavior and properties of the roving. Especially, the tendency of the roving to slip off the mandrel needs to be investigated. One possible solution to overcome this problem is the usage of binder. These polymeric materials can be activated, commonly by temperature, and then become tacky. This can (locally) increase the adherence of the roving to the surface on which it should be wound.

In this thesis, the dry fiber filament winding process with binder rovings is studied. The process and its characteristics are presented and compared to established processes, namely wet and prepreg winding. Based on these findings, experiments were conducted to examine specific challenges. Building a dry winding system based on robotic winding machinery, showed some new aspects in the practical implementation, especially in handling tasks. With appropriate adaptions and adjustments, the process proved to be suitable for the winding of geometrically complex shapes such as a cone. Experiments on the friction behavior of (activated) binder rovings on an aluminum mandrel showed an increase in available friction and hence design possibilities. Several parameters were tested, which proved to be comparable to values stated in literature for the non-binder rovings and generated new knowledge for the binder rovings. As an important process parameter, the monitoring of the roving’s profile via

a laser light sectioning sensor is presented. Experiments with binder and reference material have been executed in various settings. Based on an earlier developed algorithm, the so-gained data was evaluated and interpreted. It could be shown that the light sectioning method is a suitable technique for inline monitoring.

In dry fiber winding a preform is produced which then needs to be infiltrated with resin to produce the final part. The quality of a resin injection or infusion process is strongly dependent on the flow of the liquid through the porous media. While permeability has been discussed extensively in literature, the capillary flow in bindered rovings has not been examined yet. Capillary rise experiments show that the velocity increase of the straightened binder rovings is larger than the obstruction by binder particles. When activating the binder, the flow velocity decreases due to absorption by the rovings and blocking of the flow channels.

Depending on the desired part specifications, dry fiber winding can be a viable option. Further consideration of the cost and the resulting part quality needs yet to be done.

KURZFASSUNG

Faserwickeln ist ein seit Jahrzehnten bewährter Prozess in der Herstellung von Verbundwerkstoffen. Er erfährt zunehmend wieder Beachtung durch die steigende Nachfrage nach Transport- und Speichersystemen für Gase, insbesondere Wasserstoff. Neben der Prozessautomation und -überwachung, die für moderne Produktion unerlässlich sind, gelangen auch neue Designs, Prozessvarianten und -modifikationen in den Fokus der Forschung. Eine solche Prozessvariante kann das Trocken(faser-)wickeln sein, bei dem, im Gegensatz zu den etablierten Verfahren Nass- und Prepregwickeln, die Fasern ungetränkt verarbeitet werden. Die Benutzung nicht imprägnierter und nicht verdrillter Faserbündel, sogenannter Rovings, birgt Herausforderungen aber auch Möglichkeiten. Einerseits kann die Prozessgeschwindigkeit und das Potential für eine Automatisierung des Prozesses gesteigert werden, andererseits ist ein weiterer Prozessschritt nötig zur Tränkung der Verstärkungsstruktur. Die entscheidende Variation im Wickelprozess selbst, ist das unterschiedliche Verhalten und die veränderten Eigenschaften des Rovings. Dies kann zu einer Erhöhung der Produktionszeit und -kosten führen. Besonders die Neigung des Rovings vom Kern abzurutschen muss untersucht werden. Eine Möglichkeit dieses Problem zu lösen ist die Verwendung von Binder. Diese polymeren Materialien können, meist thermisch, aktiviert werden und werden klebrig. Dies kann (lokal) die Adhäsion des Rovings an der zu bewickelnden Stelle erhöhen.

In dieser Arbeit wird das Trockenwickeln mit bebinderten Rovings untersucht. Der Prozess und seine Besonderheiten werden vorgestellt und mit den etablierten Prozessen Nass- und Prepregwickeln verglichen. Basierend auf diesen Erkenntnissen werden verschiedene Aspekte in Experimenten untersucht. Der Aufbau eines Trockenwickelprozess auf einer bestehenden Robotik-Wickelanlage zeigte einige neue Aspekte in der praktischen Umsetzung auf, insbesondere beim Handling. Mit geeigneten Adaptierungen und Einstellungen konnte die geometrisch komplexe Form eines Kegels trocken bewickelt werden. Experimente über das Reibungsverhalten (aktivierter) bebinderter Rovings auf einem Aluminiumkern zeigten eine Erhöhung der Reibung und daraus resultierend mehr Designmöglichkeiten. Mehrere Parameter

wurden untersucht, die für nicht bebinderte Rovings die Literaturwerte validieren, während sie für bebinderte Rovings erstmals erhoben wurden.

Als wichtiger Prozessparameter wird die Überwachung des Rovingquerschnitts mit einem Lichtschnittsensor untersucht. Versuche mit und ohne Bindermaterial wurden mit verschieden Einstellungen durchgeführt. Basierend auf einem zuvor entwickelten Algorithmus, wurden die so gewonnen Datensätze ausgewertet und interpretiert. Es konnte gezeigt werden, dass die Lichtschnitttechnik eine geeignete Methode zur Prozessüberwachung sein kann.

Beim Trockenwickeln wird ein Vorformling (Preform) produziert, der dann mit Harz getränkt werden muss, um das finale Bauteil zu erzeugen. Die Qualität eines solchen Bauteils hängt maßgeblich vom Fluss der Flüssigkeit durch die poröse Struktur ab. Während Permeabilität hinreichend in der Literatur behandelt ist, wurde das kapillare Fließverhalten noch nicht untersucht. Versuche zur kapillaren Steigung zeigen, dass die Geschwindigkeitserhöhung der ausgerichteten, bebinderten Rovings höher ist als die Behinderung durch Binderpartikel. Bei Aktivierung fällt die Geschwindigkeit jedoch, da der Binder vom Roving absorbiert wird und Fließkanäle blockiert.

Abhängig von den gewünschten Bauteilspezifikationen kann das Trockenwickeln eine interessante Option sein. Allerdings müssen zur finalen Bewertung ein Kostenvergleich und eine Untersuchung der Bauteilqualität durchgeführt werden.

TABLE OF CONTENT

ABBREVIATIONS AND SYMBOLS

List of abbreviations:

Abbreviation	Term
(A)DFP	(Automated) Dry Fiber Placement
AFP	Automated Fiber Placement
ATL	Automated Tape Laying
CAD/CAM	Computer-Aided Design/ Manufacturing
CF(RP)	Carbon Fiber (Reinforced Polymer)
DOF	Degree of Freedom
DSC	Differential Scanning Calorimetry
FFT	Fast Fourier Transform
FSM	Finite State Machine
GUI	Graphical User Interface
IR	Infrared
LCM	Liquid Composite Molding
(L)LSS	(Laser) Light Sectioning Sensor
LVV	Lehrstuhl Verarbeitung von Verbundwerkstoffen
NaN	Not a Number

NCF	Non-Crimp Fabric
NDT	Nondestructive Testing
PLC	Programmable Logical Controller
PSA	Pressure Sensitive Adhesive
TCP	Tool Center Point
TDS	Technical Data Sheet
RTM	Resin Transfer Molding
VAP	Vacuum Assisted Process ®
VARI	Vacuum Assisted Resin Infusion

List of symbols:

Symbol	Unit	Description
$\#'$		d#/ds
$\#''$		d²#/ds
$\vec{b}$		Binormal vector
$c(s)$		Curve in space (parametrized by arc length)
E, F, G		Coefficients of the first fundamental form
g	m/s²	Gravitational acceleration

k_g		Geodesic curvature
k_n		Normal curvature
$\vec{k}$		Curvature vector
L, M, N		Coefficients of the second fundamental form
$\vec{n}$		Normal vector
r	m	Radius
$S(u,v)$		Surface in space with parameter u and v
t	s	Time
$\vec{t}$		Tangent vector
z	m	Height
α	°	Winding angle
θ	°	Contact angle
κ		Curvature
λ		Slippage tendency
μ		Friction coefficient/ Coefficient of friction
τ		Torsion

1. INTRODUCTION

1.1 INTRODUCTION & MOTIVATION

Fiber-reinforced polymers (FRP) are used for applications where good mechanical properties and a low component weight are demanded. Many industries such as automotive, aerospace, sporting goods, construction, or energy transport and storage make use of these materials regularly [1]. Hereby, the most common technique for the manufacturing of axisymmetric composite parts is the filament winding process [2–5]. Reinforcing fibers are wound in layers around a rotating mandrel in a predesigned pattern. It can be considered a low-level, early-stage precursor for modern additive manufacturing processes [6].

Filament winding is a well-established process that has been around since the 1940s, mostly in aeronautical/-space applications [3,4]. In the last two decades, approximately, complexity and output numbers have evolved significantly through automation [4]. For example, modern filament winding facilities are able to produce some hundred thousand cylindrical pressure vessels per year [5,7]. Yet, ‘classic’ filament winding parts such as rocket housings, tube nozzles, fuselages, or shafts are still in development given the ongoing demand for space exploration parts and aviation in general [8,9]. Being one of the favored processes for the manufacturing of energy transportation and storage systems, interest in application and research has been rising in recent years. Especially the containment of hydrogen as a part of the energy cycle of the future plays a key role in studies [10–16].

Not only the part complexity has evolved but also the corresponding processes and machinery. For example, a robotic end-effector was developed to be able to use filament winding in a joining process [17–19]. Other modern research areas tackle the environmental impact by investigating the usage of recycled [20] or biobased [1] materials for unidirectional reinforced composites.

With an increasing number of parts and rising complexity, novel approaches in processing can be necessary. Splitting the process into winding of a dry, i.e., not

impregnated, roving, and a subsequent liquid composite molding (LCM) process can be such an option. A prominent example is the production of dry wound pressure vessels which are then coated to protect them from impact loads [21].

Dry (fiber) winding as a method to produce preforms for LCM is described in literature, but little research has been done on the process itself and its implications. Compared to the more established wet and prepreg winding, dry winding has a different impact on the fiber adherence during processing which then influences the possible winding patterns. A possible solution is the use of binder material to increase adhesion. Besides, it is a two-step process. This means that the subsequent process as well as the preparation and handling in-between have to be considered. The thesis at hand will focus on the technological aspects of this process. Yet, it is also very clear that the final decision on which process to use is based strongly on cost aspects (after the technical feasibility is confirmed).

Filament winding in general is one of the most cost-effective manufacturing processes for composites [12]. Nevertheless, composite parts, especially those made with carbon fibers, are still costly. Material cost will make up for 40-90 % of the total cost depending on the output rate [22]. This means that the efficiency of highly automated processes such as filament winding is predominantly dependent on the material cost which is lowest for dry fibers. Although continuous processes (e.g. filament winding) and LCM already have an overall market share of about a quarter in composites production, it is expected to grow even further due to the replacement of manual processes [23]. The key question in the end will be if savings in raw material cost will justify a more complex production process. Depending on available equipment, part complexity, part properties, and the aimed output rate, this decision will need to be made individually every time. This work tries to aid this decision-making by providing information on the technological feasibility and hence narrowing down possible manufacturing scenarios.

1.2 SCOPE AND OBJECTIVES

Specifically, this thesis looks closer at an automated dry fiber filament winding process. The common thread in this constellation will be, almost literally, an epoxy binder roving[1]. Figure 1 shows a schematic of the thesis' scope. Binder rovings are in the center and their behavior, suitability, and specialties will be discussed with respect to the filament winding process, automation, and LCM processing. Structure and objectives of the thesis will be presented hereafter.

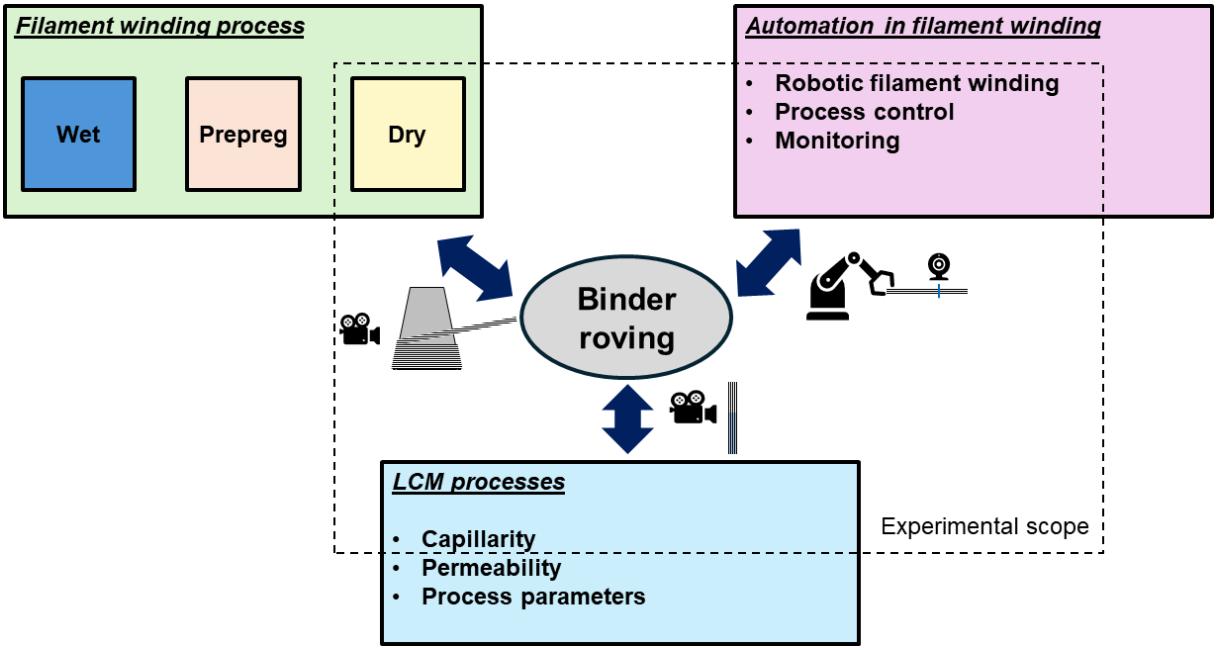

Figure 1: Overview of the thesis' scope

Some aspects will only be investigated theoretically via a literature review while others will be a part of the experimental section. The dashed line in Figure 1 shows the scope of the experiments within the principal topics.

Chapter 2 presents the state of the art as the basis for the experiments. First, the filament winding process is presented in general. Then, the specifics of dry winding are explained considering path planning, resin impregnation, and process control. Main challenge in designing a dry winding process is the avoidance of fiber slippage.

[1] *Sometimes it is also called binder tape. This notation will not be used here to avoid confusion with thermoplastic tapes.*

Mathematical boundaries are presented as well as processing possibilities. Here, especially the binder material class is highlighted as a promising solution.

The next section in the literature review is automation. Focus is on the control and monitoring techniques that are established in filament winding. Emphasis is laid on non-destructive testing methods, such as the laser light sectioning which will be used in the experiments. Another aspect of automation will be the presentation of robotic filament winding as it is established in the laboratories of the Processing of Composites Group (German: Lehrstuhl Verarbeitung von Verbundwerkstoffen-LVV).

Resin flow in LCM processes is the last section of this chapter. Several results have been published on the influence of binder on the permeability of textiles during resin infusion. These will be presented here in an overview. Influence of binder material on the capillary flow has not yet been examined to the knowledge of the author. That is why the basics of capillary flow and its measurement for composites are presented to prepare for the experimental chapter.

In **Chapter 3,** the dry filament winding process and its implementation at LVV are presented. After introducing the used binder rovings, the given equipment and the modifications for dry winding are explained. In experiments with a specially designed mandrel, the coefficient of friction between binder roving and mandrel is measured in different configurations. The so-determined coefficient is an important parameter for path planning in dry winding. Such values are not available for binder rovings yet. In the last section of this chapter, the methods, challenges, and practical solutions for executing dry winding are presented. A conical mandrel representing a challenging shape to be wound on without auxiliaries is prepared, wound, and finally infused with resin. Insights of that procedure are reported to get a deeper understanding of the characteristics of the dry winding process.

Process monitoring is the key aspect of **Chapter 4**. Since automation and monitoring are a wide field, only a specific sensor type is selected here and presented in detail for the profile monitoring of binder rovings. For that, a test rig designed for the testing of roving properties is used. The rig setup, modifications of that setup, and the programming are introduced. An algorithm was developed in the frame of a bachelor thesis and a journal publication for the evaluation of the recorded data. This code is

adapted to be used for the profile determination of binder rovings. Experiments were conducted to observe the influence of the sensor's exposure time, background materials, process speed, roving tension, geometrical changes, and binder activation. Applicability of the generated code, measurement influences, and a comparison to non-bindered rovings are at the center of the investigation.

The third and last experimental **Chapter 5** tackles the capillary flow in binder rovings. Capillary rise experiments were performed on a test rig developed in a previous thesis [24]. Influence of binder particles on capillary flow is not well-investigated. Especially the activation of the binder material, which is crucial for its processing, has the potential to completely change the flow behavior. That is why the focus of the research here lies on the change in capillary flow after a previous activation of the binder. Temperature, pressure, and duration of the activation are deemed to be most influential. Additionally, a comparison was made between roving with binder and the same type of roving without binder. The assumption that foreign material will hinder, and hence slow capillary flow is tested for its validity.

In the conclusion, a SWOT analysis is executed to summarize the results of this thesis and to point out the current state of the dry filament winding process.

2. STATE OF THE ART

2.1 THE FILAMENT WINDING PROCESS

The principle of filament winding is rather simple. Fibers are wound around a rotating mandrel under defined tension and in a predefined pattern [3]. Precise placement of the fibers depends on the coordination and design of machinery, mandrel, and processes. In the following section, a general overview of the filament winding process is given, and in the next section, the specifics of dry winding are pointed out.

2.1.1 WINDING MACHINES

Winding machinery can roughly be categorized by the available axes determining the degrees of freedom (DOF) and the construction type [5,25]. These constructions are typically lathe, portal/gantry/plotter, and robotic-style winding machines [5,25].

The selection of the proper winding machine depends strongly on the part to be manufactured [26]. Dimension, weight, and complexity have to be considered. The most simple setup for a filament winding system is a classic, lathe-style type with only two DOFs, namely carriage and mandrel rotation [27]. Complex winding machines as well as robots provide six degrees of freedom (6DOF) for the movement of the payout-eye, three rotational and three translational [28]. On top of that, a minimum of one DOF is needed for the rotation of the mandrel. Machines with multiple spindles can increase the throughput rate strongly and hence improve the process efficiency [29]. One such solution for certain mandrel forms can be a ring winding head [5,30]. Various deposition units are mounted on a ring and enable a fast deposition over a small distance. When the payout eye is stationary and the mandrel is moveable, these machines are so-called tumble winders [3,31,32]. For some parts, a vertical mounting of the mandrel in a winding machine is also beneficial, i.e., for very large parts to avoid deflection [33,34]. Robotic filament winding machines will be presented in Section 2.3.1 in the frame of automation.

Yet, a highly sophisticated but costly winding machine may not be necessarily the best choice. Low cost and a certain flexibility of the equipment are important reasons for a decision [35].

2.1.2 MANDREL

The mandrel, or (winding) core [36], is an important component of most winding processes. In classic winding applications, e.g., for vessels, tubes, shafts, or housings, the fibers are deposited around an axisymmetric, rotating mandrel. Figure 2 shows typical mandrel forms, which all have certain requirements for the mandrel material and design. In general, the mandrel should be without sharp edges which might damage the fibers, as well as concave parts which can lead to fiber bridging [37].

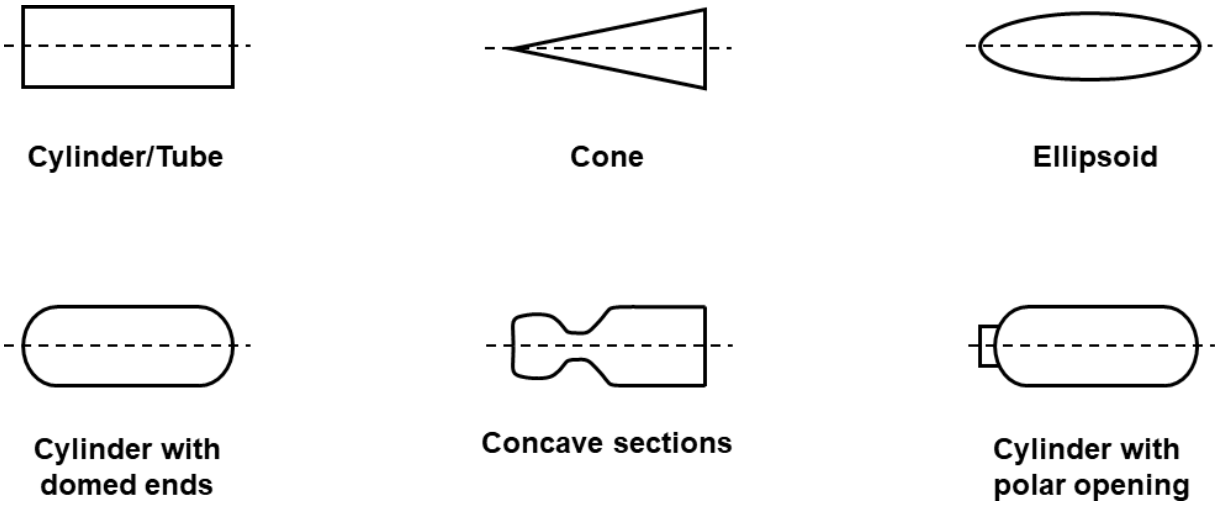

Figure 2: Typical mandrel forms (adapted from [5])

Conical, cylindrical, and mandrels with a one-sided opening can be removed after the winding [5]. Nevertheless, this can still be challenging and might cause additional effort or cost [8]. For these kinds of mandrels, any solid material such as metals, wood, or polymers can be used. Other possibilities of removal after winding, are the usage of collapsable, inflatable, dismountable, or soluble mandrels [5,26,29,36–38]. These solutions all require a costlier process step but may be the only choice for certain part designs, especially those with undercuts.

If the mandrel does not need to be removed it can stay inside the part and even provide functions, such as a diffusion barrier or corrosion protection [5]. Especially for (hydrogen) pressure vessels, the so-called liner can minimize gas permeation [10,39].

While the aforementioned mandrel forms are still the majority, new designs are also possible with modern-day winding machinery. More complex, non-axisymmetric

shapes such as elbows, t-joints, or plates are manufactured [8]. Consequently, mandrels also rise in complexity.

In the last years, processes have been developed that are called ‘core-less’ or ‘mandrel-less’. In these usually robotic winding processes, no mandrel is used. The roving is wound around pins or gaps on a plate to create some kind of grid or truss structure. [40–42]

2.1.3 PROCESSING

In the following, a typical process flow for a modern filament winding process is presented. In these four groups, the tasks can vary strongly depending on the choices made until then. It should also be noted that in the development of a filament winding routine often trial and error experiments are required [31]. Consequently, steps or sequences may be repeated until a satisfactory result is achieved.

2.1.3.1 Product and process design

Design of the part to be manufactured is the basis for all the manufacturing processes. The design can already determine or exclude some processing options, e.g., dealing with concave segments or very large parts. A CAD model can be created with a given shape and possibly calculations and/or a FEM model can be done with given strength specifications. So far, this is a common procedure in part design.

In filament winding, now also the mandrel has to be designed geometrically, functionally, and material-wise. This also strongly depends on the part to be manufactured, e.g., is it demoldable, or are elevated temperatures needed during processing?

2.1.3.2 Winding path planning

Once the specifications are clear, i.e., which strengths are required and how thick is the part allowed to be, the winding path, the resulting winding pattern, and the thickness buildup can be calculated. The classic and simplest selection of a winding path is a geodesic. It can be calculated analytically in many cases and provides a stable deposition because no friction is needed to hold the fibers in place [43]. A geodesic is the shortest path between any two points on an arbitrary surface, e.g., a great circle on a sphere or a straight line on a plane [44–46]. Generally speaking, the

winding path is modeled as a curve on a surface in three-dimensional space [32]. Based on the calculus of variation, a set of differential equations can be set up which need to be solved. An analytical solution is not always possible or even requested since numerical solutions can be easier for a computerized system. Zhang et al. [43] give a thorough review of solution approaches.

In the following, the basic equations used in filament winding are presented based on [47]. First, geodesic paths then non-geodesics. For a more detailed insight into the respective mathematics, the work of Koussios [31,32,48] and various books on differential geometry [45,46,49–52] are recommended.

Figure 3 shows a model of a fiber deposited on a mandrel, i.e., a curve on a surface. The curve $c(s)$ parametrized by arc length can be described by the Frenet–Serret formulas [28,52]. The tangent $\vec{t} = c'$, normal $\vec{n} = \frac{c''}{\|c''\|}$, and binormal $\vec{b} = \vec{t} \times \vec{n}$ unit vectors span a trihedron in $\mathbb{R}^3$.

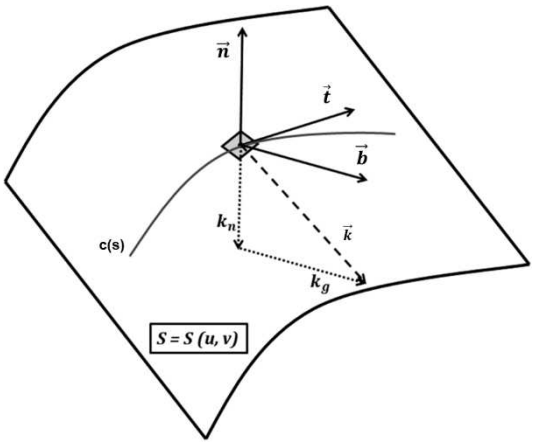

Figure 3: Curvature of a path on a surface (adapted from [47,53])

With curvature $\kappa := \|c''\|$ and torsion $\tau := \langle \vec{n}', \vec{b} \rangle$, the Frenet-Serret formulas are:

$$\begin{pmatrix} \vec{t} \\ \vec{n} \\ \vec{b} \end{pmatrix}' = \begin{bmatrix} 0 & \kappa & 0 \\ -\kappa & 0 & \tau \\ 0 & -\tau & 0 \end{bmatrix} \begin{pmatrix} \vec{t} \\ \vec{n} \\ \vec{b} \end{pmatrix} \tag{1}$$

While the Frenet-Serret formulas describe a curve in space, the first fundamental form expresses how a surface inherits the natural inner product of $\mathbb{R}^3$. It then allows for geometric measurements, e.g., the length of a curve, solely depending on the surface. [51,52]

For a parametrized surface *S(u,v)* the differential arc length is defined as [52,53]:

$$I = ds^2 = Edu^2 + 2Fdudv + Gdv \tag{2}$$

With $E = |S_u(u,v)|^2$, $F = S_u(u,v) \cdot S_v(u,v)$, and $G = |S_v(u,v)|^2$ being the coefficients of the first fundamental form.

While the first fundamental form describes the intrinsic properties of a surface, the second fundamental form concentrates on extrinsic properties. It characterizes the relationship between normal and tangential space, i.e., analogous to the curvature of a curve [44].

It is defined for the surface *S(u,v)* and the unit normal vector $\vec{N}$ as [53]:

$$II = Ldu^2 + 2Mdudv + Ndv^2 \tag{3}$$

With $L = \frac{\partial^2 r}{\partial u^2} \cdot \vec{N}$, $M = \frac{\partial^2 r}{\partial u \partial v} \cdot \vec{N}$, and $N = \frac{\partial^2 r}{\partial v^2} \cdot \vec{N}$.

The curvature vector $\vec{k}$ in Figure 3 is composed of the normal (k_n) and the geodesic (k_g) curvature [53]. With help from the fundamental forms the normal curvature can be described as:

$$k_n = \frac{II}{I} \tag{4}$$

The geodesic curvature k_g can be defined as:

$$k_g = \frac{d\vec{t}}{ds} \cdot (\vec{N} \times \vec{t}) \tag{5}$$

Two basic approaches are common to determine a geodesic. Either the minimal arc length is calculated or a geodesic curvature equaling zero is searched.

In case of the minimal arc length the Euler-Lagrange differential equation is used which leads to [46,47]:

$$\frac{\frac{\partial E}{\partial v} + 2v_u \frac{\partial F}{\partial v} + \frac{\partial G}{\partial v} v_u^2}{2\sqrt{E + 2Fv_u + Gv_u^2}} - \frac{d}{du}\left(\frac{F + Gv_u}{\sqrt{E + 2Fv_u + Gv_u^2}}\right) = 0 \tag{6}$$

When determining the geodesic curvature becoming zero, a set of ordinary differential equations with the help of the so-called Christoffel symbols can be set up. These equations are quite difficult to solve analytically and closed-form solutions cannot generally be found [54]. For the definition of the equations and possible numerical solution approaches, the following sources are referred to: [54–56].

Most parts produced in filament winding are surfaces of revolution. This can significantly simplify the computation of the geodesic curvature. Liouville's formula provides an equation for the geodesic curvature which can then be set to zero to calculate the geodesic [47,51,57,58]. It can also be used in the proof of Clairault's relation [4,51,59]. This simple and well-known equation is valid for geodesics on arbitrary surfaces of revolution:

$$r\,sin(\alpha) = const. \tag{7}$$

With r being the radial distance to the winding axis and α the winding angle, i.e., the angle between roving and the winding axis.

The constant is often equal to the polar opening since the winding angle there is $90\,°$ [4,60]. Another consequence that can be deducted, is that geodesic winding is only possible when the polar openings, e.g., for a pressure vessel, are equally large [60].

This shows already that not every shape can be wound geodesically, even simple geometries such as a tube or pressure vessel. Also, in geodesic winding, the path is fixed as soon as winding angle and position/radius are given [28,61].

Apart from the cases where a geodesic wound part is desired but must be varied (locally), most modern processes rely on non-geodesic paths. With the introduction of computer-supported path planning the increased effort of calculation has become less

relevant [54]. Enhanced design freedom and the possibility to wind more complex shapes on the other hand justify the addition of complexity.

If the roving deviates from the geodesic path, a friction force is needed to keep it in place and prevent (catastrophic) slippage. The condition for that is given by [58,62–65]:

$$\mu \geq \left\| \frac{k_g}{k_n} \right\| \tag{8}$$

With k_g being the geodesic curvature, k_n the normal curvature, and μ the coefficient of friction (henceforth also called ‘friction coefficient’ for short). A force-based definition and the measurement of this coefficient will be presented in Section 2.2.2 with respect to dry winding.

The resulting equations for the calculation of the fiber path are even more difficult to solve due to the extra term. Typically, a solution is generated numerically for example by the Runge-Kutta method [58,66]. An overview of analytical solutions for common shapes is given in [65].

The farther away from the geodesic path, the more friction is needed to stabilize the roving. Design opportunities are not limitless. Commonly, paths close to the geodesic are chosen because only low friction force is needed. Consequently, they are called semi-geodesic [28,37,59,67–69].

Finding a parametrization and solving differential equations can be exceedingly difficult or even impossible. Discretization can then be an option. Liang et al. introduced the so-called quasi-geodesics which define a piecewise curve described by the Clairault equation extended by a friction term [63]. Other discrete models are presented in [70–73].

In any case, fiber bridging has to be considered [28,59]. Fibers lift off in concave areas of the mandrel must be avoided [37,74]. To prevent this the normal force acting on the roving $\overrightarrow{f_n}$ must be larger than the outward-directed normal of the surface $\vec{n}$ [37,61,71,73]:

$$\overrightarrow{f_n} \cdot \vec{n} \leq 0 \tag{9}$$

Which can also be expressed by the geodesic curvature being smaller than zero [57,73,75]:

$$\overrightarrow{\kappa_n} \leq 0 \tag{10}$$

While bridging is usually avoided by part design and path planning, it can also be suppressed during processing, e.g., by pneumatic devices [76] or local application of extra material [4].

Nowadays, winding paths are predominantly generated in specifically designed winding programs. Commercially available software has been developed, often originating in university research (e.g., Aachen [77], Leuven [78], Delft [79], Nottingham [80]). Some programs are CADWIND [77], CADPATH [81], CAWAR [28,37,61,67,78], Cadfil [80], ComposicaD [82], FiberGrafiX [83], TaniqWind Pro [79], and Abaqus/Simulia (plugin ‘Wound Composite Modeler’) [7,84].

Figure 4 shows a sequence of preparing the winding pattern before processing [47]. After a model of the mandrel is created, a possible winding path is calculated based on the given specifications, e.g., winding angle, and available friction. Machine control data can then be derived with given machine specifications. If the upcoming simulation is collision-free, the covering pattern can be determined. It then defines the degree of coverage, the thickness, and the processing sequence. A more detailed analysis of these steps regarding the equipment at LVV is given in Section 3.2.3.

Having a geometrical model of the part and a winding strategy, calculations on the mechanical properties can be made. Depending on the desired accuracy, different methods such as finite element analysis (FEA) or classical laminate theory (CLT) can

be used. If these criteria are also satisfied, the machine control data can be generated to be able to start production.

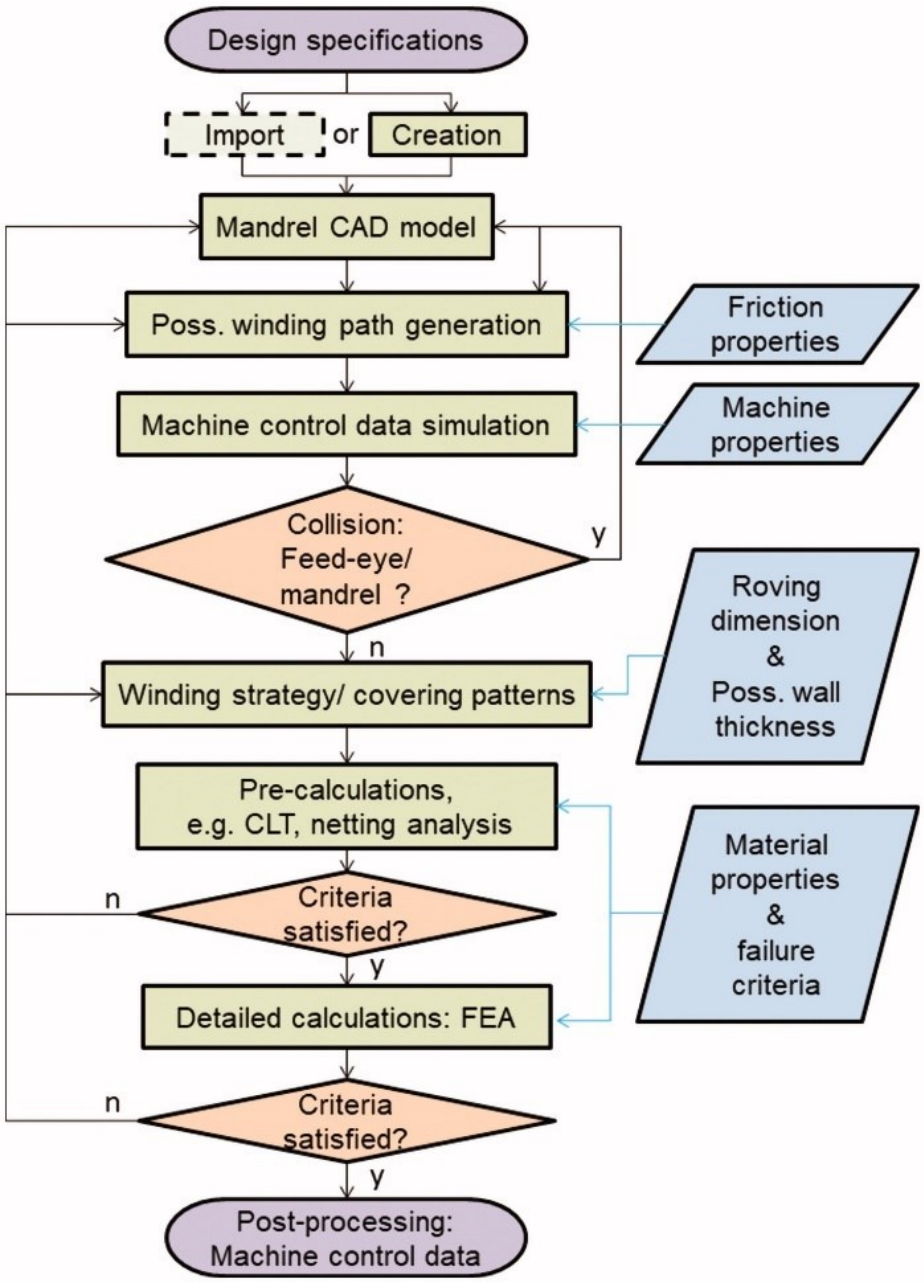

Figure 4: Flowchart on winding pattern generation [47]

Machine control data is generated based on the machinery's dimensions, motion parameters, and the planned deposition path. Two different approaches for the machine movement relative to the mandrel are common [4,10,47,85]: A constant free fiber length tangential to the surface is easier to calculate but can cause either too large movements, too close approaches, or even crashes. A more elaborate method

is to define an enveloping frame around the mandrel which should not be entered by the machine. It requires more effort in computation but provides movements that are more secure and possibly faster.

2.1.3.3 Winding strategies and process parameters

Most important parameter for the design of the winding trajectory is the winding angle. It not only determines the number of possible winding paths (if any exist), but it also strongly influences the properties of the final part. Depending on the expected load, the designer selects an angle that fits the mechanical requirements but has to keep in mind that a winding path calculation is still feasible. Often, various angles are used in different layers. Classically, the range of winding angles is divided into three categories. A winding angle close to 90 ° is called hoop or circumferential winding. It is typically used for the cylindrical section of pressure vessels [26,47]. Polar winding is done with angles close to 0 ° around the polar openings of the mandrel. Both polar and hoop winding, are the extreme cases of helical winding which stands for winding angles between 0-90 ° [4,26,47,86]. Figure 5 shows these three winding strategies.

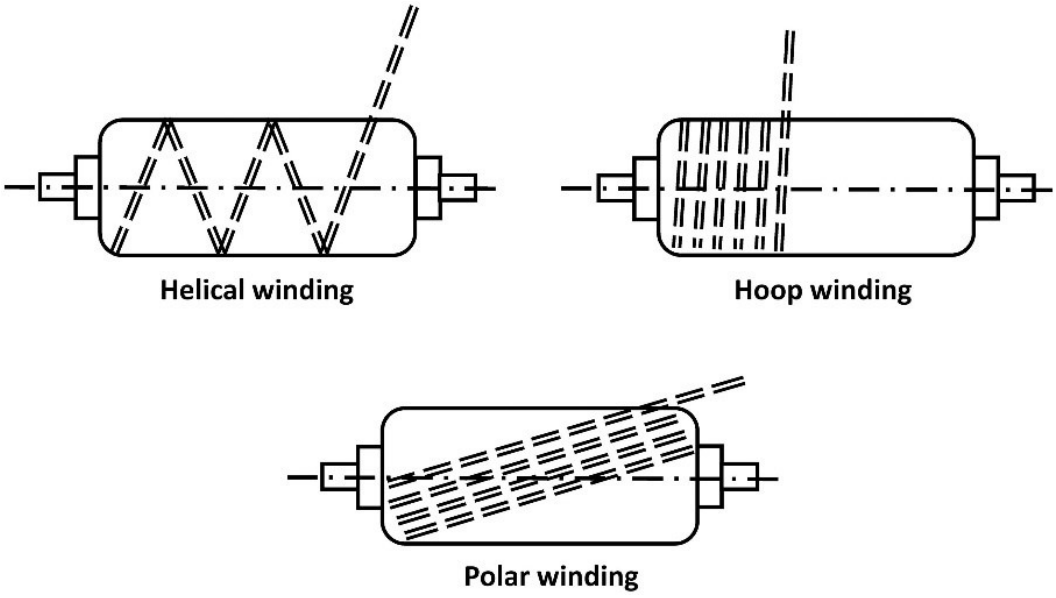

Figure 5: Winding strategies on a pressure vessel [47]

When all the geometrical parameters are determined, the most important parameters that influence the process are speed and tension.

In most cases, the winding process is optimized for maximum output, i.e., efficiency, which is predominantly affected by the possible winding/ carriage speed. Many aspects can be identified that could lead to a reduced process speed, e.g., too much fiber damage, worsened deposition accuracy, limited detection rate of sensors, or extra time needed for material application or activation [3,27]. If no process-related aspect hinders the speed, only the winding machine specifications defy the maximum possible speed. Typical winding speeds are in the range of 1-10 m/min [13]. For dry fiber winding the speed can possibly go up to several meters per second [13,87]. The deposition amount can be between 45-180 kg per hour [33].

The other important process parameter, roving tension, can influence the mechanical properties of the final part by affecting void content and fiber volume fraction and is also crucial for fiber guidance and possible fiber damage [3,37,88–90]. During fiber guidance, the tension should be low to avoid abrasion, fiber breaking, or spreading [33]. A too-low tension though can lead to wrinkles or folding of the rovings and consequently defects [89,90]. Tensioning units, e.g., springs and dancer units, are commonly applied in the winding system.

In which way the mechanics are affected depends on the load case: for fiber-dominated loads a higher tension leads to increased strength whereas for matrix-dominated loads a lower tension leads to better results [88].

2.1.3.4 Postprocessing

After the winding process is completed, the part has to be removed from the winding machine together with the mandrel. Then, wet or prepreg wound parts are commonly cured in an oven, sometimes in an autoclave, or by other heating methods [5,33]. To avoid dripping and resin accumulation at the bottom, the part is usually rotated constantly [5]. Dry wound parts have to be handled carefully to prepare them for the upcoming LCM process.

If the mandrel is not supposed to stay inside after curing, it has to be removed. Depending on the mandrel type, various methods can be applied. Generally, it can be stated that this step has to be executed carefully. Especially, mechanical removal can

require high forces and is often done with specialized appliances. Finally, the part can undergo classical postprocessing steps such as deburring or coating.

2.1.4 WET WINDING/ IMPREGNATION

Wet winding is a classic, simple, and cost-effective method to produce parts in filament winding [34]. Rovings are impregnated during the process and then deposited. Figure 6 shows the basic setup of a filament winding machine for wet winding. The rovings are guided from the creel through a resin bath and are then laid on a cylindrical mandrel in a lathe-type winding machine.

A crucial part of this process is the impregnation of the roving(s). It is commonly the limiting factor for the winding speed since the rovings need to be in contact with the resin long enough to ensure proper wetting [3,91].

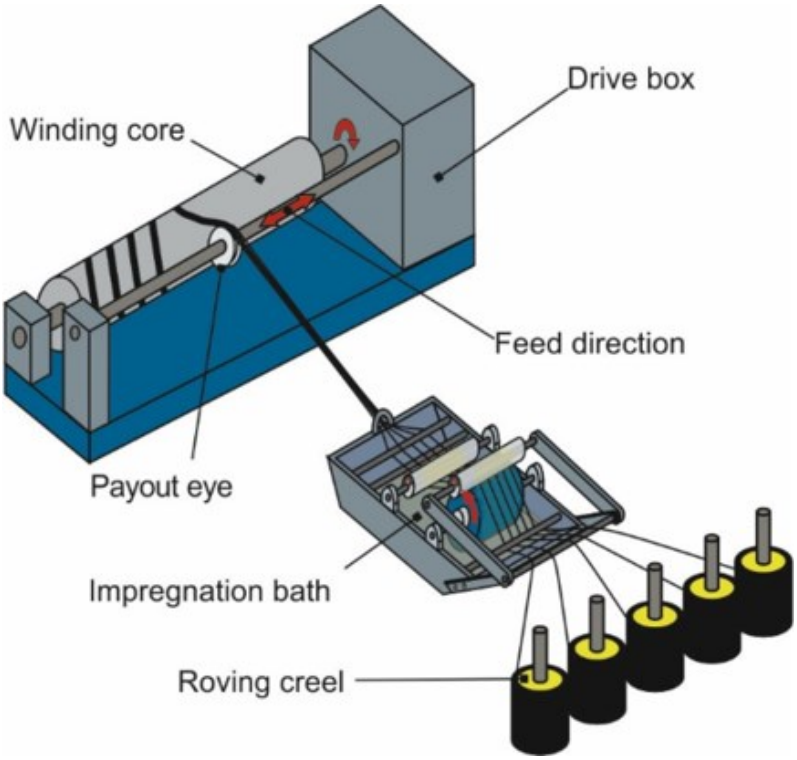

Figure 6: Schematic of a winding machine setup for wet winding [36]

A typical impregnation method in wet winding is the resin bath. It can either be drum-type (as in Figure 6) or dip-type (held down by rods) [3,92]. Often, resin baths are heated to lower the viscosity of the resin and facilitate impregnation [5,29]. The excess resin is removed with resin scrapers [3]. Both are well-established and rather simple

solutions [36]. More elaborate impregnation units have been developed to increase process speed, reduce waste, stabilize process parameters, and minimize potential hazards. In these units, the rovings are impregnated in closed boxes under pressure. A special development is the siphon impregnation unit, where the roving is guided through a sinusoidal path and is impregnated by capillary and hydrostatic forces [36,92].

Roving tension, twisting, and spreading are important parameters to be considered before the roving is guided through the impregnation unit [2,3]. Nevertheless, an in-line impregnation bears the risk of improper or inhomogeneous wetting of the roving [91]. Moreover, a resin bath, or in the case of an impregnation unit at least the impregnated fibers, can be hazardous both in case of safety and cleanliness [12,36,91].

2.2 DRY FIBER FILAMENT WINDING

Dry fiber filament winding (or short: dry winding) in the context of this work deals with non-impregnated and binder rovings. In some literature, this term has also been used for what is described as prepreg winding in the frame of this thesis, e.g., in [4,29,87,93–95]. In [29], the process is denoted as ‘post-impregnation’. For this reason, this section starts with a comparison between wet, dry, and prepreg winding. Then, the fiber slippage and its avoidance are regarded as the main challenge in dry winding. Finally, binder materials and the property ‘tack’ are presented in preparation for the experimental section.

2.2.1 COMPARISON WITH WET AND PREPREG WINDING

Research in filament winding strongly concentrates on wet winding because it is the best established and relatively simple method to produce wound parts. Prepregs are often considered as the costly alternative which may raise part quality. Dry winding is often just mentioned as a method to produce preforms but only a few results have been published with parts manufactured with non-impregnated rovings [3,38,96].

Advantages and disadvantages of the three methods that can be identified in the literature are summarized in Table 1. The comparison is explained afterward.

Table 1: Comparison of winding methods [10,12,13,29,47,91,96,97]

PROCESS	ADVANTAGES	DISADVANTAGES
WET	• Lower raw material cost • Simplified material storage • Variability in resin and additive selection • Established process	• Less control of resin content • Lack of variability • Cleanliness • Resin accumulation • Tradeoff quality/speed • Poor external finish
PREPREG	• Precise resin content control • Better mechanical properties • Faster processing	• Higher material cost • Material storage (shelf life) • Handling (unfreezing) • Less material variability
DRY	• Precise resin content control • Better mechanical properties • Faster processing • Lower raw material cost • Simplified material storage	• Second process step necessary (impregnation) • Preform handling • Danger of slippage

The major advantage of wet winding is that is a well-established process. That means that many machines are available as well as the knowledge of how to use them, e.g., setting up process parameters or handling the resin. Materials can be stored as in any other composite manufacturing process. Only the storage conditions of the resin have to be regarded. Also, by purchasing the resin, additives, and rovings separately, cost savings and the flexibility to adapt the resin system to the respective needs are given. Wet winding also has some disadvantages, especially when it comes to high-performance parts and/or high output numbers. The necessity of the roving to stay in

the resin bath/impregnation unit as long as it is fully impregnated limits the speed of the process sometimes drastically. Another big issue is the handling of excessive resin and the resin distribution within the roving. This has various effects on the process. The guidance must be adapted, which reduces the flexibility of possible movements. Also, the roving or the part respectively must not stand still as this would lead to resin accumulations at the bottom. Poor surface quality and unimpregnated areas can also occur. Especially an open resin bath can be hazardous to the health of workers, e.g., by toxic fumes. Hence, safety equipment must be installed additionally. Eventually, wet winding is a rather dirty process that requires a lot of cleaning effort. This includes resin dripping from the rovings as well as preparing the resin bath for filling.

Prepreg winding's advantages lie in the fast processing and the well-defined properties of the material. Consequently, high-performance parts can be produced faster and with less scrap. The major drawback of prepreg materials is the cost. Towpreg (prepreg tows/rovings) material itself is already more expensive than rovings and resin bought separately. On top of that it has a limited shelf life and needs to be stored in a refrigerator. This means that storage costs and more detailed production planning will be necessary. When unfreezing the prepregs they have to be checked for excessive moisture which could impair the properties of the material. In addition, only some towpreg materials are commercially available. That means that either a lot of money is required to develop a prepreg system with the desired properties or the selection of material is rather limited.

In Table 1 it seems that dry winding would combine the advantages of wet and prepreg wetting. It can be as fast and productive for high performance as prepreg. But it also has the flexibility in resin selection, simplified storage, and less cost just like wet winding (if binder rovings are used the cost will be higher but usually still below those of prepreg). While the dry winding process itself certainly can be fast and (cost-) efficient, it has some repercussions that need to be considered. First of all, a subsequent impregnation step is required. In an LCM process, high-quality parts can be produced but it is an additional process that needs resources. Depending on the desired output numbers it has to be evaluated if the cost is still lower than with prepreg material. This could for example be the case when a functional LCM machinery is already given. Also, another process step comes with other challenges that are not

part of the winding process, i.e., mold-filling behavior such as race tracking or fiber washout. After a dry winding process, only a preform is produced. This means that it has to be transferred to the LCM process workstation. Handling a preform can be very tough in order not to damage or relocate the structure. It could be necessary here to develop and build special mandrel types that can provide stability during winding, transport, and possibly also during the impregnation process. In the dry winding process itself, the biggest issue is the increased potential for slippage. This will be explained further in the upcoming section.

Regardless of the impregnation method, the fibers need to be spread in the right manner to enable a good coverage of the single fibers [98]. In prepreg winding or winding with binder rovings, this is already taken care of by the material supplier. In wet winding or dry winding without binder, the fiber guidance has to be adapted to provide a proper surface for the resin/binder to adhere to the fibers.

2.2.2 FIBER SLIPPAGE IN WINDING AND ITS PREVENTION

As discussed earlier, winding of non-geodesic paths requires a certain degree of friction to keep the roving stable on its path. Equation (8) already defined the coefficient of friction as the main criterion to avoid slippage. It will now be regarded in greater detail with respect to the acting forces (based on [47]).

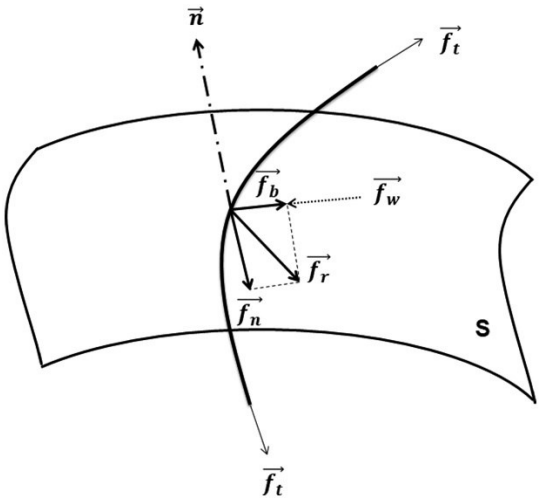

Figure 7: Forces acting on a fiber placed on a surface [47]

Many forces act on the roving which is deposited on the surface *S* in Figure 7. The roving itself is tensioned with $\vec{f_t}$ according to the process specifications. Caused by the

tension, a resulting force $\overrightarrow{f_r}$ points towards the center of curvature. This force is composited by a lateral $\overrightarrow{f_b}$ and a normal force $\overrightarrow{f_n}$. The normal force can be compensated by the mandrel surface while the lateral force has to be equalized by a friction force $\overrightarrow{f_w}$. Hence, that friction force must be larger than the lateral force [61,67,99]. The relation between lateral and normal force is defined as 'slippage tendency' λ [28,61,67,99]:

$$|\lambda| = \frac{\|\overrightarrow{f_b}\|}{\|\overrightarrow{f_n}\|} \tag{11}$$

The slippage tendency must always be smaller than the friction coefficient to avoid slippage [61]. This and equation (8) lead to the following criteria for the friction coefficient μ [65,100]:

$$|\lambda| = \frac{\|\overrightarrow{f_b}\|}{\|\overrightarrow{f_n}\|} = \frac{\|\overrightarrow{f_t}/R_g\|}{\|\overrightarrow{f_t}/R_n\|} = \left\|\frac{R_n}{R_g}\right\| = \left\|\frac{k_g}{k_n}\right\| \leq \mu \tag{12}$$

With R_n being the normal radius and R_g the geodesic radius of curvature.

Since most of these forces cannot be measured during processing, it is important to determine the friction coefficient experimentally. Obviously, a good knowledge of the available friction is crucial for the calculation of fiber paths [100]. A general overview is given in [18,100]. End of the 1970s, the coefficient was determined via hoop winding on a sphere and calculated based on the distance where the slippage occurs [60,62]. Wells and McAnulty improved the accuracy of this method by replacing the mandrel with an elliptical shape and using a camera to record and being able to rewind [64]. They also introduced a differentiation between initial (the roving starts to move) and final/catastrophic (complete separation) slippage. Di Vita et al. used the same setup testing prepregs [101]. Based on the same approach, Koussios and Bergsma [100] introduced a new mandrel shape to facilitate the measurement and make it more accurate. Its surface profile is in a linear relation to the carriage distance which makes programming as well as identifying the slippage point easier. This setup has then also been used by other authors [18,99,102,103] and will also be used in this thesis. Other

test setups are based on a moving sled [18,104] or a capstan (drum) [105–107]. In most studies reviewed here, it is stated that the influence of tension and speed changes on the coefficient of friction is negligible [32,60,62,64,99,100,102,108]. Only Di Vita et al. [101] found that for carbon prepreg rovings a higher tension also leads to a higher coefficient of friction.

Various influences and configurations have been tested that led to ambiguous results which should be examined further [100]. In frame of this thesis, only dry carbon fibers on a metallic mandrel (aluminum) are under consideration which also represents the most critical phase for slippage in filament winding. The values determined for this scenario vary around the value of 0.2 ± 0.05 [18,60,62,64,100,102].

The safest way to avoid slippage in filament winding is using geodesic paths or just small deviations with high safety factors on the coefficient of friction. Since this reduces the design freedom drastically, other solutions are sought. Keeping the rovings in place can be solved mechanically, e.g., by pins or rings, or physically/chemically through adhesion. A tackiness between the surface can be established by additional material(s). Those will be presented in the following section.

2.2.3 BINDER MATERIAL & TACK

In order to create adhesion between mandrel and roving various approaches can be executed. Manipulating the mandrel surface, e.g., by grinding or coating, can have an effect on the frictional behavior. Yet, aspects such as part removal, repeatability, or mandrel specifications have to be considered. That is why this approach is not tackled here but it is recommended to check if this would be an option for a planned process. When trying to increase adhesion on the roving side, one wants to achieve the frictional properties of a wet roving or even better. If a completely impregnated roving is not wanted, as in dry filament winding, the treatment of the roving’s surface with binder material is recommended.

2.2.3.1 Binder material

Materials that can provide the required tack for non-slippage in dry filament winding are called binder or tackifier [109]. They can either be thermoplastic or thermoset. A detailed summary of available binder types is given in [110]. The most commonly used

types are epoxy and thermoplastic polyester or polyamide [109,111,112]. Thermoset binder, such as epoxy in this thesis, can be activated (reversibly) by temperatures above cross-linking temperature whereas thermoplastic binder need to be molten prior to application [113]. Depending on the used materials, binder can be applied to the reinforcement in numerous ways. Solvent spray, veil, commingled yarn, hotmelt, and powder are typical methods [109,114–118]. Every method has advantages and disadvantages which have to be evaluated for the concrete use case, e.g., sprayed binder provides a better distribution than powder binder [119]. Commonly, the percentage of binder applied to a textile ranges between 4-10 % of the composite's weight [109,111,120]. Another important aspect is the remaining binder. It can be soluble in the matrix resin or remain as a different particle [121,122]. If the binder is not dissolved in resin, it can be used to control compaction, thickness, and dimensional tolerances in general [123].

Exemplary advantages of binder technology are improved handling, reduced slippage, less scrap after cutting, the possibility to place inserts, producing shelf-stable semi-finished products, stabilizing the preform for an infusion, and local property modification [124].

While binder material is classically used for preforming, in recent years it has been employed with unidirectional materials in processes such as dry winding and (automated) dry fiber placement ((A)DFP) [125–130]. A special case in processing is the 'online' application of the binder to reduce cost and use its properties more efficiently [116,125,131,132].

Depending on the type, application form, solubility, activation, and other material and process properties, the presence of binder materials will change the characteristics of the final composite. The influence on permeability and (capillary) flow will be discussed in Section 2.4. Binder materials influence the compaction behavior of fabrics strongly [133]: Mainly depending on the compaction temperature, the stack acts differently under compaction. Varying binder viscosity leads to binder movement to specific areas which leads to a different nesting and relaxation behavior, e.g., for high temperatures binder flows in the lower layer which 'dries out' the upper layer which then shows larger relaxation.

Many studies state that in most cases the binder influences the mechanical performance of a part in various ways but mostly negatively [130], e.g., thermoplastic/non-reactive systems can reduce mechanical properties but also improve impact resistance [134]. It can also lower the glass transition temperature of the final product [123,134].

2.2.3.2 Tack

As the alternative name ‘tackifier’ suggests, binder materials provide tack. It is defined in ISO 472:2013 as a “property of a material that enables it to form a bond immediately on contact with another surface, which can be an adherend or another layer of adhesive” [135]. Most prominently, tack was investigated for pressure-sensitive adhesives (PSA) and prepregs [136]. A relation between tack and the coefficient of friction in prepreg winding was investigated in [108]. After (partially) curing an already wound layer in a certain time, tack and friction increase which can be beneficial for the next layer to be wound. Bindered reinforcements for composites show similar behavior as prepregs but to a smaller extent. In the frame of this work, a measurement method for bindered rovings in robotic dry winding was presented and published in [137]. Only the main results are summarized here while for further information it is referred to the publication and its references.

Binder materials are usually applied only on surfaces. That means that contrary to prepregs, there is no adhesive holding the fibers together in a perpendicular direction. In the common probe test method, this led to fanning of the roving which made the measurements unreliable. To overcome this issue and to be closer to the winding process, the experiments were performed on a heated plate. The roving was laid down for one meter, pressed down with a roll, and then pulled off by the winding head on the winding robot. The resulting force was measured via a load cell.

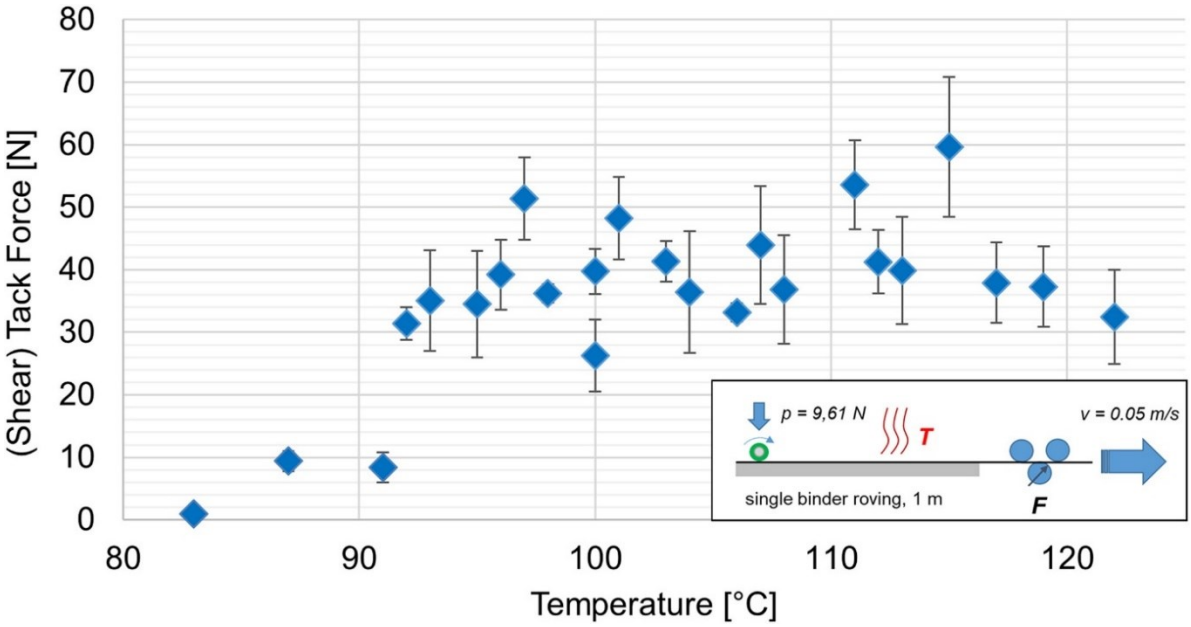

Figure 8: Effect of temperature on tack in robotic dry winding [137]

As a main result, Figure 8 shows the influence of temperature on the resulting force. Even for temperatures slightly below the given activation temperature, a sufficient tack could be observed. Yet, it correlates well with the measured onset temperature in the DSC diagram of the binder (see Figure 15). This experiment also showed that the force required to shear off the roving does not rise significantly for binder activated at a higher temperature.

In further modifications of the setup, it could be seen that a higher compaction pressure and a higher haul-off velocity led to a slightly higher tack force. The twisting of the roving had no notable effect.

2.3 AUTOMATION IN FILAMENT WINDING

The term automation covers a broad area of aspects. Figure 9 shows the so-called automation pyramid. It displays the distinct levels of automation in a company.

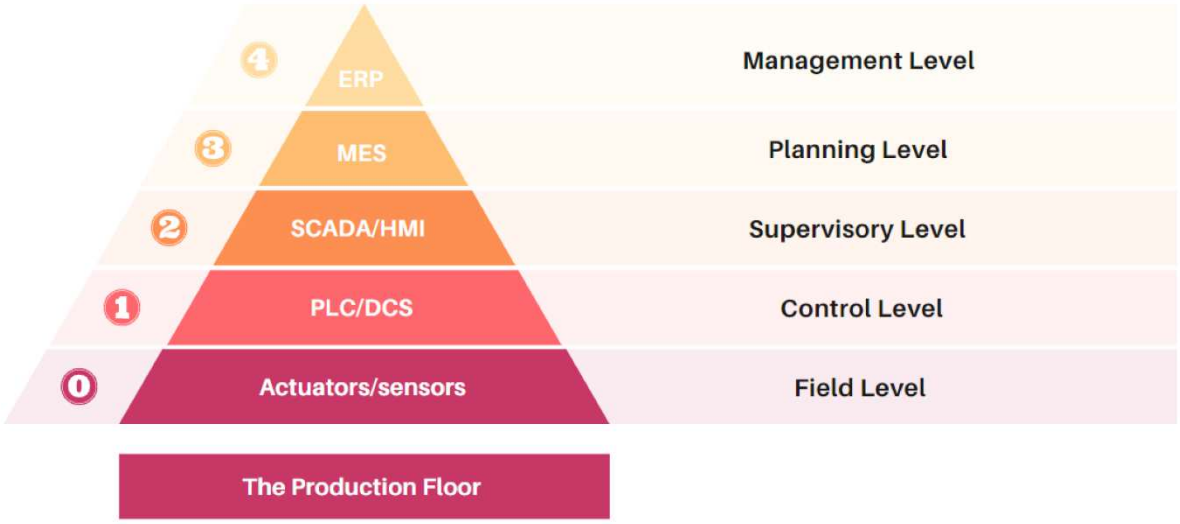

Figure 9: ISA-95 (IEC 62264) Automation pyramid [138]

The two top levels 3+4 cover the management (ERP=Enterprise Resource Planning) and planning (MES=Manufacturing Execution System) functionalities. Both are rather on a management, resp. strategic, planning level and can cover whole factories. Levels 0-3 can be often seen even at a single machine or a single process, for example, filament winding. Supervisory level 2 contains concepts such as the human-machine interface (HMI) or the supervisory control and data acquisition (SCADA). Data is processed in order to interact with a human operator or to be monitored and eventually trigger alarms or events [138]. Level 1 tackles control systems such as a PLC or distributed control systems (DCS). These systems are standard in modern machinery, also in filament winding. Field level 0 deals with sensors and actuators.

Experimental and development work executed in this thesis covers the field and the control level with small parts of the supervisory level. Yet, the data generated there is crucial to the upper levels since they are the basis for the decisions made there. For example, the answer to the question of whether a dry filament winding process is a suitable option can be supported by data generated in experiments with the machine.

Out of the many aspects of automation, two will be highlighted in this section because of their relevance to the thesis at hand: Robotic filament winding as the used machine setup and the usage of sensors and control data for process monitoring in filament winding. For further reading on the history of automation in filament winding, chapter two in [4] and for an extensive, contemporary review of Industry 4.0 in composite manufacturing, [139] is recommended.

2.3.1 ROBOTIC FILAMENT WINDING

Even though ‘regular’ filament winding machines nowadays cover six degrees of freedom [38], it is worth having a look at robotic filament winding. Industrial, anthropomorphic robots usually also cover 6 DOFs but a more established in industry and cheaper than a specially developed filament winding machine [3,28]. An example is displayed in Figure 10. Robotic winding is particularly interesting for research and development facilities or any other manufacturer that needs to wind a variety of complex shaped parts in a low to medium quantity [140]. Early research on robotic winding was executed in the 1980s [3,86] and has evolved with the progression of robotics up to collaborative systems these days [25,41].

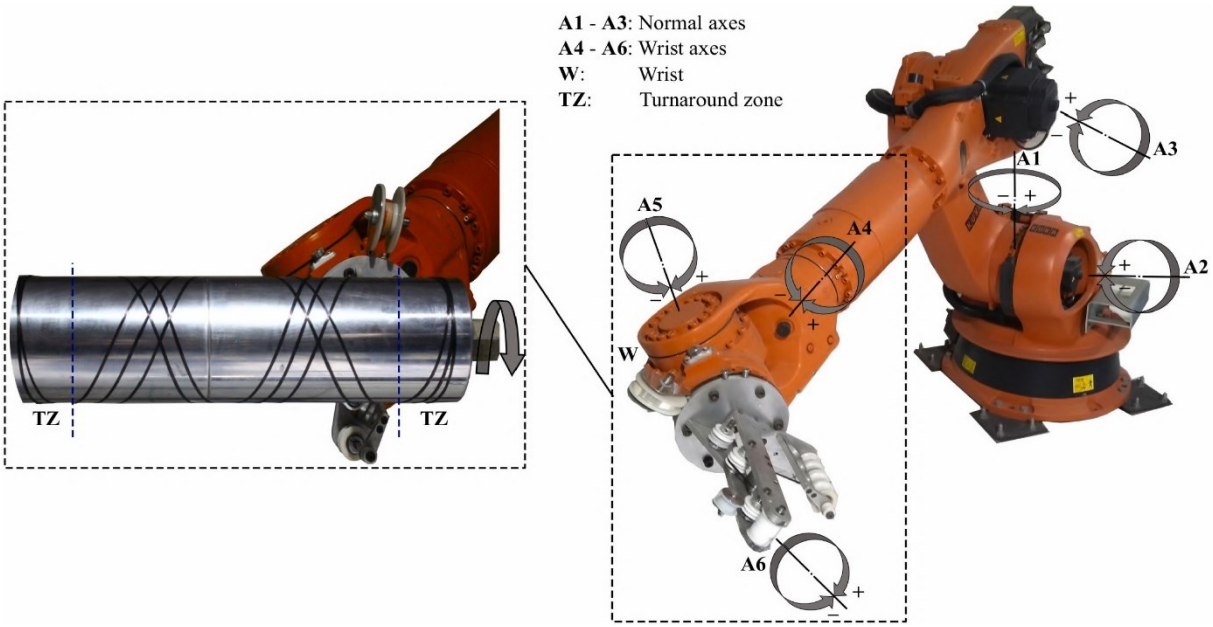

Figure 10: DOFs of an anthropomorphic winding robot for cylinder manufacturing [141]

A new challenge that arose with robotic filament winding is collision detection. Due to the many degrees of freedom and the complex movements, the probability of causing

a collision either with the part, the axis, other parts of the equipment, or even the robot itself rises [27,28]. In path planning and simulation this has to be considered carefully. Especially, the definition of the free fiber length (or the enveloping contour respectively) is of significant importance. The selection of a safety distance can have mixed effects on the process efficiency. A larger distance means also more distance to be covered but also the robot can possibly facilitate faster movement speed due to the gained security [142]. Also, specific challenges associated with robots need to be regarded, e.g., singularities, angle velocity and acceleration, or joint angle limitations [35]. Another factor of path planning in robotic winding that needs to be considered is the number of points. On the one hand, many points can provide a smoother and more accurate movement and thus less potential to lose tension, on the other hand, it also increases winding time [27,142]. As for the winding parameters in robotic winding, roving tension should be kept constant and rather low. Winding speed should not be too high to ensure an accurate fiber deposition [140,142]. Robots are often also an essential part of modern process concepts such as ring winding [143], joining with winding [18,19], or creating open truss [41] or isogrid [144] structures. Table 2 summarizes the pros and cons of robotic filament winding.

Table 2: Advantages and Disadvantages of robotic filament winding [12,27,145]

Advantages	**Disadvantages**
Other tasks can be performed by the robotic system, e.g., quality control	Accuracy might be lower if the control cannot couple the winding axis properly
A robot is less expensive than a winding machine with similar capability	Mandrel size is limited by the robot's workspace
Due to mass production better quality (control) of the machines	Less efficient for parts with simple geometries
Possibly faster for parts that allow medium accuracy	

2.3.2 PROCESS MONITORING IN FILAMENT WINDING

Looking at process monitoring in filament winding, one can differentiate between the monitoring of the process parameters and the inspection of the part. Both can be processed further in the main controller to inspect and adapt the process if necessary. The control of parameters required for the proper functionality of the process is usually already implemented in the machine by the manufacturer, e.g., speed and acceleration. Depending on the complexity of the machine, other sensors can be implemented as well but don't have to be. For example, roving tension can be measured separately and then controlled with a PID controller [146]. Often, the tensioning control system is already implemented in the creel [2]. In robotic winding, tensioning can also be implemented in the deposition head [74,89,137].

While the monitoring of process parameters is often taken care of already by the machine supplier, the inspection of the produced part is still a big topic in research. Early efforts in robotic filament winding used ultrasonic C-scans for defect detection [28]. However, most papers concentrate on the related processes AFP, DFP, and ATL. Here, several extensive reviews on (inline) monitoring and non-destructive testing (NDT) are available [147–149]. In these processes, the detection of gaps and overlaps is of crucial importance, because they can easily happen and change the properties of the part significantly [150]. In filament winding, this can also be an issue but to a lesser extent. Due to spreading behavior depending on parameters such as tension, surface curvature, and wetting, the deposited (wet) roving will most likely have a different shape [2]. Binder rovings on the other hand show a similar behavior to tapes and can be treated accordingly. Figure 11 shows the challenges for edge detection in wet filament winding. While the cross-section is mostly modeled to be rectangular, in the actual process it is not [2]. When viewing the deposition from the top, the focus depends on the winding method. For several layers of hoop winding the contrast is low when deposited. When a hoop layer is wound on a helical layer, the contrast is low compared to the previous circle but high against the last (helical) layer. These different behaviors have to be considered when setting up a monitoring process.

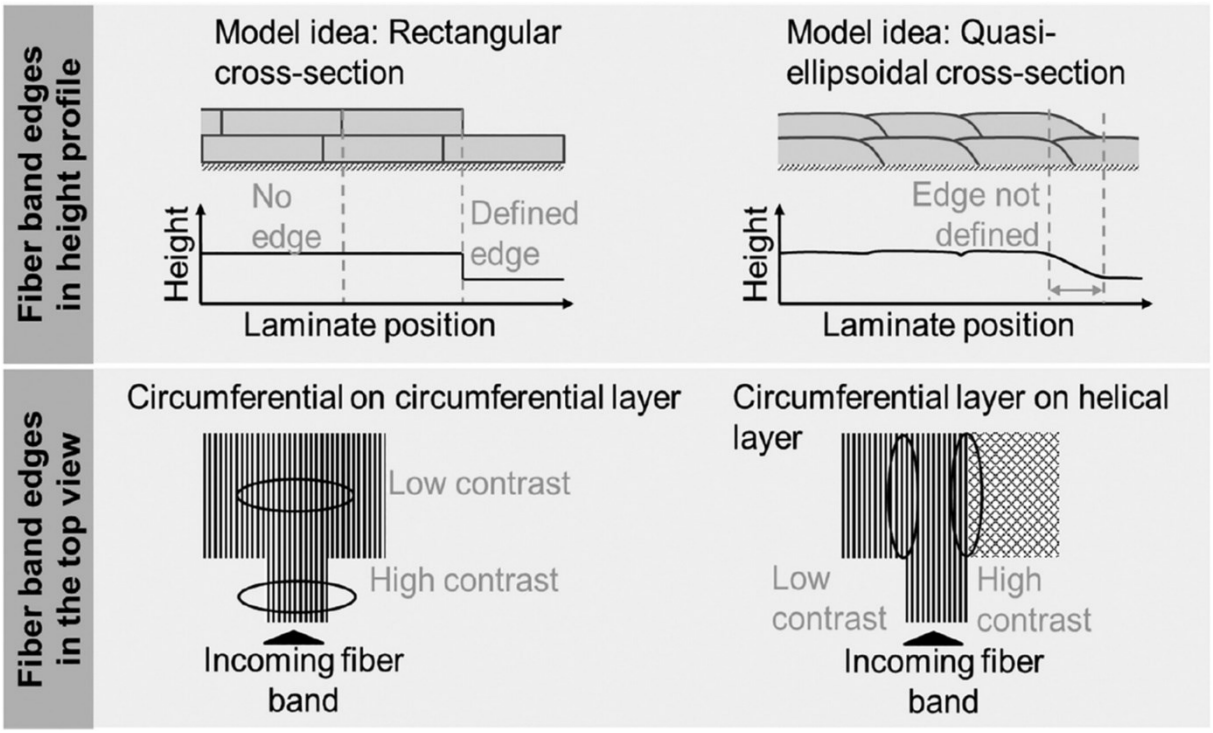

Figure 11: Edge detection in (wet) filament winding [2]

In general, the inspection of surfaces or profiles in composite manufacturing comes with some challenges. Tactile sensors might influence the wet resin or damage the cured resin. Contactless, non-optical measuring methods are often too slow for the monitoring of continuous manufacturing processes such as filament winding or AFP. Hence, optical (and thereby contactless) methods are generally preferred. [151,152]

Yet, optical measurement of composites can be challenging due to the color of the fibers. Black carbon or shiny glass fibers can cause a lack of light intensity or unwanted reflections [153].

Optical monitoring techniques for continuous composite processing can be roughly divided into three major categories: thermography, laser-/ machine vision, and profilometry [147]. For other techniques mentioned in literature such as fiber Bragg grating sensors (FBG) or interferometry and for deeper information on the presented methods, it is referred to the previously mentioned reviews.

Thermography is particularly suitable for the detection of foreign objects and debris [2,147,154]. A transmission-style measurement is also possible by preheating the previous layer [155]. It can be an option in wet filament winding since the roving edges

coalesce and cannot be recognized by vision-based systems anymore [2]. Machine vision systems, optionally with laser projectors, capture images of the surface and then apply image processing algorithms [150,156,157]. The challenge with these systems is to create a high-quality image (lighting and detection hardware) and then find a suitable algorithm for the processing of the so-gained data.

Most machines that are described in literature make use of some kind of profilometry sensor. Especially, the (laser) light sectioning sensor ((L)LSS) is the focus of research [151–153,156,158–163]. This type of sensor will also be used in Section 4 of this thesis. As mentioned previously, it would be difficult to detect the roving edges in an already deposited layer. Yet, this method is suitable for dry and bindered rovings. It can also be used not only after deposition but also during the fiber guidance in the winding machine. By that, parameters such as the width or defects and anomalies such as twists can be detected before the roving is placed on the mandrel.

2.4 INFUSION OF BINDERED MATERIALS

2.4.1 RESIN FLOW IN LCM PROCESSES

Dry fiber filament winding produces preforms [96]. To obtain a composite part, this preform has to be filled with resin. Liquid composite molding (LCM) summarizes a group of processes to fulfill that goal. Roughly speaking they can be split into vacuum-driven (infusion) and pressure-driven (injection) processes. Figure 12 shows an overview of typical processes in this spectrum. As can be seen there, the resin transfer molding (RTM) process contains many subcategories. Many of them with the support of a vacuum, as indicated by the dashed line. Depending on the application and desired output, multiple processes can be chosen for a wound preform. On prototype level, the infusion processes are easier to handle. When it comes to high-performance and medium-size output numbers the RTM processes are the method of choice.

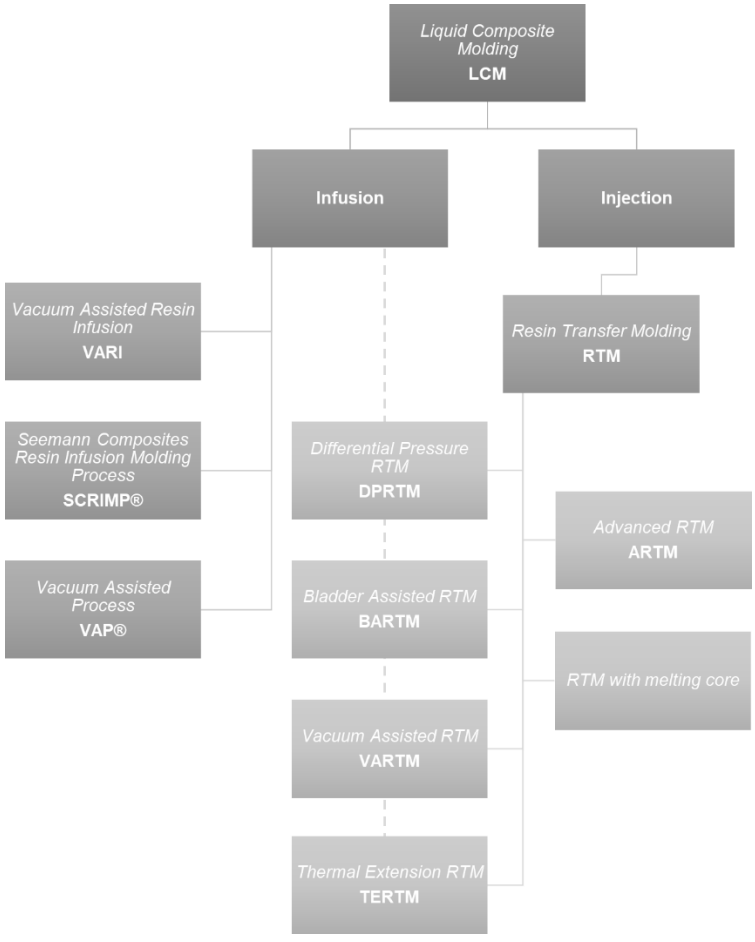

Figure 12: Selective overview of LCM processes (adapted from [5,164])

All these processes (and possible derivates) connect that a good impregnation of the reinforcing structure is mandatory for a high-quality part. A key aspect to achieve this is the impregnation velocity. On the one hand, it determines if the process is fast and hence (cost-)efficient [165]. On the other hand, it also affects the part quality. The main challenge is to find the maximum velocity at which close to no voids are created. Voids, pores, fiber washout, and other defects caused by deficient impregnation can have a large influence on the mechanical properties of the part [166,167].

The flow in a typical textile preform can be modeled as ‘dual scale’ [165,168–172]. Two types of pores can emerge depending on the fluid flow and the position in the textile. This mechanism is depicted in Figure 13. The driving forces that enable flow can be split into viscous/pressure-driven and capillary-driven [165,170,173,174]. Depending on the velocity of each effect, micro or macro voids can develop in the textile [170,173]. If the capillary forces are too high, i.e., the pressure-driven flow is relatively small, the fluid progresses faster through the rovings, the so-called ‘fingering’ [170,174]. This might lead to voids in the pore spaces of the textile. If the injection pressure is too high and the mold is filled quickly with resin, this can lead to the rovings being dry on the inside. A thorough overview of void formation and its consequences is given in [172].

Many studies have been performed to find an optimal injection velocity [165,172,173,175]. Yet, processing conditions are commonly unique and depend on many parameters. While some general statements can be made, the individual process usually needs pre-trials or a reliable flow simulation.

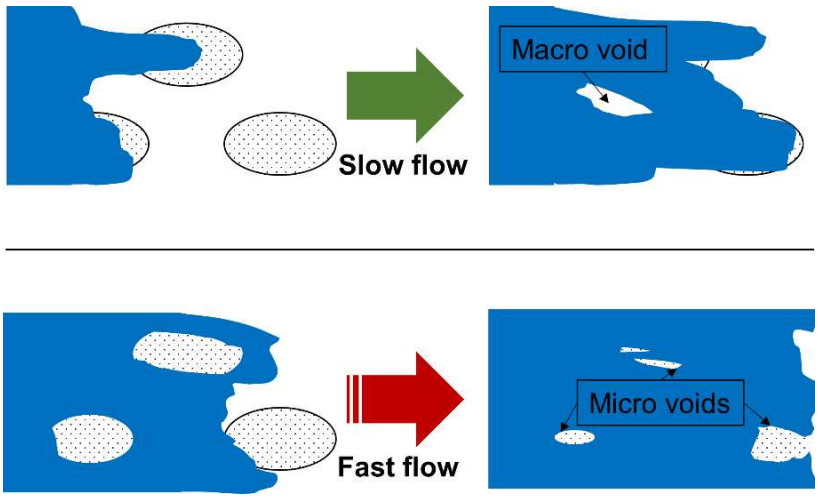

Figure 13: Dual scale flow model (adapted from [165])

When it comes to the processing of bindered textiles, the prediction of the actual flow is even more complicated due to the presence of additional material in the pore spaces; this also counts for other materials such as stitching yarn [174,176]. Not only is the binder a foreign material, but it also can interact with the infiltrated fluid. It can dissolve, react, or just be washed out by the resin [121,122].

The flow in reinforcing textiles can be modeled by various approaches. The most popular (and simplified) equations are the Darcy equation for permeability of a porous medium [177] and the Lucas-Washburn equation for capillary flow [178,179]. In the following two subsections, these two aspects will be discussed. First, an overview of permeability studies on bindered material will be given. Since many results are already available, permeability will not be investigated further in this thesis. Then, capillary flow phenomena will be examined. Although numerous studies handle capillarity, only a few exist which also include the possible effects of binder material. In the experimental section, capillary flow experiments of binder rovings will then be performed.

2.4.2 PERMEABILITY OF BINDERED TEXTILES

The permeability of polymer composites is a unit that describes the property of the reinforcing structure (porous medium) to let a polymer (fluid) pass through it. Usually, it can be divided into three principal directions, two in-plane, and one through-thickness [180]. It is one key parameter in the design of LCM processes. Permeability determines the possible filling speed and hence cost efficiency and (mechanical) properties of the final part.

Binder materials are an additional material that needs to be considered when planning to use an LCM process to fill a fibrous reinforcement with resin. The presence of a binder will influence the injection/infusion in many different, sometimes opposed, ways. In the field of permeability, many studies have already been published presenting these different aspects. In the following, a brief overview will be given on the state-of-the-art of binder influences in various preforming and LCM processes.

Binder location, concentration, and material specification can influence permeability strongly [115,181,182]. Especially for anisotropic materials, binder can affect the flow differently in the principal directions [181]. Shih and Lee state that the location of the binder has a great effect on the permeability [167,183]. They also found that

permeability decreases with higher binder content for fabrics activated at 80 °C whereas it increases for those activated at 160 °C. Also, the higher activation temperature and the consequent absorption of the binder into the rovings lead to more voids. Rohatgi and Lee state that permeability is affected more by the blocking of large pores between the rovings than by blocking of interlayer pores [176]. Dickert investigated the influence of binder and its activation on the permeability and mechanical properties of carbon NCFs [115,182]. It is concluded, that for the mechanical properties, the binder location and the activation temperature related to that have a larger influence. High activation temperatures lead to a highly viscous flow that reorganizes the binder distribution and hence the adherence of the fibers. Concerning permeability, different mechanisms were identified, too. Depending on binder type and concentration, the binder particles either widen the flow channels and increase permeability or block them and decrease it. Zeng et al. examined 3D woven reinforcements with binder yarn. They concluded that the binder has a significant impact on the permeability, especially in weft direction, due to the varying degrees of compaction [184].

2.4.3 CAPILLARY FLOW IN TEXTILE REINFORCEMENTS

Minimizing the void content of a part is crucial for any LCM production process. As depicted in Figure 14, the optimal resin flow velocity is where micro- and macro-voids are minimal. Thereby, the resin flow velocity is driven by viscous and capillary forces.

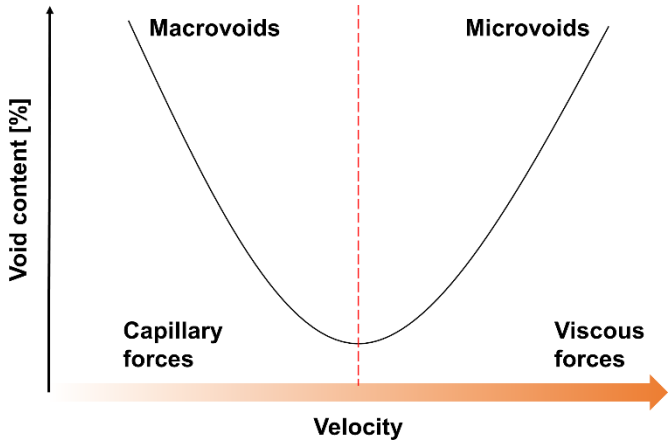

Figure 14: Void content depending on driving forces (adapted from [175])

Viscous forces originate in the hydrodynamic injection (under-)pressure and act on the reinforcement structure. Permeability is the key parameter here to optimize the

process. During a very slow injection, capillary forces will dominate and could lead to macro voids when the resin in the rovings flows faster than in the interlayer regions and pores. Optimizing this flow is necessary for a high-quality product. For a good overview of capillarity in composite manufacturing, the review paper [185] is recommended.

Often, this process is associated with the term ‘wicking’. It stands for the spontaneous, capillary-driven absorption of liquid by a porous medium [166,186]. Capillary forces originate in pressure differences due to different surface tensions between a solid material, entrapped air in a pore, and a fluid [185]. In composite manufacturing, this is the polymer filling the fibrous reinforcement structure. Since resin or even thermoplastic polymers have a greater viscosity than for example water, the process is much more dependent on interface velocities [185]. Also, capillary flow of resin can be influenced by curing reactions. For that reason, neat resin or a test fluid is commonly used in studies on capillary flow [187].

Basically, all experimental methods to determine the capillary flow are based on the dipping of a textile reinforcement structure into a container filled with a (test) fluid. The evaluation can then either be by the weight loss of the fluid or by monitoring the flow into the textile. Both acquisition methods can also be done simultaneously. [171,172,175,185,187–201]

Many adaptions have been made to this basic setup, e.g., with an IR camera [175], translucent [171] or fluorescent lighting [193,202], or the addition of an injection unit [203]. For further reading on the experimental determination of capillary flow in composites the following review (sections) are recommended: [185,186,193,202].

After the information on the capillary behavior is gained, it has to be processed. Here, various approaches mostly based on the Darcy, or the Lucas Washburn equation can be observed. Many models and adaptions have been published which will not be presented in the frame of this thesis. For this and the derivation of parameters such as the capillary pressure or the capillary number, the reader is referred to the already mentioned reviews and cited articles.

Yet, if bindered textiles are used, their influence is usually neglected. Rohatgi and Lee [176] found the highest capillary pressure for unbindered textiles, followed by those with binder on the surface, and then the ones with binder absorbed by the rovings. They conclude that the absorbed binder can be a reason for an inferior fiber wetting by the resin.

In this thesis, only a single binder roving is regarded. Filament wound preforms are expected to have different flow behavior than fabrics. So, as a first step, the capillary flow at roving level is investigated to get a first impression of the influence of binder material. Similar experiments on single fibers and tows without binder have been performed by Wang [204] and Qiu [205–207]. They provide insight into the wetting behavior (surface tension, contact angles, etc.) on micro- and mesoscale.

In further research, experiments with patches of wound structures should be executed to get a realistic impression of the flow in bindered, wound preforms.

3. DRY FIBER FILAMENT WINDING

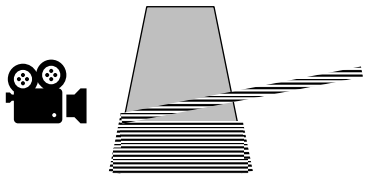

3.1 MATERIAL

Studies on bindered composites usually deal with semi-finished textile reinforcements such as rovings or tapes in 1D and weaves or NCFs in the 2D case. Often, the binder is applied online or previously on a specifically designed apparatus. While there are many bindered fabrics available, the market for bindered rovings is small. In the frame of this thesis, only one epoxy bindered roving system was commercially available to the author. This roving will be used in all experiments in the upcoming chapters.

Tenax®-E HTS40 X030 by Teijin Carbon Europe GmbH (Wuppertal, Germany) is based on a 12K roving coated with ~ 7 % binder. The preliminary product data sheet [208] constitutes the activation temperature at ~120 °C which has to be achieved thoroughly in all areas where adhesion is desired. Temperatures above 160 °C must be avoided to exclude curing reactions which could impair the repeatability of the activation. The binder roving is based on a 12K roving of the same manufacturer: Tenax®-E HTS45 E23. This roving is used as reference material for unbindered processing. The cost increases for the binder roving by 80 % with respect to its unbindered basis.

Since the binder's name and properties are not specified further in the technical datasheet (TDS), differential scanning calorimetry (DSC) was performed on a DSC 1 (Mettler Toledo Inc., US/Switzerland) to validate the given parameters. For this measurement, the binder was dissolved from the rovings by butanone/ methyl ethyl ketone (MEK). After vaporization of the solvent at 80 °C the binder was removed.

Figure 15 shows the setup and the result of the DSC measurement of the binder material. The peak is at approximately 100 °C. This shows that binder activation is to be expected at even lower temperatures than the 120 °C specified in the datasheet. It is merely the upper limit where the manufacturer guarantees the activation.

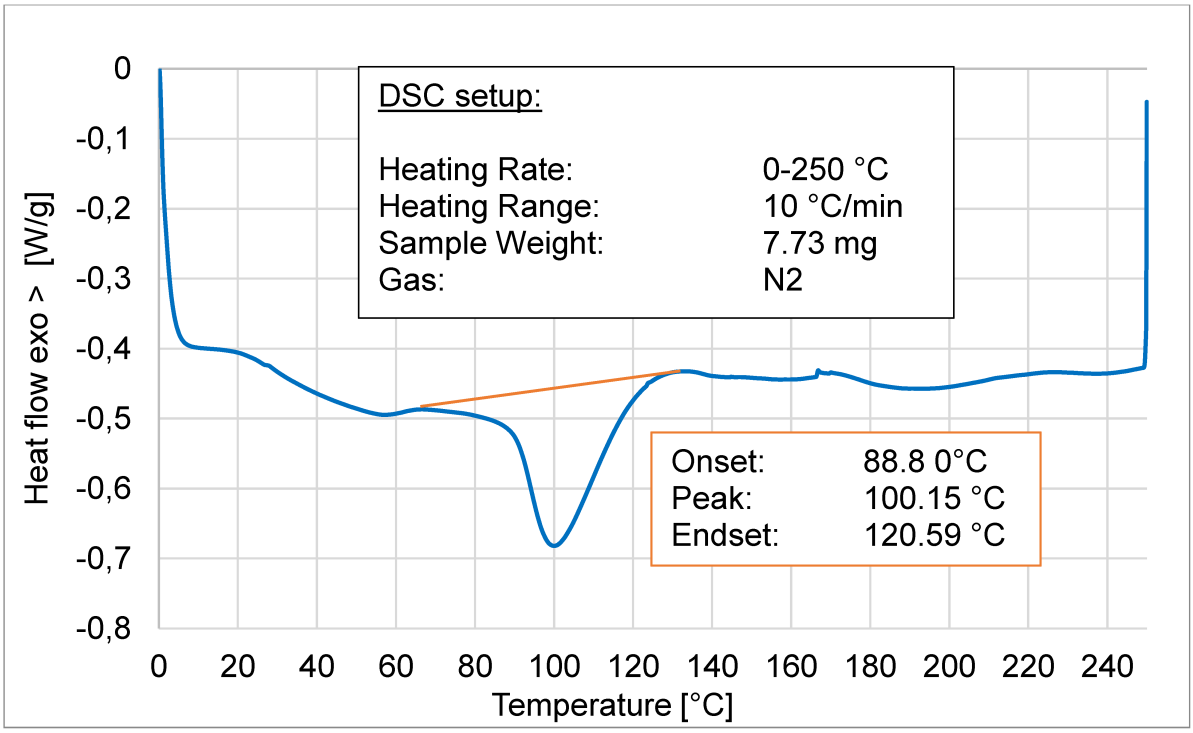

Figure 15: DSC measurement of binder material from HTS40 X030 (similarly published in [137])

3.2 DEVELOPMENT OF A DRY FIBER WINDING SETUP AT LVV

At the beginning of this work, only basic equipment for robotic filament winding was available at the 'Processing of Composites' group (LVV- Lehrstuhl Verarbeitung von Verbundwerkstoffen). Consequently, the first task in the frame of this thesis was the development of a robotic end-effector and the design of a mandrel that could be used for the research of dry fiber winding. In the following, the developed parts will be presented shortly and their relevance for this thesis will be explained. The two main aspects are automation (robotics, PLC, communication) and dry fiber winding (mandrel design, tension control, path planning).

3.2.1 FILAMENT WINDING EQUIPMENT

3.2.1.1 Robotic filament winding setup

The existing winding setup at LVV consisted of a robot KR150 R2700 extra (KUKA AG, Augsburg, Germany), a rotational axis KPF1-H250 (KUKA AG, Augsburg, Germany)

with a splined shaft, a self-built ring winding head, and some auxiliary equipment. Figure 16 shows the setup including the newly developed mandrel and winding head.

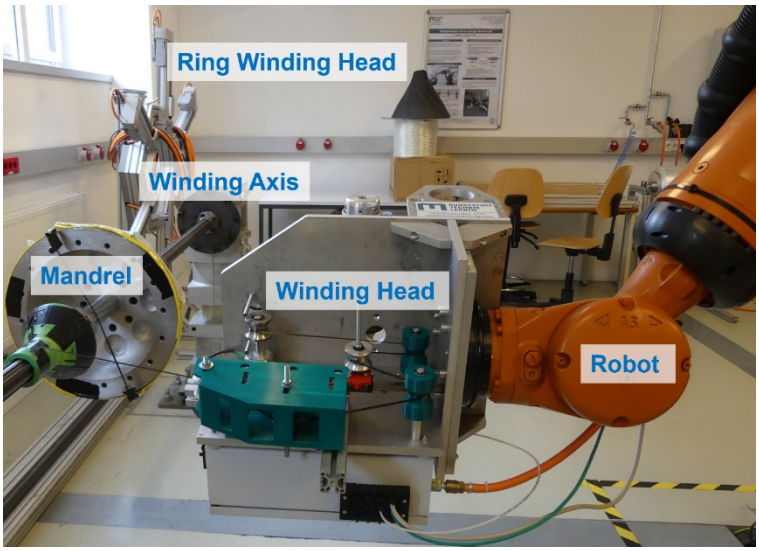

Figure 16: Overview of the winding equipment at LVV

The combination of a 6-axis robot with an external axis allows multiple degrees of freedom for dry fiber winding. Complex shapes can be wound on, and process automation and control can be established flexibly. The main components of a robotic winding machine are commonly the robot, a winding head as a robotic end-effector, a winding axis, and a mandrel. Furthermore, important for the design and the control of the process are suitable winding software and overall control, e.g., via PLC. A resin bath or other injection units can be omitted for dry or prepreg winding. Optional equipment can be sensors, fiber guidance units, heating devices, pins, tackifier spray, tape, pressing devices, and spool changers to name a few.

3.2.1.2 Mandrel

When investigating the processability of binder roving for dry fiber winding, a suitable mandrel is required. A general requirement for a winding mandrel is the absence of larger concave areas on the mandrel. Avoiding fiber-bridging without additional auxiliary components is usually not possible unless the shape and the designed winding paths can be selected accordingly. Simple structures such as tubes provide few possibilities for research on fiber slippage and its control.

Consequently, the chosen structures at LVV were cones. Two aluminum mandrels were manufactured for the different experiments. One mandrel to measure the coefficient of friction is based on the design published in [99,100]. The other mandrel with a concrete case of application is a jet engine nose cone, originating in a project.

While the mandrel for the friction experiments is clamped on one side in a three-jaw chuck, the nose cone mandrel is attached on both sides to the splined shaft of the winding axis. For ease of manufacturing and cost reasons, both mandrels are designed without the possibility of heating them. The nose cone mandrel has some notches on the backside to reduce weight and hence simplify handling. Figure 17 shows CAD drawings of both mandrels.

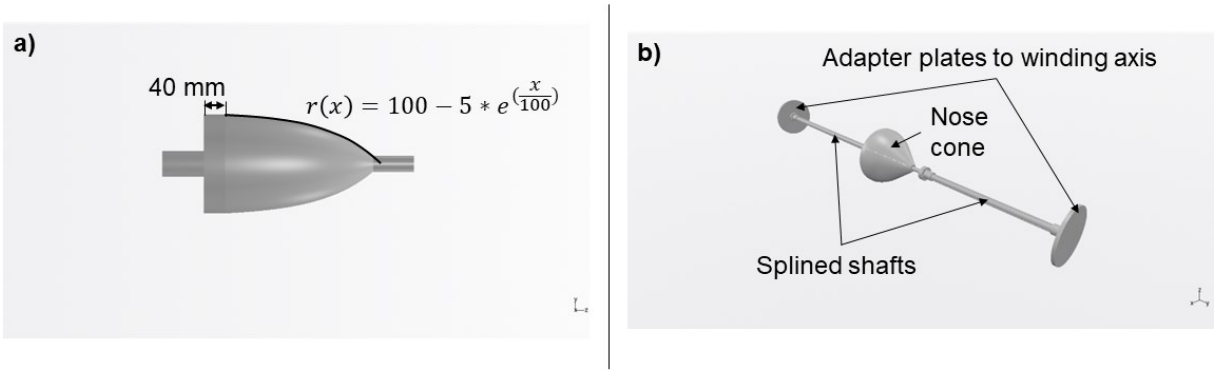

Figure 17: Winding mandrels: a) Friction experiments b) Nose cone

The specific shape of the mandrel depicted in Figure 17 a) allows the direct determination of the coefficient of friction. When slippage occurs during hoop winding of a roving, the carriage of the machine correlates with the coefficient. The equation for the surface given in the figure can be derived by solving an ordinary differential equation deduced from the definition of the friction coefficient and inserting the geometric properties [99,100,102]. The nose cone mandrel in Figure 17 b) was manufactured according to the drawings of the project partner. Here, both ends of the mandrel are connected to spline hubs on the splined shaft. The flange on top of the mandrel needs to be demountable to remove the wound preform from the mandrel. Both mandrels were used in winding experiments which will be presented at the end of this chapter.

3.2.2 DEVELOPMENT OF A WINDING HEAD

Fiber deposition in robotic filament winding is done by a (often self-built) device mounted on the robot's flange. The main purpose is the correct placement of the roving according to the calculated path. Doing that, many side tasks emerge to ensure the accuracy and quality of the winding. This means that the winding head usually carries sensors and other devices to control the roving's tension, guidance, and overall quality aspects.

The winding head developed at LVV was devised to be multifunctional. Mainly designed for dry fiber winding, it should also be possible to wind towpregs or tapes and to do wet winding with an additional impregnation unit. To increase the output and/or to enable hybrid winding two spool holders with separate roving guidance were designed. The frame of the winding head is manufactured with aluminum plates to be able to add or modify components easily. It is screwed on the robot's flange and supplied with electricity, pressurized air, and a PLC data connection via the cable conduit of the robot.

Figure 18 shows the CAD design of the winding head. While the mounting of two spools is possible, only one is usually installed. It is clamped on a pneumatic expansion shaft which can be activated by a valve on the front side of the shaft. To control tension and to prevent movement of the spool after a stop, a pneumatic brake is installed. It is controlled manually or via PID controller in the PLC. To ensure that the roving is unwound and correctly guided, two 3D-printed parts are attached to the movable guiding rolls ('Mickey Mouse ears'). After the roving is guided through the top plate of the winding head it is redirected by 90°. This roll is mounted on a load cell which measures the roving tension and gives feedback to the PLC for the tension control. The load cell was calibrated by measuring the weight of a bucket of water. With the measured tension data, it is possible to control the tension by adjusting the pressure level on the brake via PLC.

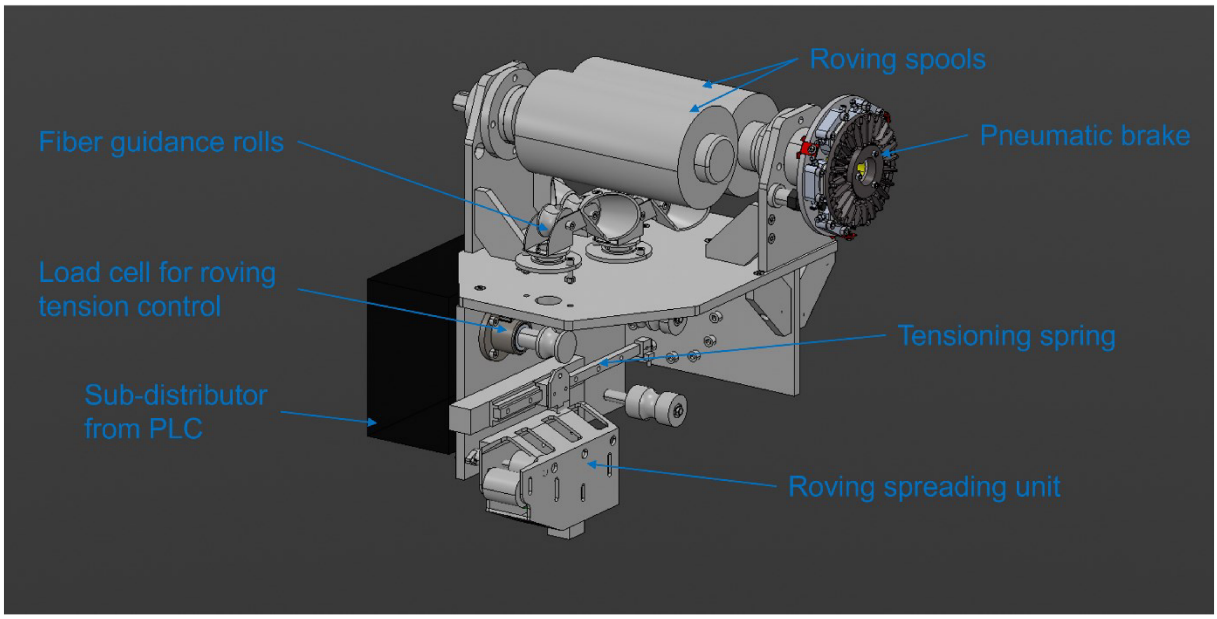

Figure 18: Winding head for dry fiber winding

A major issue in the dry winding experiments was the loss of fiber tension caused by the motions of the robot. Since the roving cannot actively be pulled back, a spring is installed on a linear axis. With that, small movements where the roving would slack can be compensated. For larger deviations, the path planning must be changed. The last unit before fiber deposition is a housing with three rolls at different heights. To spread the roving, the lowest roll has a convex surface. This helps minimize twists and other guidance errors and helps provide a more uniform roving for the deposition. On this winding head, only rolls were installed. Experience shows that ceramic eyelets and other common guiding elements are less suited for bindered or prepreg rovings. They can increase friction drastically and hence cause damage to the rovings. In the middle of the last roll on the winding head, the tool center point (TCP) is placed. In robotics, this point defines the origin and orientation of the tool's coordinate system. Usually, the movements of the robot are set up in the tool coordinate system in reference to the base's coordinate system, in this case, the winding axis.

The winding head proved to have good usability in the winding trials, yet some improvements can still be made. Tension control is still difficult to achieve due to the various redirections and the usage of the spring. Moreover, the redirecting causes notable fiber damage which needs to be avoided by smoother guidance. Another challenge is the location of the roving on the spool. At the edges, the roving tension

peaks due to the roving being dragged over the edge. The installation of the guiding shields on the first roller improves the unwinding significantly. Yet, when it comes to the edges an increased distance could help. Additionally, the rovings are not always placed without twists by the manufacturer. This cannot really be compensated during the fiber guidance and can only be reduced by a suitable spreading unit.

3.2.3 PROCESS CONTROL AND AUTOMATION

The robotic dry fiber winding process comes with a high degree of (possible) automation. Robotics itself is a widespread field that allows many possibilities but also makes the process more difficult to design and control. Consequently, a large aspect of process design is the communication and control between the various machines and devices.

The design of a winding process starts with the determination of the winding pattern according to the strength requirements and the mandrel's topology. Especially for dry fiber winding, the calculation of the winding path is a crucial step for the feasibility of the whole project. One major advantage of binder rovings is that, when activated, the rovings provide more tack for the adhesion on the mandrel surface. Yet, this is also the reason why specifications will be pushed to the boundaries to allow more design freedom. After the winding path is computed to be stable, it needs to be ensured that the winding machine can follow this path without collisions, losing fiber tension, or other possible damages. When the machine path is generated, the other process parameters such as tension or velocity need to be defined before the process can be started.

Figure 19 shows the process flow of the robotic filament winding equipment at LVV and the respective programs to set up the process and control it. In the following section, the key aspects and possible challenges will be presented.

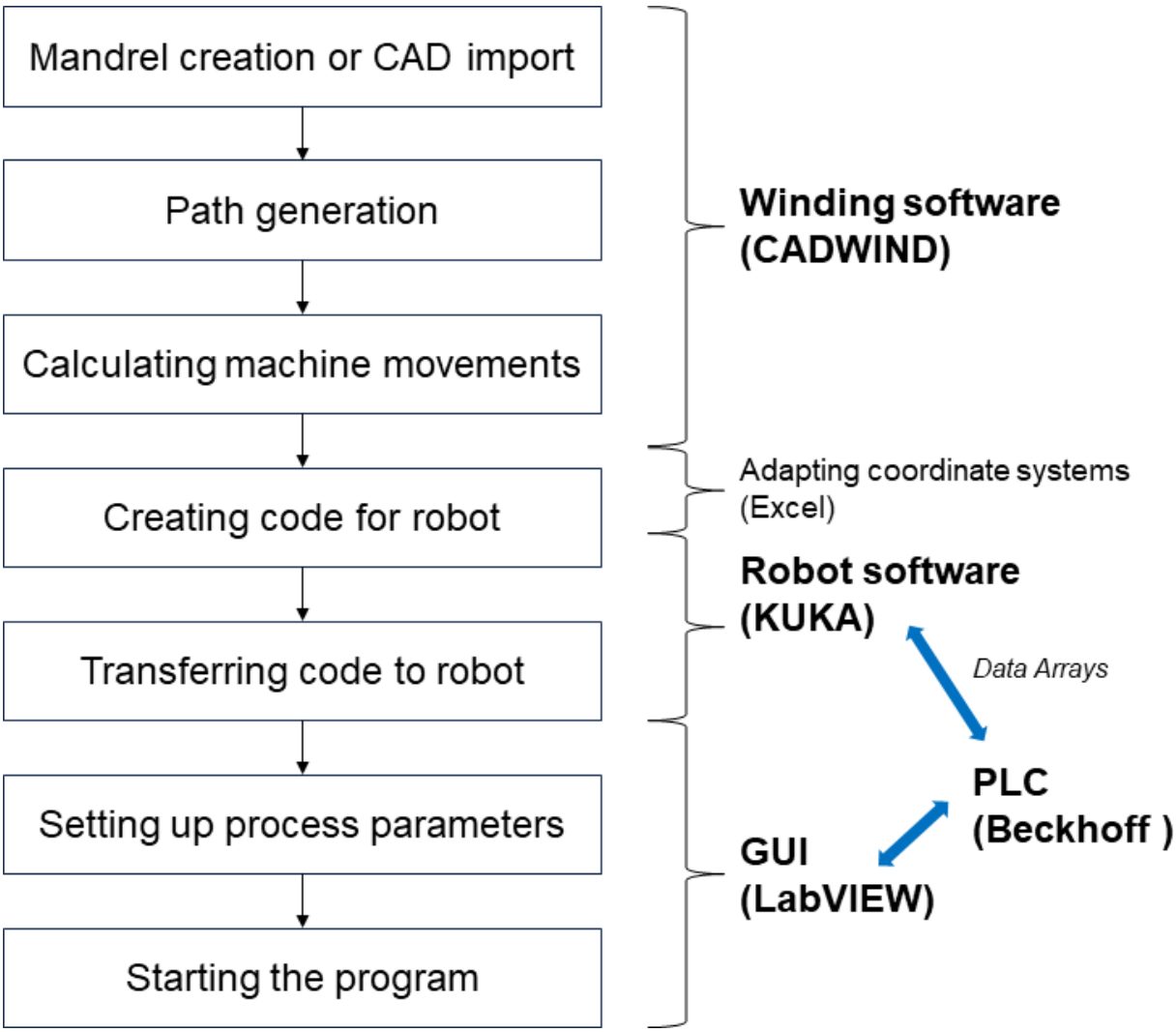

Figure 19: Winding process flow at LVV

Given a suitable mandrel, the process design starts with creating a winding simulation. First, the mandrel must be created in the winding program. At LVV, CADWIND® (MI MATERIAL innovative GmbH, Aachen, Germany) is used and explained hereafter [77,85]. Simple forms can directly be created in the program, while the conical mandrels used in this work must be imported. Although 2D (.dxf files) and 3D (.stp/.step files) imports are supported, attention has to be paid to the surface properties. The winding program must be able to identify the surface to dissect it and create sections (‘frames’). These can then still be refined in a text file.

Based on this mandrel model the winding paths are created. Circumferential (hoop) winding is necessary for the friction coefficient experiments which can easily be designed manually. Winding on the nose cone requires non-geodesic winding paths.

These can be designed by assigning a friction coefficient to the different segments. Other required input parameters here are the winding angle, the roving dimensions, the number of layers, the definition of starting and turning positions, dwell on the edges, and the desired degree of coverage. If the calculation of the winding path has one solution, it is displayed directly. In the case of multiple solutions, the user can select based on the degree of covering, the required cycles, and the pattern. The displayed results are shown in Figure 20 for a non-geodesic winding on the ‘friction mandrel’.

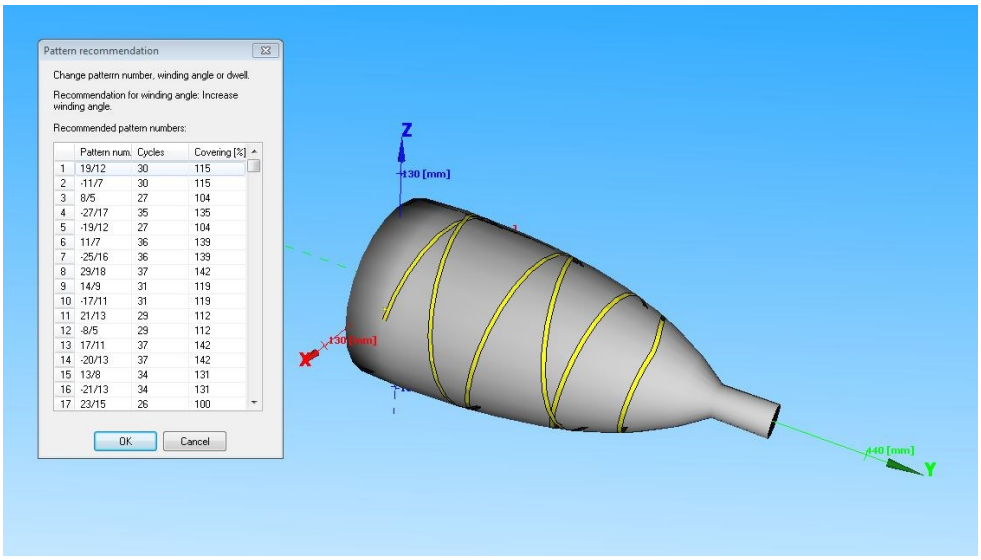

Figure 20: Winding pattern selection in the filament winding software

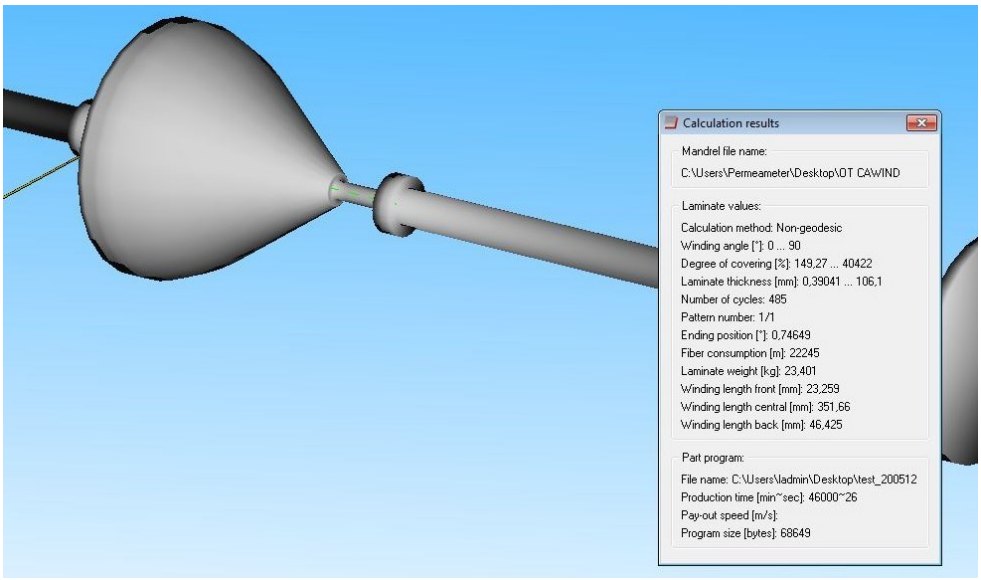

Figure 21: Winding path results for non-geodesic winding on the nose cone

Yet, even if computational solutions are generated, this does not mean that they are also feasible. Figure 21 shows such a result for the non-geodesic winding on the nose cone with a friction factor of 0.1. This shows that, despite the improvements in filament winding software, experience and/or trial-and-error are required in selecting the winding pattern. Also, this choice might be strongly limited by the design specifications and could lead to a conflict between dimensioning and manufacturability.

After the winding pattern is chosen, the machine commands for the respective winding path must be generated. Here, robotic filament winding is shown to be more complicated than conventional winding machinery. Unlike modern winding machines which can provide a similar number of degrees of freedom, a robot is not primarily designed for the winding process. This can be seen by the fact that the calculated motions would lead the robot to crash with itself. That is why vertical and yaw motions are usually not considered in LVV's programs to force the robot to execute simpler movements with less danger of crashing. Also, these complex curves usually consume more time which makes the process less efficient.

Another issue that is worth mentioning in robotic winding, is the necessity to test the complete winding program for possible errors, particularly collisions with the mandrel, the floor, or the robot itself. In a self-built filament winding setup, the separate components need to be adapted to work together. The filament winding software provides solely the location where the TCP has to move alongside the winding path depending on preferences such as a safety distance or a defined area around the mandrel. When teaching these points to the robot, the movements must be checked for feasibility. Only after a trial at slow speed, the actual planned process speed can be tested (if possible). The winding axis at LVV for example is built for positioning and not for winding purposes. This leads to error messages in the testing phase because the planned acceleration cannot be reached.

In robotics, various coordinate systems are recommended to operate the robot efficiently. The main coordinate system is called 'world' and is commonly based in the center point of the robot (called 'robroot' with KUKA). Referring to this system, coordinate systems for tools and bases can (and should) be taught. By that, the robot knows the location and orientation of the tool center point and a characteristic point of

the basis one wants to work with, e.g., the center of a chuck. The filament winding software usually lays its coordinate system in the center of the mandrel (depending on the model). Figure 22 shows the used coordinate systems for the given winding equipment.

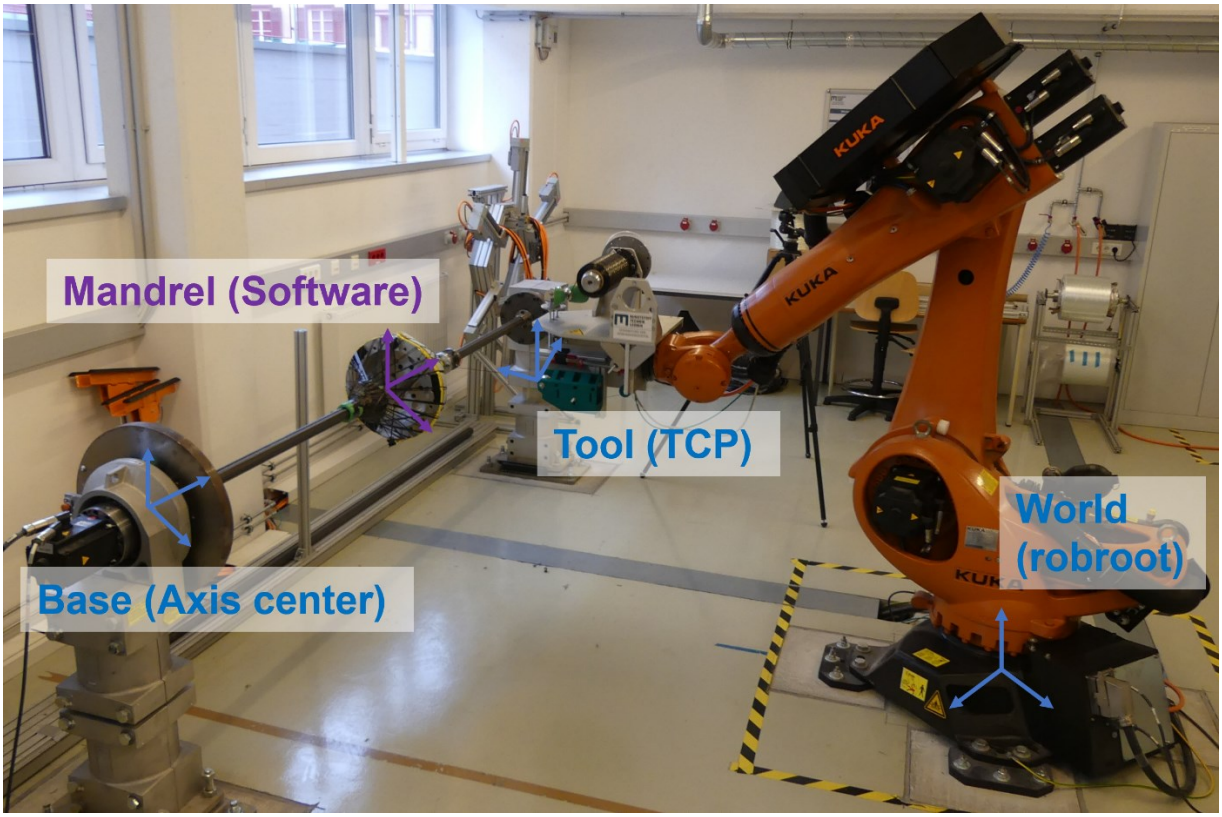

Figure 22: Different coordinate systems in the winding process

While the transformation between the robot's coordinate systems is calculated automatically by the robot control when a new tool/base is programmed, the transformation to the winding software's system must be done by the user. The most practical solution was to note the robot's coordinates at the starting position that is fixed in CADWIND. New coordinates in the adapted system can then simply be calculated in a spreadsheet editor. Alternatively, the mandrel design file could be altered with an offset. However, this would be impractical and less clear. Also, programming the new coordinates in the robot's programming language KRL (KUKA robotic language) is not practical due to the lack of suitable commands for the calculation and the danger of introducing a higher susceptibility to errors.

Once the robot program is created successfully and uploaded to the robot control, the movement along the desired winding path can be executed. Yet, for a complete process design other parameters have to be monitored and controlled. As indicated in Figure 19, a PLC (Beckhoff Automation GmbH & Co. KG, Verl, Germany), was installed as the main ‘controller’ for the overall process control and especially the monitoring of safety devices. The robot and the distributor on the winding head act as ‘devices’. While the distributor is connected to the PLC in real-time via EtherCAT (fieldbus system by Beckhoff), the robot communicates via an EtherCAT bridge terminal. The PLC, the robot, and the user interface (LabVIEW, National Instruments Corporation, Austin, Texas, U.S.) exchange data cyclically. Three arrays with Boolean, 16-bit, and 32-bit data are exchanged. The PLC’s cycle time usually is 10 ms. Communication with the graphical user interface (GUI) can lag though because LabVIEW on Windows operating systems is not real-time compatible without Add-ons. This cyclic data exchange allows the user to control and monitor all relevant parameters on a control computer via a GUI, which is depicted in Figure 23.

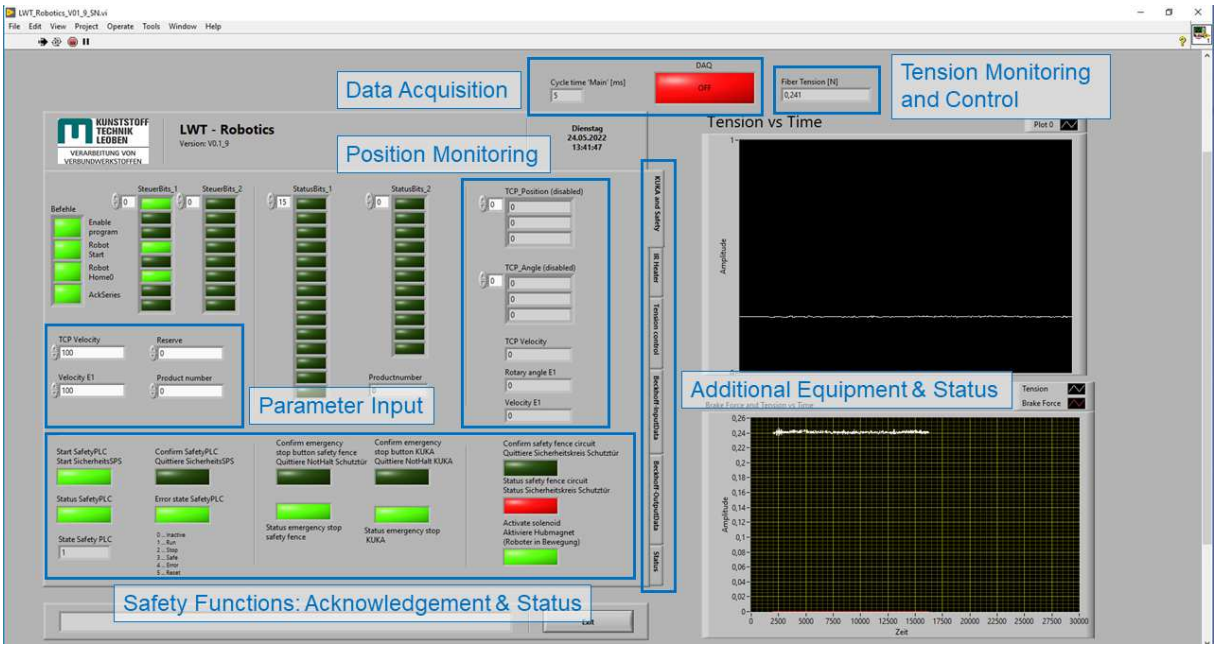

Figure 23: Filament winding GUI in LabVIEW

The primary purpose of this interface is the status display and acknowledgment of the various safety features, e.g., the safety PLC components, the security fence and gate, and the emergency buttons. The robot’s position can be displayed as well as the

velocity can be predefined. Additional features were implemented with the development of the winding head. Two diagrams show the current values of the roving tension, respectively the brake control. The tension data can be stored at the touch of a button. With increasing data volume, the storing process requires more resources and hence slows the cycle time of the ‘main’-process. To track this behavior an additional display is placed. Besides this main tab, others are created for additional functions and to track the status of the communication and the values of the data arrays that are exchanged. In the ‘tension control’ tab, the brake force can be changed manually, or a PID controller can be started. The ‘IR heater’ tab can trigger infrared heating lamps and set their output level. Generally, it can be stated that this system is open to the implementation of additional sensor and control equipment and that it can be adapted very individually with data access on almost every level.

3.3 EXPERIMENTS ON THE FRICTION COEFFICIENT

One major drawback of dry rovings compared to impregnated ones is that their friction coefficient is significantly lower. Possible winding pattern and hence design freedom is reduced. Binder material applied to the dry rovings can, after activation, raise the friction coefficient again. In this section, experiments based on the work in [99,100,102] were performed. The goals were the comparison between bindered and unbindered rovings, the validation that velocity and tension have no influence on the coefficient, and the investigation of the effect of binder activation.

Figure 24 shows the experimental setup. The mandrel is mounted on a lathe chuck on the winding axis. A measuring tape is placed behind it for reference. The winding head mounted on the robot is moved parallel to the upper surface of the mandrel at a fixed distance. A camera films the whole experiment. Depending on the respective setup, a binder or reference roving is mounted on the expansion shaft, and the pneumatic brake is adjusted. The standard configuration of the brake was 10 % of the maximal force which led to a force of 15 N +/- 5 N on the roving. Experiments with different tension levels had the values of 5 %, resp. 5 N +/- 3 N (low tension) and 20 %, resp. 32 N +/- 5 N (high tension). In the experiments where the binder should be activated, a heat gun is placed under the roving to activate the binder on the lower side before it touches

the mandrel. Additionally, for experiments with a heated mandrel, the mandrel was kept in an oven at 130 °C for at least one hour. After the binder is adherend to the mandrel an additional cleaning step was necessary to prepare the mandrel. A mold cleaner was applied to remove the binder and isopropanol to degrease the mandrel afterward.

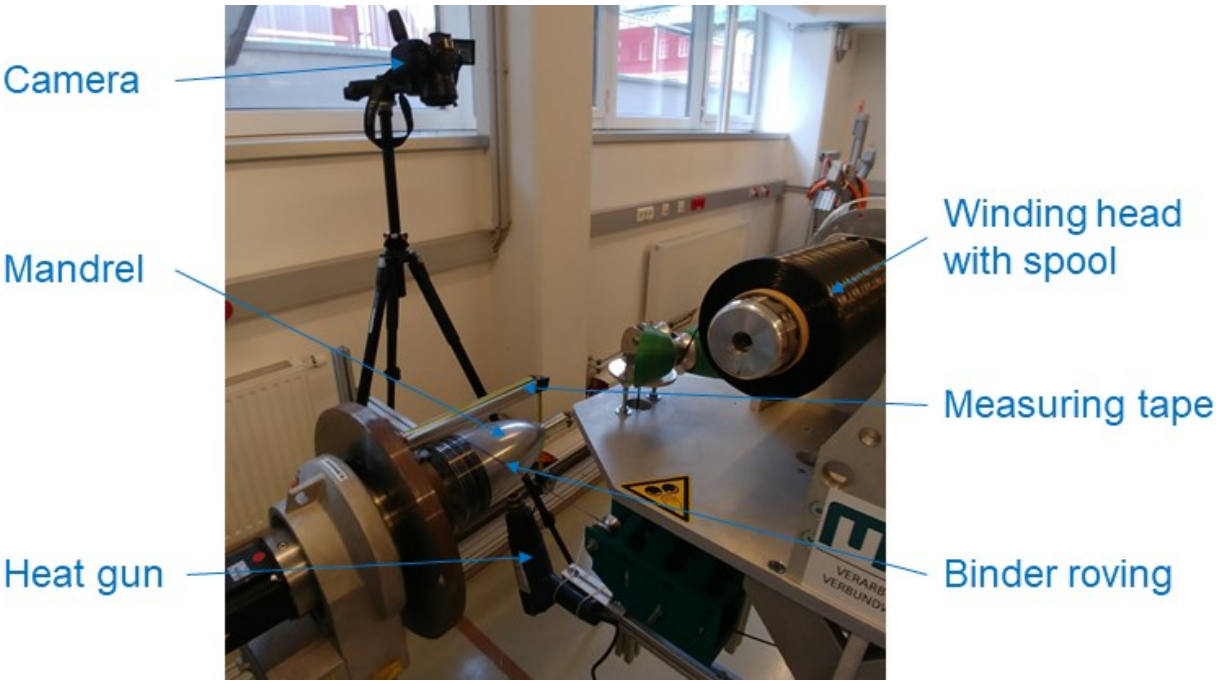

Figure 24: Determination of the friction coefficient experimental setup

The exponential function of the mandrel surface given in Figure 17 a) allows the determination of the friction coefficient by the carriage of the machine, here the robot. Different methods can be used to specify the exact carriage position when the roving slips. Recording of a drop in friction force as well as optical evaluation, e.g., by the reference measuring tape, can be executed. In these experiments, the determination via video proved to be most practical and accurate. By tracking the times when the roving passes the cylindrical area until it catastrophically slips and multiplying this time with the carriage velocity, the covered distance is calculated. This is also marked in Figure 26. As previously mentioned, the radius of the mandrel at the point of slippage can then be calculated, and by that the coefficient of friction between zero and one (resp. the percentage).

In the first experimental series, the untreated rovings were examined. The green bars in Figure 25 show the results. It can be seen that the values are all around the value of 0.25. This has already been tested in [102] and it lies between the reported values in the literature for dry CF winding (0.33 in [99], 0.15 in [100]). Similarly, the chosen modifications of speed and roving tension show no significant effect.

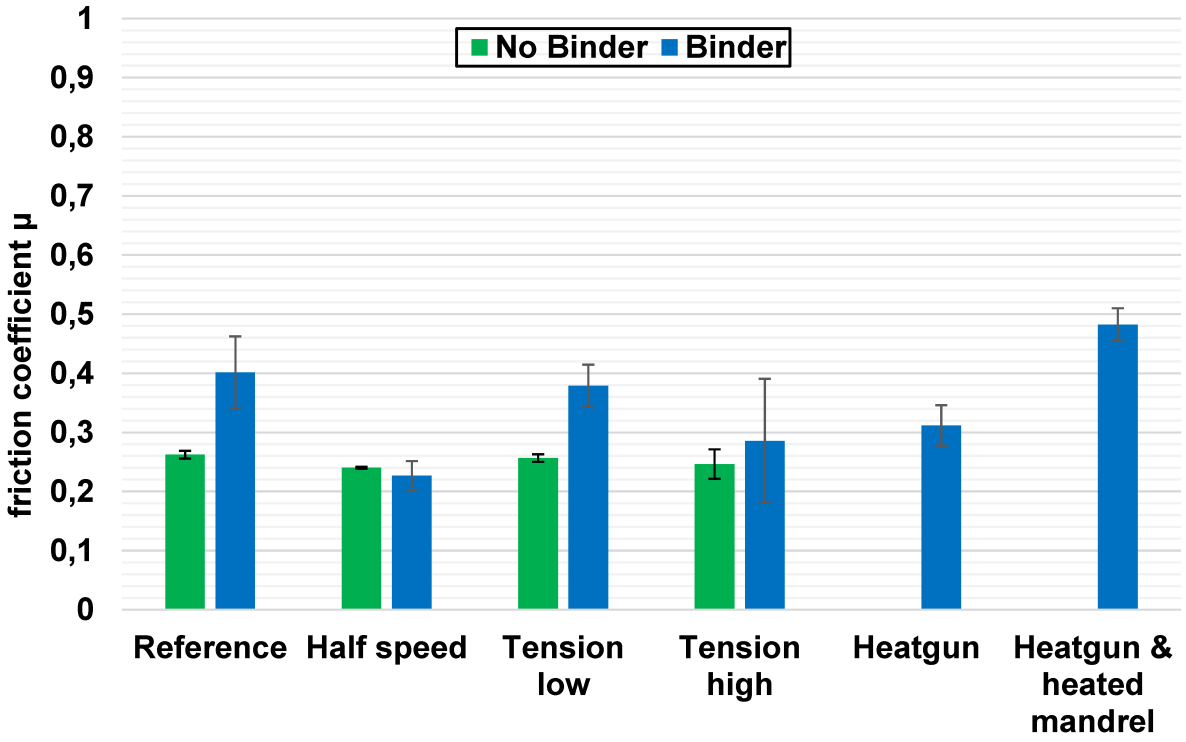

Figure 25: Results of the friction coefficient experiments for binder and untreated rovings

A more versatile result can be observed for the experiments of binder rovings. Trials with the reference configuration already show a significant increase in the friction coefficient to 0.4. Yet, the standard deviation also rises strongly. Reducing the speed leads to results comparable to those of the rovings without binder. The rougher surface and the more uniform width cause a higher friction of the binder rovings on the mandrel surface. At reduced speed, the rovings slip due to inaccuracies in the laydown and the resulting spreading of the previously laid roving. This behavior is similar to the rovings without binder.

Contrary to the velocity, the roving tension still has no significant effect on the friction coefficient. For high tension the coefficient is reduced but with a high standard

deviation. Experiments with high tension are more susceptible to inaccuracies in the laydown which could lead to slippage. On the other hand, the tension keeps the roving deposition stable. In [102], the roving spool was only braked to avoid running the spool after a tension loss. There, the friction coefficient was negligibly low because of the pre-tension of the wound-up roving.

While the experiments with binder rovings at room temperature were only for comparison, the interesting results arise from those experiments with activated binder. Lacking a heated mandrel, the activation of the binder proved to be difficult. When trying to heat the mandrel with a heat gun, melting of the binder particles could be observed. But as soon as the roving touches the mandrel surface it cools down and the binder loses its adhesive properties. The resulting coefficient in Figure 25 is even slightly lower than the reference coefficient. This can be attributed to the softening of the roving which can facilitate spreading behavior.

To overcome the lack of mandrel heating, it was pre-heated in an oven at 130 °C so that a sufficient binder activation temperature (~120 °C) during the experiments could be guaranteed. The heat gun was used to also ensure that the binder was activated before coming into contact with the mandrel. With the binder activated, the friction coefficient could be raised to 0.48. This significantly increases the range of possible designs. Yet, the raise is not as high as for tackifier sprays (which have other disadvantages though) [102].

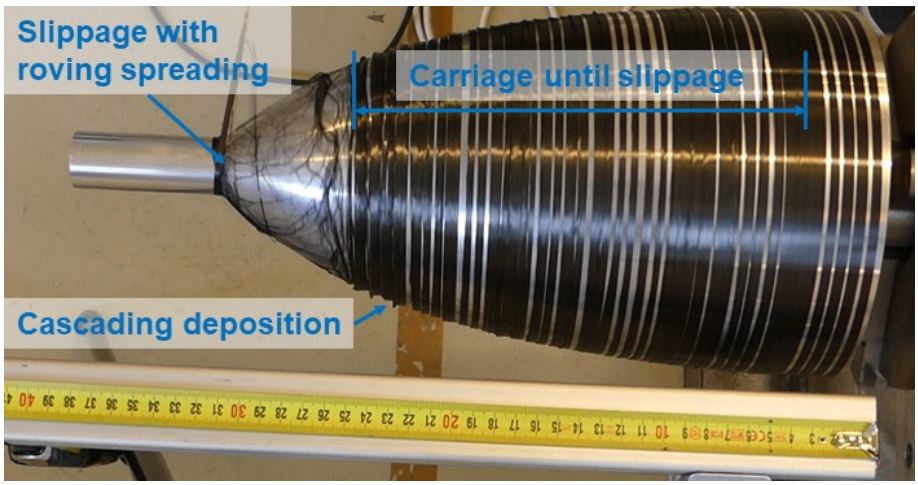

Figure 26: Roving slippage in an experiment with a heated mandrel and heat gun

Figure 26 shows the reason for the earlier slippage of binder rovings. Unlike a spray, the binder material is just applied to the roving. Under tension, it is still relatively stiff. This leads to a steplike deposition of the roving in the area of the mandrel with a high curvature. These steps can easily be touched and torn off by the following deposition turn. Activated binder softens the roving's inner cohesion which makes it more susceptible to being spread and ripped off by axial force.

3.4 WINDING ON A CONICAL MANDREL

As a demonstrator with practical application, a conical structure planned as an aircraft turbine nosecone should be wound with robotic dry filament winding. With this being part of a project, only the insights considering the process and its pros and cons will be presented here. In these trials, experience in handling dry rovings should be generated. Binder was not used in order to neglect its influence on the resin infusion and to reduce setup complexity, i.e., no heating devices. Path and process design as well as the overall setup were adapted to produce the part in a two-step process consisting of dry filament winding and an infusion process.

3.4.1 MANDREL AND PATH DESIGN

A conical mandrel comes with specific challenges for the filament winding process. Geodesic paths are commonly the chosen winding pattern [37,209]. Deviations require a certain friction between roving and surface or auxiliary pins. Also, the wound layers on a cone usually thicken the shell on the tip disproportionally without changing the paths non-geodetically [210]. Figure 27 shows a comparison of three different mandrel types generated in CADWIND, namely a cone, a pressure vessel, and a sphere. The color scheme shows how much the chosen winding paths deviate from the geodesic path, i.e., how much friction force is required. While for the pressure vessel, the danger of slippage is only present in the turning zones, it is apparent on almost the whole surface of the cone. The sphere shows a more colorful scheme, meaning that the geodesic behavior changes drastically locally. In this case, the geodesic path is a great circle. Hence, small deviations are required which lead to this ununiform picture.

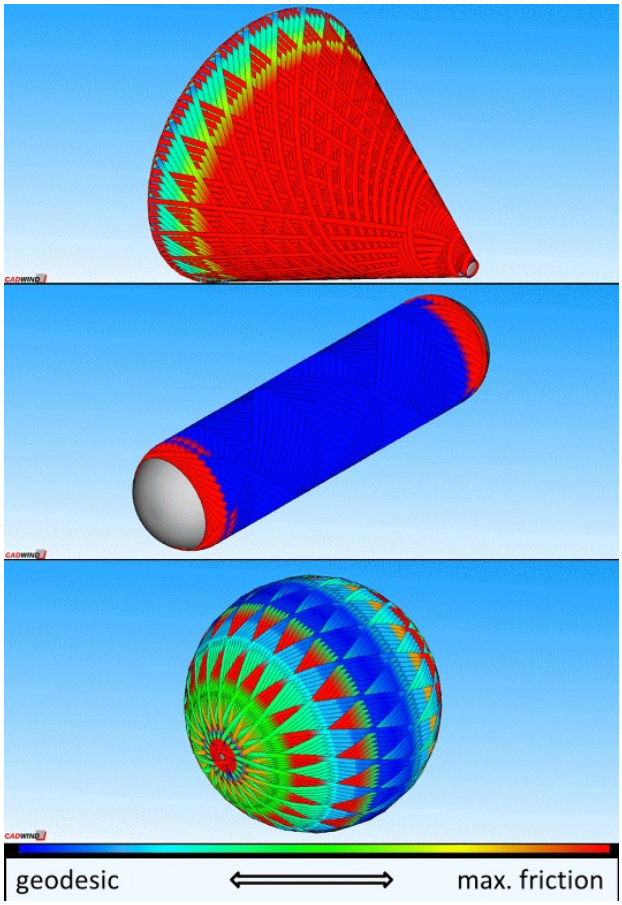

Figure 27: Exemplary winding patterns of a cone, pressure vessel, and sphere. Color scheme showing the degree of deviation from the geodesic path. [47]

Finding a winding path on a cone with a reasonable friction factor for dry winding proved to be not feasible. Additionally, pre-trials with sprayed tackifier showed that raising the friction in this manner leads to a bad winding result and makes demolding of the preform almost impossible.

To overcome this situation, the concept of a double-sided cone was selected. This patented method is already used in the production of turbine nose cones [210,211]. A major benefit of this tooling concept is the possibility to produce two preforms at the same time. At LVV the double-mandrel is only used in the simulation. In the process, a regular cone was used while on the other side, a 3d-printed shell was produced to provide a turning zone. Figure 28 shows the simulation result of various parameters of this mandrel in CADWIND. A friction factor of 0.2 was used which works well with dry rovings. Nevertheless, as Figure 28 a) shows, the deviation from the geodesic path is high all over the mandrel. This means that the risk of slippage is still high.

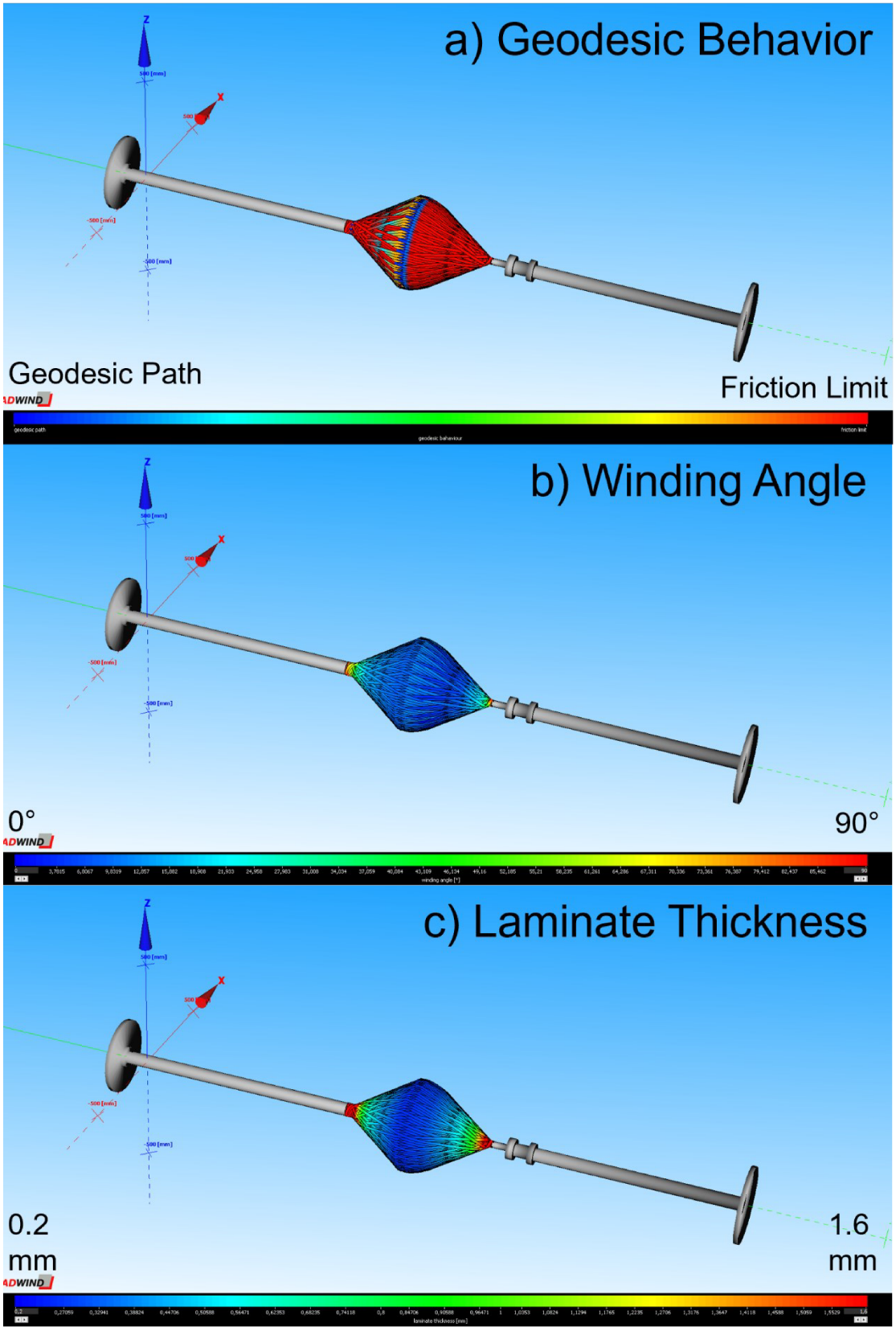

Figure 28: Color schematic of different winding aspects in CADWIND: a) geodesic behavior, b) winding angle, c) laminate thickness

The used countermeasures are described in the next Section 3.4.2. Figure 28 b) shows the distribution of the winding angle. While it is close to zero in the middle, it becomes maximal, i.e., 90°, at the turning zones. Both extreme cases can lead to challenges in processing. The last image Figure 28 c) gives an indication of the thickness distribution of the laminate. It varies between 0.2 mm for a single layer and 1.6 mm at the ends, i.e., the thickness increases eightfold.

This setup provides feasible winding patterns for the given machinery with full coverage of the mandrel after a second iteration. Drawbacks are the thickening at the tip and the material waste on the coreless side of the ‘double’-mandrel.

3.4.2 PROCESS CONTROL

During the dry fiber filament winding trials, a couple of observations could be made. Some of them are general filament winding issues, some others can be attributed to dry fiber winding. Figure 29 shows the three main categories of challenges that could be identified. In the following, they will be explained in greater detail and solution approaches will be presented.

a. Tension loss b. Fiber damage c. Layup errors

Figure 29: Typical winding errors in dry fiber filament winding

a. Tension loss

Many winding patterns and the respective machine movements calculated in the simulation could not be executed due to a tension loss of the roving. It then sags and the positioning of the roving after the tension is reestablished is not reliable anymore. This problem has several reasons rooted in the winding equipment at LVV. To begin with, the winding software does not address this issue. The calculated machine movements may lead to sagging of the roving and must be tested every time. Also, the

coordination between the robot and the simulated path needs to be optimized. A reduction of considered axes and the consequent reduction of degrees of freedom facilitates the selection of a suitable machine motion. Apart from the ineligible machine motions, tension control needs to be discussed. In the given setup, the roving tension is controlled by a pneumatic brake, i.e., a pre-tensioning must always be given. An active backward motion by a motorized control could not only enable more motions but also increase the control effort and the overall machinery cost. To compensate for small movements of a few centimeters, a tensioning unit, similar to a dancer mechanism, is installed. Figure 30 g) shows the guiding roll mounted on a linear axis pre-tensioned by a spring. With this unit, small movements can be compensated without losing the pre-tensioning.

b. Fiber damage

The fiber guidance is the main source of damage to the rovings. In early versions of the winding head, polymeric and ceramic eyelets were used. If the rovings were slightly damaged or fraying before, these guiding units amplified this and collected fiber material. Hence, the tension rises significantly, and ultimately the roving ruptures. To overcome this, all guiding units were replaced by rolls. They still collect some of the frayed fibers, but the damage amplification is minimized as well as the danger of rupture. Yet, sharp edges, e.g., on the mandrel, still pose a danger for roving damage. This can only be avoided by suitable winding paths and if that is not possible, then by use of auxiliary materials to cover the cutting edges.

Apart from the roving sweeping over guiding units and the mandrel in the process, it can already be damaged on the spool. It is in the nature of rovings to easily drift apart when under radial load. Not only in the production of the spools but also during handling and unwinding these forces may arise. Especially, the edges suffer from high de-spooling forces which lead to slippage and thereby damage in the underlying layer. Because of the limited space on the winding head’s surface, the first roll is relatively close to the spool and the respective roving tension is high. The rotatable pair of rolls on the winding head was lifted with two screws and 3D-printed auxiliary guiding shields were installed (see Figure 18, Figure 22, and Figure 24). With this, the angle of attack was optimized and hence the damage of the roving was reduced drastically.

c. Layup errors

Much like in the related tape-laying processes, the reliability and accuracy of the fiber deposition are crucial for the overall quality of the product. Gaps as well as overlaps should be avoided. In the case of the wound cone in Figure 29 c. small and large gaps can be observed. Overlaps are harder to determine due to the complex nature of the winding pattern and will not be regarded further at this point. In this figure, one can clearly identify one large gap and several smaller ones. The origin of the large gap is clear. Before winding, equipment for the subsequent vacuum infusion was installed. The vacuum tube leads to a local buckling where the rovings slip and leave this area blank. The exact reasons for the smaller gaps are harder to determine. Possible explanations in the cone winding trials are:

- Slippage
- Bad path calculation
- Unfitting (roving) dimensions
- Aftereffect of larger gaps

It could be observed that the simulated full coverage of the mandrel could not be achieved. This means that either the assumed (model) parameters and calculations are not accurate, or slippage occurred during the processing. A probable cause for small gaps can be found in the twisting of the rovings during fiber guidance. To reduce this change of roving width, a spreading unit was installed (see Figure 30 h). Guiding the roving over a convex-shaped roll prior to deposition leads to a more uniform thickness. Nevertheless, a complete coverage could not be reached. Therefore, a second run of the winding program was executed with a slightly modified winding angle aiming to reach full coverage. While the result improved significantly, some of the gaps remain. They can be attributed to slippage. The winding motion results in a flat deposition of the rovings on the cylindrical part of the mandrel. Here, sealant tape was placed to reduce this effect but sometimes the roving slips over the mandrel surface before it comes into contact with the tape. When this happens, the roving is fixed at a wrong position, leaving a gap at its designated position. Concludingly, it must be stated that gaps cannot be avoided totally with the given setup. Yet, with the subsequent resin

infusion process the resin flow might rearrange the filament and (partially) close the gaps.

3.4.3 HANDLING, PRE-, AND POST-PROCESSING

Besides slippage prevention, the handling of the preform is a major challenge in dry fiber winding. To overcome this issue, additional pre- and post-processing steps may be required. In the following, the preparation of the mandrel, handling, and post-processing in the winding of a cone will be presented.

A key factor for the handling is the type of mandrel. A solid mandrel can also be used during the LCM process. Thereby, it must be differentiated between mandrels that remain in the part and others that must be removed. For those mandrels, either the geometry of the part must be suitable for safe removal, the mandrel must be collapsible, or the mandrel material must be dissolvable (chemically). If the mandrel is removed before the LCM process, the handling effort increases significantly. Here, the preform has to be stabilized. This can be done either chemically by binder/tackifier materials or with additional handling devices. Whatever the choice is, it means also additional workload, time, and ultimately cost.

In the case of the conical mandrel used here, it can be demolded after the flange on the top side is removed (if the hole on the top side of the part is large enough this might not even be necessary). Consequently, the mandrel can be used during winding and LCM which simplifies the handling to a significant effect. Yet, some preparations have to be made for the resin infusion. To safely demold the mandrel, either a release agent or other release material has to be applied before winding. In the case of the later presented VAP process, this comprises of a semipermeable foil, a flow aid, vacuum tubes, and the required amount of sealant tape to make this setup vacuum-tight. For winding an imaginary double cone on a single cone mandrel, some other materials proved to be useful. Replacing the second cone, a 3D-printed structure is mounted on the spline shaft to enable to correct turnaround of the rovings in the turning zone. Due to the slippage risk in the area with the largest diameter, some sealant tape was also applied to the edge of the mandrel to fix the rovings there. For the later removal of the second half of the preform from the unused side, a metal stripe was laid on the

cylindrical part of the mandrel to be able to cut with a utility knife. Figure 30 shows the so-prepared mandrel right before the start of the winding process.

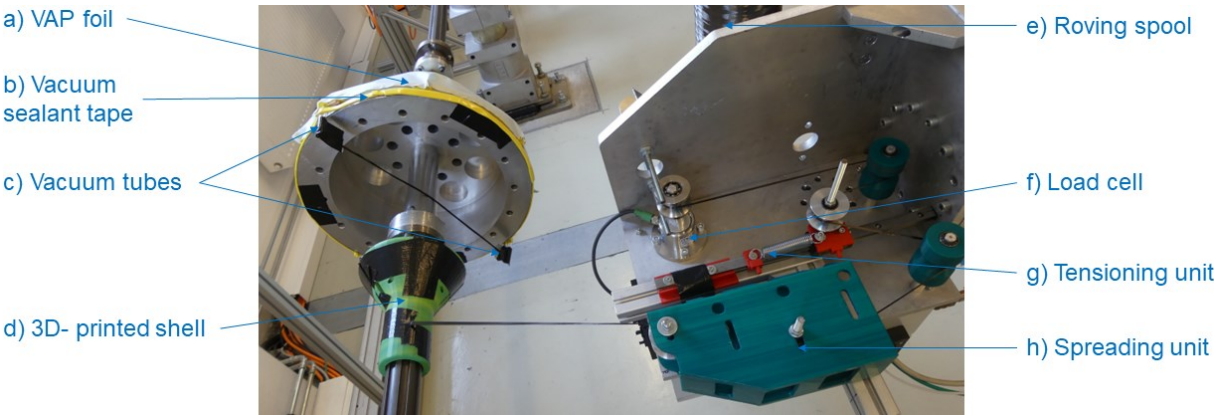

Figure 30: Starting position for dry winding trials. Mandrel prepared for subsequent VAP process.

After finishing the winding, the mandrel needs to be further prepared for the resin infusion. First, the rovings on the unused side have to be removed to be able to demount it. The rovings cannot easily be cut without destroying the preform. Therefore, a hose clamp is tightened on the mandrel's cylindrical part to keep the cut rovings in place. The rovings must be cut so that the vacuum setup will fit on the outside of the mandrel. After cutting, the mandrel can be demounted and transported to the LCM workplace.

3.4.4 VACUUM INFUSION

Due to the size of the part and less (specific) equipment needed, a vacuum infusion process was preferred over a vacuum injection process, such as RTM. In pretrials, simple VARIs were set up directly on the winding axis. None of them produced satisfactory results. The mandrel would have to be rotated during the infusion to avoid resin accumulations which is not possible with the vacuum tubes.

After removing the mandrel and placing it in a three-jaw chuck, a vacuum bag was applied. Here, both infusions from the bottom and the top failed to deliver satisfactory results. When applying vacuum against the incline of the cone, the preform closed at some point in the middle. This results in a poor vacuum on the broader side of the cone and consequently a bad resin flow. When applying the vacuum on the broad side and setting up the infusion at the top, the mold gets fully filled. Yet, the thickened part at

the top was not completely filled. This area of the preform is so densely packed that the resin will flow predominantly over the surface and back into the resin trap instead of impregnating through-thickness.

To overcome this issue, a through-thickness impregnation approach was chosen. The ‘vacuum assisted process’ (VAP) is a patented process with a semipermeable foil that allows airflow but no resin flow [212].

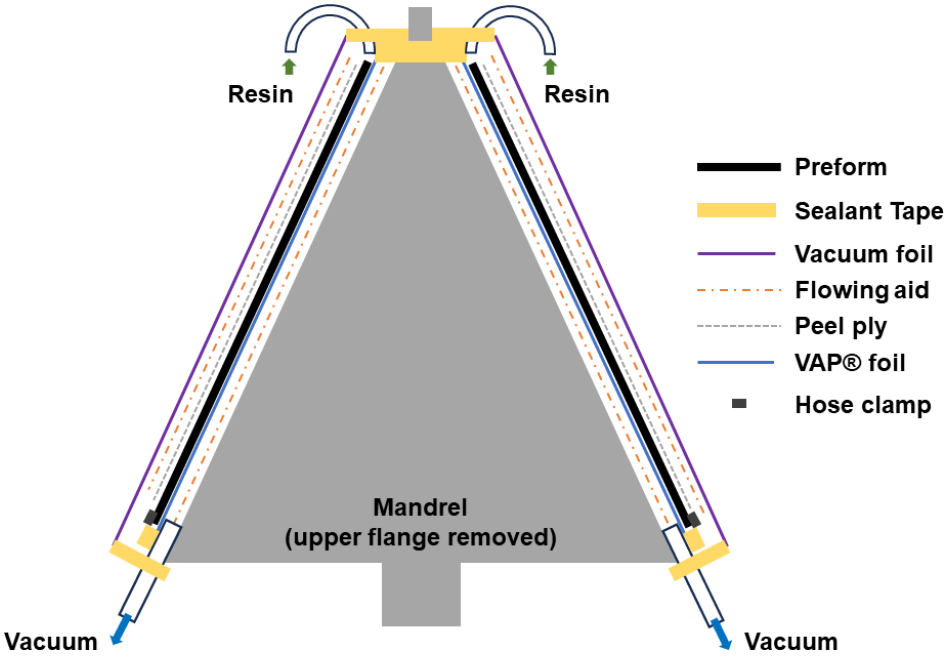

Figure 31: Schematic of the vacuum infusion of a conical preform

As described in the previous section, the VAP membrane was applied and sealed before the winding process. For better air distribution, a flowing aid was put underneath. Vacuum tubes were also already installed. Figure 31 shows a schematic of the complete resin infusion setup. To prepare the wound preform for infusion, a ‘classical’ VARI setup was placed on top. This means a peel-ply layer for the removal of the auxiliaries, a flow aid for the resin distribution, and finally the vacuum foil. A lot of effort has to be put into the proper sealing of this setup. When a good vacuum quality is achieved the infusion can start. The VAP membrane provides a vacuum all over the mandrel’s surface while the resin is distributed on the top. Through-thickness impregnation proved to deliver full filling and good part quality of the conical mandrel in general.

Figure 32: Result of VAP-infusion of dry-wound nosecone

The demolded nosecone is shown in Figure 32. A thickening at the top is clearly visible as well as the pattern of the rovings on the surface. Yet, regarding the missing postprocessing and the circumstances in manufacturing, this part can be seen as a good demonstrator.

3.5 SUMMARY: ROBOTIC DRY FIBER WINDING EXPERIMENTS

In the experiments on the friction coefficient, literature values could be validated, and new values for binder rovings were introduced. The carriage velocity can have an influence on the measurement of the friction coefficient. For low velocities, the possibility of a roving to spread and to be ripped off by the upcoming turn increases. Activating the binder has a significant effect on the friction but not as much as possibly hoped for when looking at the adhesive properties of the material. In this context, it should be noted that this test setup with its curved mandrel is prone to minimal deposition errors (i.e., twists, width changes) which lead to a spreading of the roving. Nevertheless, such a complex-shaped mandrel represents the desired freedom of design which is the main (intended) benefit of dry winding process design.

Trials to wind and infuse a conical mandrel showed up some challenges in dry winding. A better understanding could be generated of what the specific requirements are for this type of process and how to deal with them. The two major factors are slippage prevention and handling during the process. Both are affected by various process parameters, given equipment, and the design of the desired part. In the case of the cone wound in these trials, the issues could be managed to various degrees and a part of good quality could be produced. It can be stated that the process is feasible in many cases, but the process(es) has to be well planned and executed.

4. AUTOMATED ROVING INSPECTION IN DRY WINDING

This chapter is based on the publications [213,214]. The algorithm developed there is presented briefly and then validated for the usage of binder rovings in dry fiber filament winding.

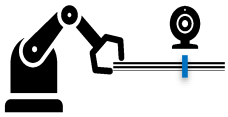

Modern filament winding machines are often part of a highly automated manufacturing line. Many aspects of a production process are covered by the term automation such as process monitoring and control, sensors, data recording, and handling tasks. The robotic filament winding equipment at LVV with its PLC implementation already gives the opportunity to customize the process control. Moreover, this system allows sophisticated movements of the robot and has a complex control architecture. For this reason, an existing test rig for the investigation of roving properties was adopted. This rig allows the testing of various sensors and (control) setups while continuously winding a roving or similar types of material, e.g., tape.

As mentioned previously, process control is gaining more attention also in filament winding. In the frame of this thesis, a special kind of sensor for the profile measurement of a roving will be tested: the laser light sectioning sensor ((L)LSS) or just profile sensor. It works on the principle of laser light triangulation and provides the height profile of the specimen at a certain time instance. This type of sensor has already been used in the (gap/overlap) control of ATP/AFP processes [151,159,160,215], for rovings [161,162], in DFP [216], and even in preforming [152,158]. Here, the usability of binder rovings in winding shall be evaluated. An already developed algorithm [213,214] will be used to examine various configurations and to determine the best recording parameters on the roving test rig. After an introduction to the test rig, the sensors, and their programming, the used algorithm will be presented. In the experimental section of this chapter, rovings with and without binder will be measured and compared. Various process parameters and modifications will be tested.

4.1 ROVING TEST RIG SETUP AND CONFIGURATION

4.1.1 ROVING TEST RIG SETUP

The roving test rig presented here has been built for the examination of the impregnation behavior of a single roving.

It was designed with two rotatable axes and one linear axis to be able to unwind and wind a roving on a spool. This basic concept is well-suited for the testing of various sensor types. In its original setup, a rotary encoder and a tension sensor were already installed. Various adaptations have been made for the investigation of binder deposition and the winding of spherical mandrels. This can be seen in the picture of the test rig in Figure 33.

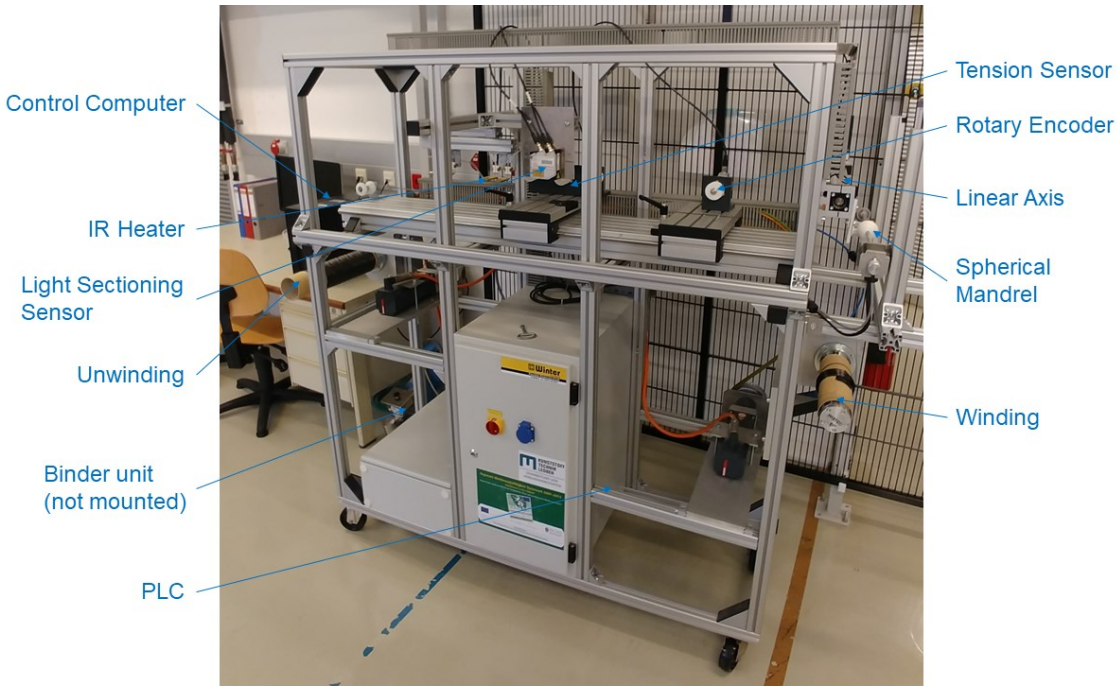

Figure 33: Roving test rig at LVV

The experiments conducted here require the winding and unwinding axes, the light sectioning sensor, the control units, and the IR heaters to activate the binder.

The roving spool is put on the pneumatic expansion shaft on the unwinding side. Controlling the tension of two coupled axes in this case is not helpful. The two motors used are too powerful for effective control. That is why the roving tension is solely given

by the force required to unwind it from the spool (in some of the experiments a brake force is put on the spool). The light sectioning sensor is mounted in the middle of the test rig with a distance of about 66 mm to the roving, depending on the background material. Four infrared heating elements with a total power of 1 kW are placed between the unwinding unit and the sensor to heat the upper side of the roving. A guiding eyelet mounted on the linear axis ensures the positioning of the roving in the middle. On the winding side, an empty paper spool is fixated on the pneumatic expansion shaft. After pulling it through the guiding elements, the roving is attached there. Other equipment from the figure is not used here. A bungee cord for braking the unwinding spool, a screwdriver for splitting the roving, and various plates as background materials were used in the respective experiments.

4.1.2 PLC PROGRAMMING & EXPERIMENTAL PROCEDURE

Before measuring the rovings, a program has to be written and a user interface has to be created. Though process development aims for inline monitoring during the robotic filament winding process, this task will be examined on the test rig in this study. Two reasons for that can be given. First, changes in machine setup and programming of a working machine can lead to problems with existing programs. In the second place, the effort to mount the sensor and the complexity of the machine movements are drastically reduced when working with an almost linear movement of the roving. Nevertheless, such things as background inclination, roughness, reflectivity, or deflection can be considered. Another issue worth mentioning here is that the given setup is not real-time capable which would be essential for inline monitoring. The currently given hard- and software setup of the sensor does not support this. That is why the data is first recorded and then evaluated in MATLAB (The MathWorks Inc., Natick, US-MA). It can be stated that the experiments performed on the test rig represent a realistic industrial environment and the test of the capability of the sensor for measuring binder rovings is legit. To fully implement an inline control system further equipment modification and installation steps are required. But this does not diminish the results of the tests conducted here.

As a first step to set up the experiments, the required equipment has to be wired to the PLC and configured. The PLC and the control software TwinCAT3 are provided by

Beckhoff Automation GmbH (Verl, Germany). Table 3 shows the used components and the respective communication with the PLC. As explained above, only one of the rotary axes is utilized to wind the roving. This axis has its own servo controller unit and is referred to as a motor unit to the PLC with its (Beckhoff-)specific data type ‘AXIS_REF’. The linear axis ensures that the roving is placed in the middle of the pathway. It also provides the option to move the roving radially which is not used in the experiments here. The linear axis is connected to a motor which is wired to a servo motor terminal. The same datatype as the one used for the radial axis is used here.

Table 3: Components of the rovings test rig and their PLC reference used in the LSS experiments

	Communication with PLC	**Number (in use)**	**Data type in PLC**
Motor (rot. axes)	Servo drive	2 (1)	AXIS_REF
Motor (lin. axis)	Terminal for servo motor	1	AXIS_REF
Limit switches	Digital in	2 (1)	BOOL
Expansion shafts	Digital out	2 (1)	BOOL
Power controller IR	Analog out	2	REAL/UINT
Power supply LSS	Digital out	1	BOOL

Two limit switches are mounted on the linear axis to restrict the travel range of the sliding carriage. Due to the fixed position in the mid, only one of those switches is needed for the initial ‘homing’ step. A Boolean signal is sent to the PLC if the switch is reached by the metallic carriage. The pneumatic expansion shaft to span the cardboard spool is also controlled with a Boolean command from the PLC. Power for the IR heater has to be set by an analog value. For the user interface, the data type has to be transformed in the program from ‘REAL’ to an unsigned integer value. The power supply of the light sectioning sensor is connected to a ‘digital out’ terminal with 24 VDC to be able to switch it on and off via the program.

Figure 34 shows the so programmed graphical user interface for the experiments. Hereafter, the experimental procedure is explained via these controls and the

underlying simple finite state machine (FSM) of the ‘main’ program which is depicted in Figure 35. It should be noted that this configuration is the bare minimum to get the experiments done and principal functions such as error-handling and safety features are not considered here.

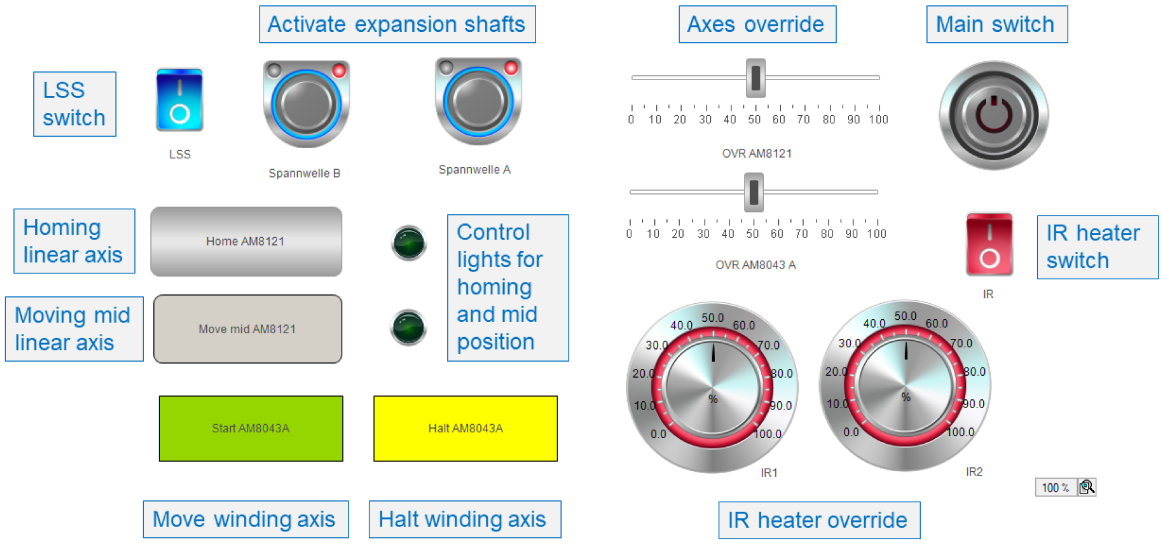

Figure 34: GUI for winding experiments with light sectioning sensor

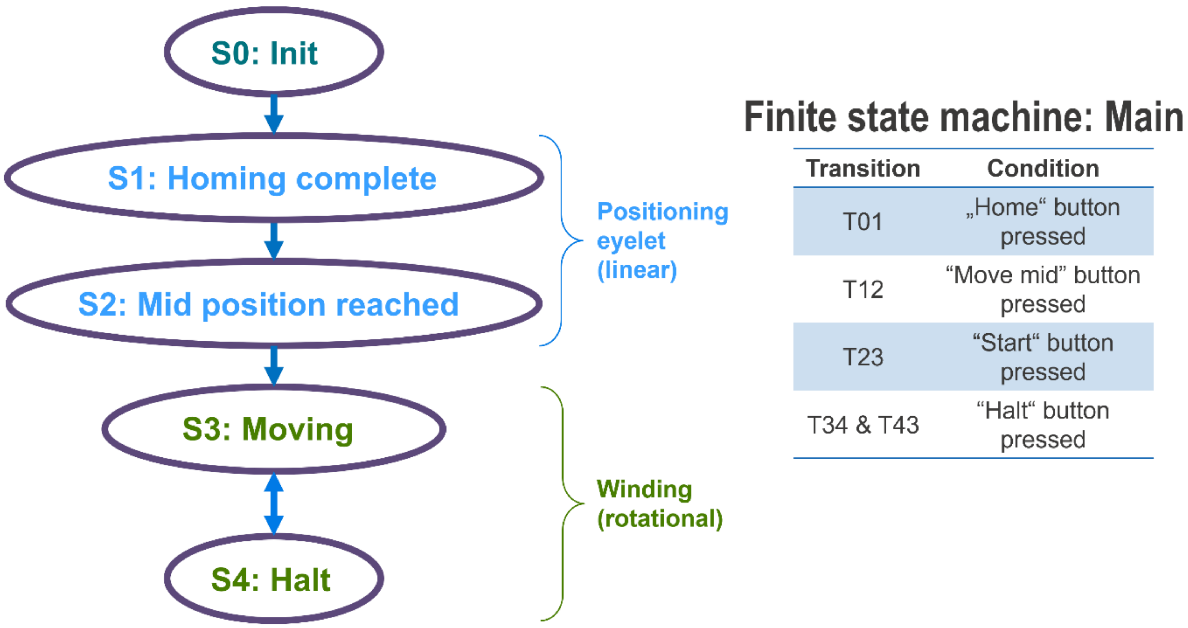

Figure 35: Finite state machine of the 'main'-program on the roving test rig

Some preparational steps have to be executed to be able to wind the roving. The main switch on the GUI provides an ‘enable’ signal to the PLC and the motors. It also functions as (emergency) stop button. Two slider bars allow the user to set the axes’ override in percent. The finite state machine is in the ‘initial’ state. Before the linear axis can be used (after starting the PLC) it needs to be homed to be able to determine the actual position of the guiding eyelet. Therefore, after pushing the respective button, the sliding carriage is moved toward one of the limit switches. When this switch recognizes the slider, a signal is given to the PLC that the homing is complete, and a green light is displayed in the GUI. This is the second state of the FSM. The next transition condition is given by pressing the button to move the sliding carriage to the mid position. This is also marked with a green light in the GUI and represents the next state. Prior to starting the winding, the expansion shaft of the winding axis has to be activated and the light sectioning sensor has to be turned on. The switches in the GUI trigger the respective output channels. States three or four of the finite state machine are active after either the ‘start’ or the ‘halt’ button is pressed. With that, it is possible to pause the winding. For the experiments with binder activation, the GUI provides a switch and two rotary power controls for two IR lamps each.

After referential experiments with three different exposure times of the unbindered roving, the binder roving was used. As a key parameter for the sensor setup, all possible exposure times available in the sensor control software were tested for usability. With the so-determined preferred exposure time, the experiments on all other parameters were conducted. These parameters were variations of the background, the brake force (tension), winding velocity, twist of the roving, splitting of the roving, and activation of the binder.

4.2 ROVING PROFILE CHARACTERIZATION WITH LASER LIGHT SECTIONING

4.2.1 LASER LIGHT SECTIONING SENSOR

The laser light sectioning sensor used in the experiments is labeled scanCONTROL 2900-25/BL by Micro-Epsilon Messtechnik GmbH & Co. KG (Ortenburg, Germany). It is built with blue laser light which has a wavelength of 405 nm. Blue laser light has a shorter wavelength than red laser light. With less intensity and penetration depth, it causes less noise and increases accuracy. It is especially recommended for transparent material or reflective surfaces. [217,218]

Although this sensor type was purchased in particular for glass fibers, it is expected that the blue light also shows some benefits when dealing with a carbon surface covered with polymeric binder powder. Figure 36 shows the sensor and its blue laser line measuring a roving on a black background plate.

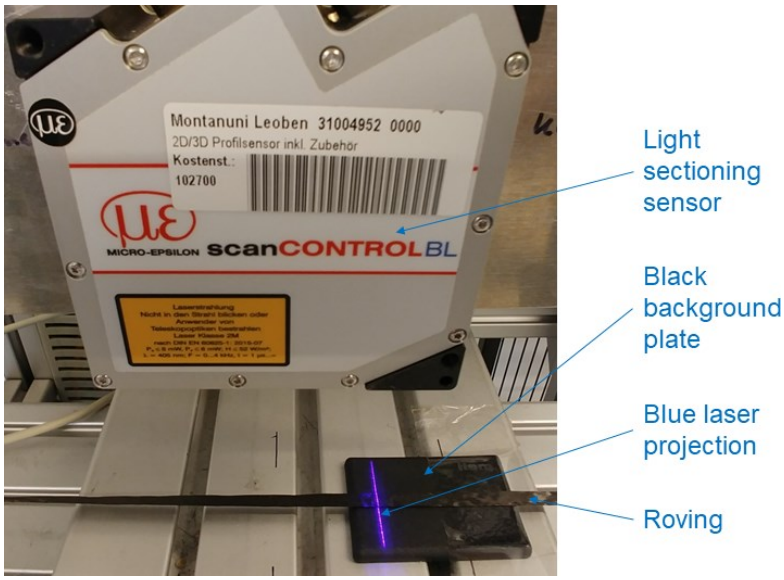

Figure 36: The light sectioning sensor (LSS) used on the roving test rig with a black background plate

4.2.2 ALGORITHM FOR PROFILE DETECTION

As mentioned at the top of this chapter, the algorithm presented hereafter is based on a bachelor thesis/conference contribution [214] and the respective extended research

journal paper [213]. Only the key aspects will be presented here. For further information, the reader is referred to these publications.

The main program is executed as a ‘live script’ in MATLAB where it calls many subroutines and toolboxes. This way, the code can be clearer, and the figures will be displayed fast and are easy to check. The overall structure of the program is displayed in Figure 37. It shows the three main steps before the analysis regarding the (filament winding) process parameters can be started. First, the datasets have to be converted into the right format and unnecessary data can be removed to make the code more efficient. After that, the data points representing the roving have to be distinguished from the background baseline. With this knowledge, the data can be separated to make the following computations possible or at least more effective and accurate.

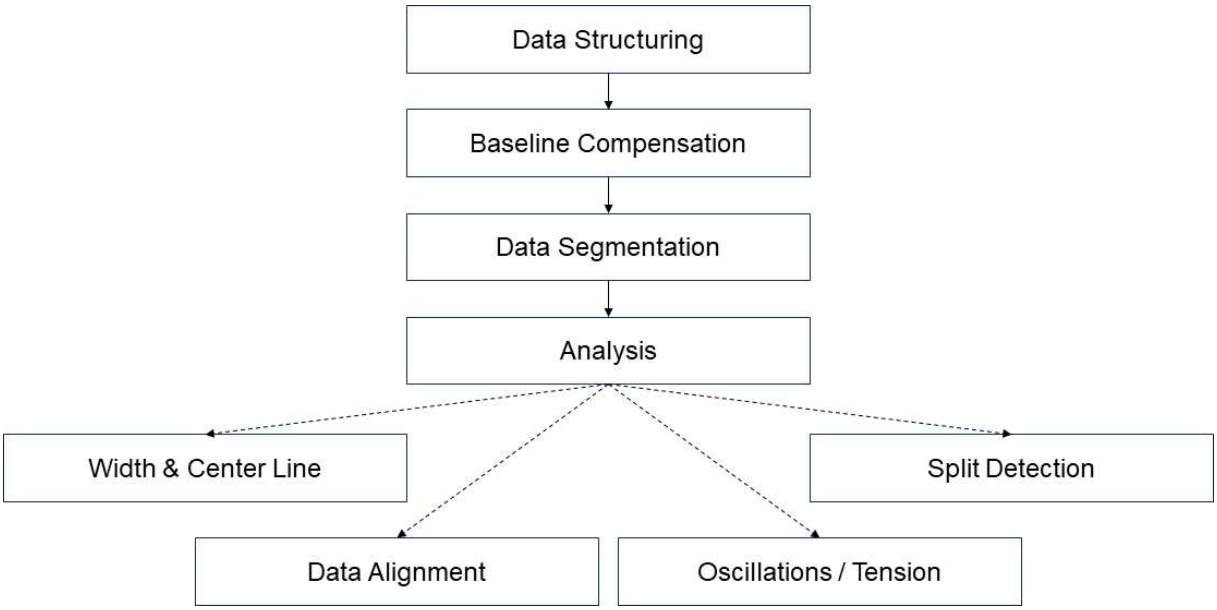

Figure 37: Structure of the profile detection algorithm

Data structuring

The selected output format from the sensor’s software is a ‘csv’-table (comma-separated value). Data is structured in three blocks containing the coordinates *x*, *y*, and *z*. These coordinates need to be imported in MATLAB and stored in the data type ‘timetable’. In doing so, each profile is associated with a certain timestamp within the measurement duration of 20 seconds. The elevation being the most interesting

parameter for most evaluations is stored in the coordinate *z*. Since the position of the sensor is stationary and the width is fixed by 1280 points in the sensor's settings, the coordinate *x* only needs to be imported once. The coordinate *y* denotes the carriage/elapsed time and can be generated easily within the code. Out of this timetable a matrix $\boldsymbol{Z}$ can be generated which contains all measured, planar heights. A typical dataset consists of 1000x1280 points (number of recorded profiles x points per profile).

Baseline compensation

When a roving is guided in the filament winding process, it usually has no contact with surfaces other than the guiding elements to reduce fiber damage. For optical measurements, a background plane is required to be able to focus and separate the object from the background. Yet, this background plane is never perfectly even and plane, especially in a production environment. To be able to perform exact calculations on the roving's geometry, the background has to be detected and then separated from the object to be investigated, here: the roving. Many things influence the relationship between object and background such as lateral movement of the roving, diameter, and inclination changes, vibrations, friction effects, and changes in optical behavior. For that reason, the baseline is detected for every single profile and afterward for the whole measurement as a tensor. The developed model is based on existing models in literature [219–221]. After a least squares polynomial approximation, outliers are detected and segmented and ultimately a tensor polynomial approximation is executed.

The algorithm for the baseline detection of each row can roughly be divided into the following steps:

I. A background profile is initialized with the *x* and *z* row data, i.e., the complete dataset.
II. The Vandermonde matrix is computed. Its inverse is computed via QR decomposition. With the assumption of a Gaussian distribution the coefficients and their covariance can be determined.
III. The residual vector and the prediction uncertainty for each point are calculated. A desired level of prediction is selected.

IV. Points within the desired degree of certainty are selected for further processing.

V. Testing if the residual vector is Gaussian, e.g., by Kolmogorov-Smirnoff test. If this is not successful, the algorithm goes back to step two.

Typically, this algorithm converges after four iterations and provides satisfactory results for most tested profiles. Figure 38 shows an exemplary dataset from the reference material, i.e., without binder. In the upper part of the figure, the polynomial approximation is shown at its initial stage and in the final stage fitting the baseline. In the lower part, the dataset is shown after the baseline compensation, i.e., the elevation is normalized, and the tilting of the background is corrected.

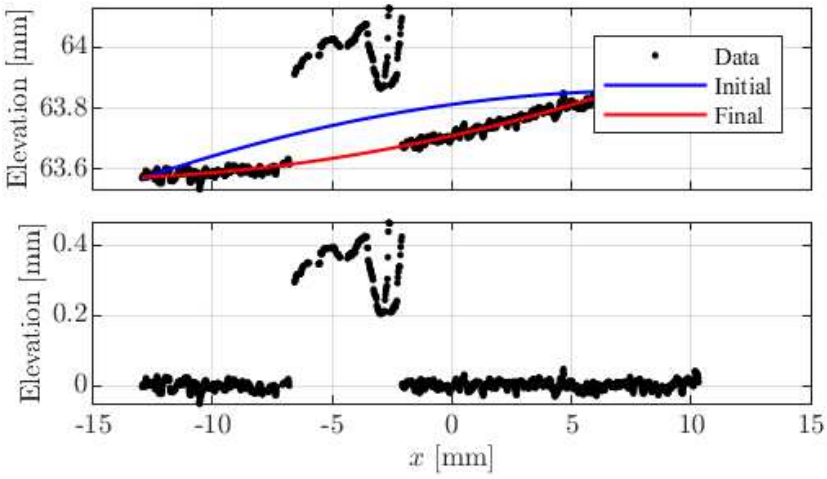

Figure 38: Baseline compensation of a single row for reference material without binder. Up: Polynomial approximation of the baseline; Bottom: Dataset after baseline compensation

Since the baseline detection of a single row can be disturbed by noise, it is beneficial for the stability and the knowledge gain to determine the baseline also in the *y*-direction. With the Vandermonde matrix of *y*, the tensor approximation can be computed and composed with the *x*-direction. Figure 39 shows the result of the application of the baseline compensation to the whole dataset. On the left side, the raw data is depicted. The surface in the center of the figure is the result of the tensor polynomial approximation. Analogous to the row data, the result on the right side shows the data with the background being a plane on the zero level.

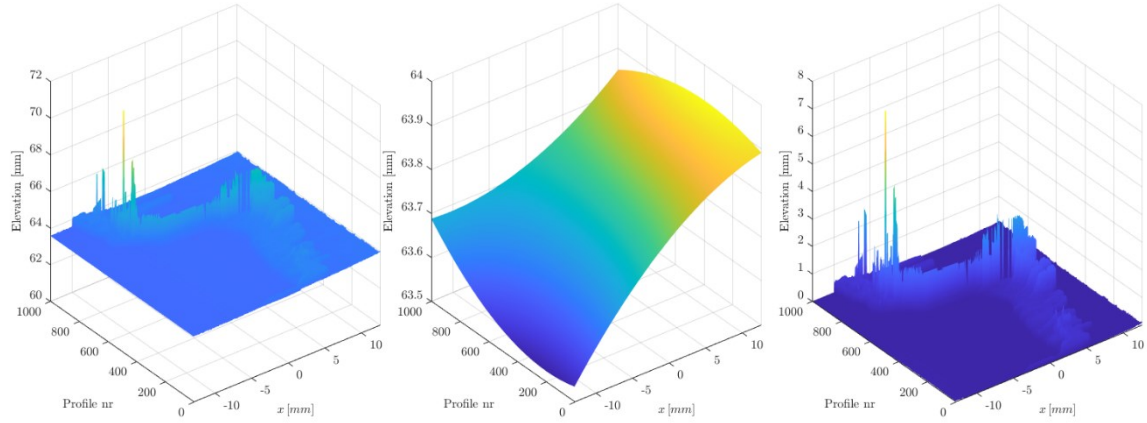

Figure 39: Baseline compensation of the whole dataset for reference material without binder: Left: Raw data; Center: Tensor polynomial approximation for base values; Right: Data after baseline compensation

Data segmentation

With the covariance of the residual given, an upper confidence interval can be computed. By that, the data can be segmented into contiguous portions for further analysis. Possible winding defects such as spreading, filament breakage, splitting, or foreign objects can be detected. This method is also the basis for some of the analyses presented in the next paragraph.

Analysis

Obvious parameters of interest for the control of the winding process are the width of the roving and its position. Designing and controlling the process requires knowledge of the roving's dimension and how it is deposited. Many process parameters and influences can affect it though, e.g., tension effects, slippage, or fiber damage.

The width of the roving can be determined by identifying the edges of the object in the dataset with a normalized base. For each row, this distance can be computed easily. Figure 40 a) shows an exemplary width profile of a carbon fiber roving without binder. In this case, (apart from an outlier) only minor changes can be seen. This means that the roving guidance and tension here lead only to slight changes due to compaction, twisting, spreading, or other possible effects.

From the same dataset, the position of the center line of the roving can be determined. In Figure 40 b) the shift of the roving from the center line is displayed. It shows a

general movement of the roving which is caused by the not perfectly straight fiber guidance between the spools, especially on the unwinding side. An outlier can be found at the same position as for the width. Apart from the general lateral movement, the shifts of the center are rather small. Hence, abrupt position changes have not happened during this measurement and only small vibrations can be spotted. Tension changes due to friction on the guiding elements are most likely to cause this.

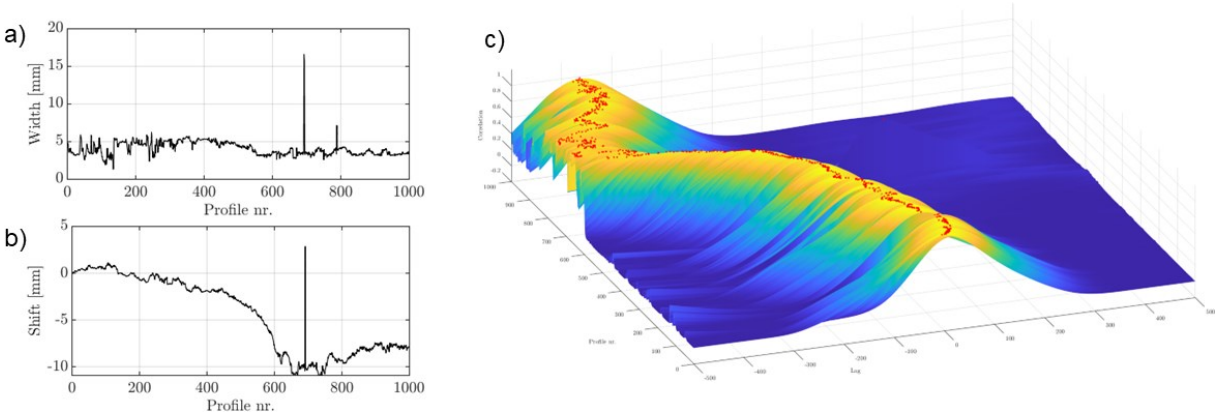

Figure 40: Analysis results for carbon fiber roving without binder: a) roving width, b) center line shift, c) cross-correlation of the centerline

Making the evaluation less vulnerable to elevation changes in the profiles, the data matrix can be normalized by applying the 2-norm. This changes the magnitude but not the structure of the data and that does not influence most analyses. With this normalized matrix, the cross-correlation can be computed. The reference profiles were selected at the starting position since they can be expected to be in the right place there. Maximum correlations in each row can then be used in a vector to estimate the position of the center line. Figure 40 c) shows the center line as a function of time. The benefit of this method is that all data points are used, and it is less susceptible to random Gaussian noise.

With the given information the roving can now be aligned to the center line. This can be beneficial for some calculations where the path is of no interest. On the left side of Figure 41, the dataset with an already corrected baseline can be seen. The right side shows the result of the alignment algorithm to the centerline.

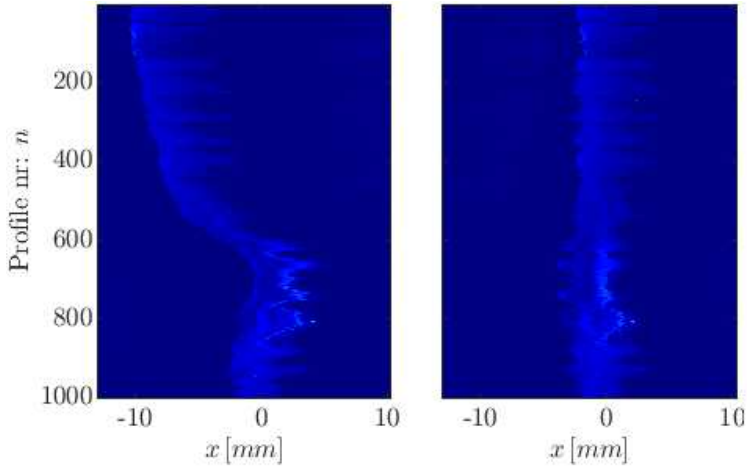

Figure 41: Left: Baseline corrected data; Right: Same data after alignment to center line

Having that much information on the geometry and the position of the roving, defects such as splitting are now easy to detect. This information is essential for efficient inline process control.

A more advanced application of this data can be found in the analysis of oscillations. This behavior is closely related to the tension acting in the process. Hence, by knowing the oscillation behavior, the process controller can analyze the tension forces in his machine and avoid friction-related damage to the roving or the equipment. A fast Fourier transform (FFT) can be applied to the whole data or for each location to know the spatial distribution. Irregularities that can be seen here should be investigated for their origin in the process setup.

4.3 PROFILE CHARACTERIZATION OF BINDER ROVINGS

One expected advantage of dry winding in comparison to wet winding is its automation potential. Since sensor equipment has not been tested yet with binder rovings, this work aims to investigate the suitability of laser light sectioning for the profile characterization of binder rovings. The chosen method is an established nondestructive testing method and inline control for related processes such as AFP. The reference material will be the respective non-bindered roving. Comparing these two types, it is apparent that the binder provides a more well-defined and constant cross-section profile. Yet, the surface has other optical properties due to the binder

particles. Also, form changes, e.g., caused by tension changes or twists, vary from the reference. A first attempt to examine the difference [213] showed that the measurements of the binder rovings were more reliable, yet left some room for improvement. Contrasting background and optimized lighting conditions were identified to improve the measurements.

The experimental setup is similar to the aforementioned publications. The specific alterations are explained in the respective subsections. First, the range of possible exposure times was determined. This value defines the amount of light that is projected onto the roving. Especially the black carbon surface is critical for (unwanted) optical effects and can easily lead to an insufficient reflection of the sensor's detector. Another important influence on the quality of the measurement is the available background. A preferred black background is compared to typical industrial background materials steel and aluminum. As process parameters, velocity and (brake) tension are examined. Typical roving defects are simulated by twisting the roving and manually splitting it. Finally, as a characteristic of binder material, it is activated to change the surface appearance and structure to observe the influence on the measurement.

4.3.1 EXPOSURE TIME

Light sectioning measurement is based on the principle of triangulation. A laser light beam is projected onto the object and a camera records the data. Especially for moving objects, the quality of the measurement is determined mainly by the exposure time of the laser light. Insufficient lighting leads to inferior-quality images while too much light input may cause motion blur and also increases the recorded noise. The given sensor provides exposure times in the range from 0.01 to 40 ms. All possible times were tested with a moving roving over a black background. A measurement time of 20 s was chosen. With 50 buffered profiles per second, this leads to 1000 profiles for each experiment. An exception is the exposure time of 40 ms. The buffered profiles per second have to be halved which makes it necessary to double to measurement time to receive the same number of profiles.

Fast exposure times lead to a triangle-shaped signal with gaps in between. Figure 42 shows this in the upper left corner for the fastest available time of 0.01 ms. The exposure time of 2 ms in the upper right corner already shows a good representation

of the profile of the roving. Yet, many ‘holes’ are visible, i.e., non-existing or corrupted data. In [213], an exposure time of 5 ms was proposed for binder rovings. The lower left corner of Figure 42 shows a profile from the current experiments. An evaluation with the proposed algorithm is possible but still, there are many datapoints missing which lead to NaN-values that need to be excluded. Apart from some noisy behavior in the foreground, an exposure time of 40 ms provides a suitable dataset for further processing. Starting from an exposure time of 5 ms the sensor data quality is good enough for further processing. Since the measurement time is doubled for 40 ms and no significant loss of quality is expected, an exposure time of 20 ms was selected for the investigations on the process parameters.

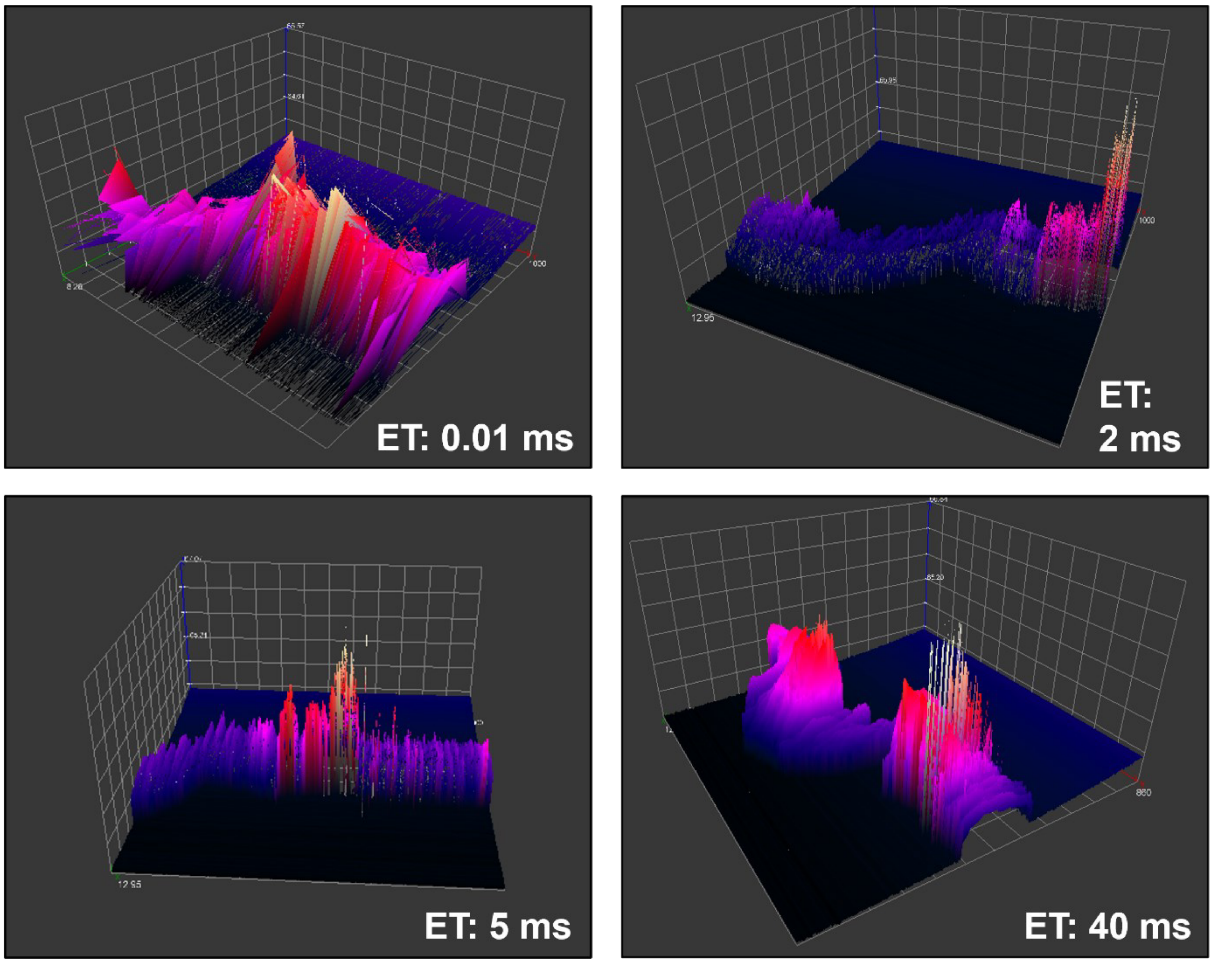

Figure 42: Moving binder roving captured with different exposure times (ET). Displayed in the sensor's software.

4.3.2 BACKGROUND MATERIAL

Another crucial factor for the quality of the measurement is the availability of a suitable background. Commonly, the winding equipment is mounted on some metallic part made of either steel or aluminum. A rather glossy aluminum and a matte steel plate were selected for testing to provide a wide range of possible metallic surface properties. The reference is a black, matte polymer cap which is used in all other experiments. Binder rovings have a more uniform surface than the reference material and due to the binder particles, it appears more greyish. This makes it easier for the sensor to detect it. Yet, the background must not disturb the reflections from the roving.

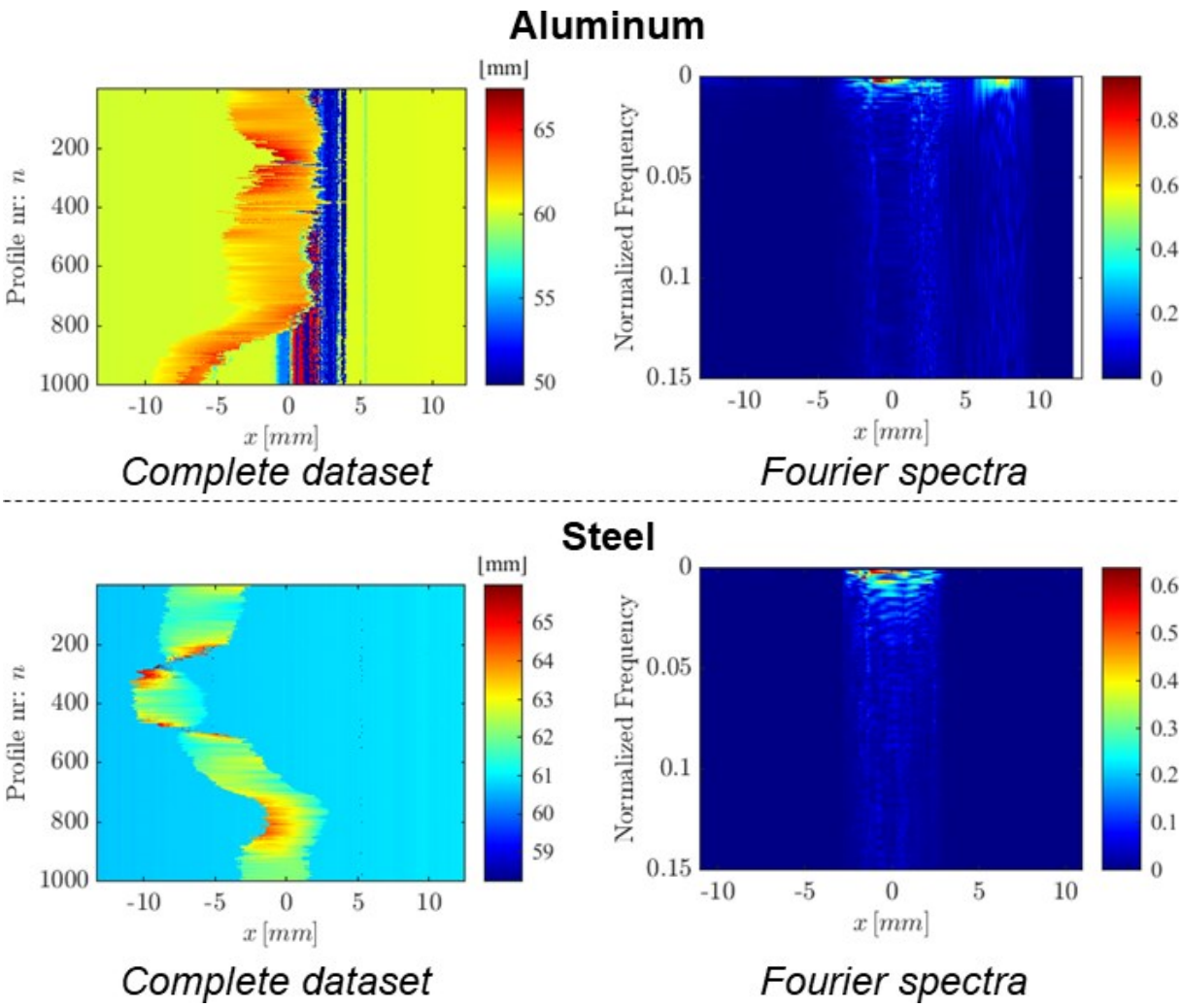

Figure 43: LSS measurements of binder rovings with different backgrounds: Aluminum top, steel bottom. Left side: complete measurement dataset, Right side: Fourier spectra for each vertical track (relative to measurement frequency)

Figure 43 shows on the left side the datasets generated from the measurements with a steel and an aluminum background. On the right side, the result from an FFT for

each *x* location is displayed. For aluminum, an area of about 5 mm width is visible which is caused by unwanted reflections from the background. This leads to the ‘recognition’ of a second dataset which is displayed in the Fourier spectrum. A shiny surface such as polished aluminum is therefore not suitable for this measurement because it can corrupt the data. The data set generated with the steel background shows a decent quality, comparable to the black cap. Only at about x= +/- 5 mm small dark lines are visible in the dataset. Here, some kind of reflection probably from the sensor’s housing is displayed in the measurement results. It is likely that this reflection can be ignored or compensated in the algorithm easily. The results here show that measurements on a matte metallic background are possible but might need some more programming effort. If possible, a black background for the area of measurement is recommended though.

4.3.3 SPEED AND TENSION

Process speed and roving tension are two of the most important process parameters in filament winding. Speed predominantly determines the overall process efficiency. Therefore, the maximum speed has to be found at which no quality loss occurs. Tension during manufacturing influences the residual stress of the preform and can have a large effect on quality aspects such as the accuracy of the layup. Consequently, the mechanical properties of the final product depend on the acting tension in the filament winding machine.

The process velocity of the test rig is controlled by the ‘override’ property in the PLC. A rotation of the winding axis of 100 °/s is defined as standard velocity (≙ 50 % override). To test the effect of velocity changes, experiments were performed with 100 % and 25 % override, i.e., double and half speed.

Observations during the experiments already showed that for a higher velocity, the roving tends to stick, slip, and jump more than in the reference. A slower motion appears also to be smoother. Figure 44 displays the datasets and the center line shift of the representative experiment. In the case of the reduced speed in the upper part of the figure, the motion shows only small lateral movement. In general, the roving moves slightly from left to right due to sliding on the first concave guiding roll directly after unwinding.

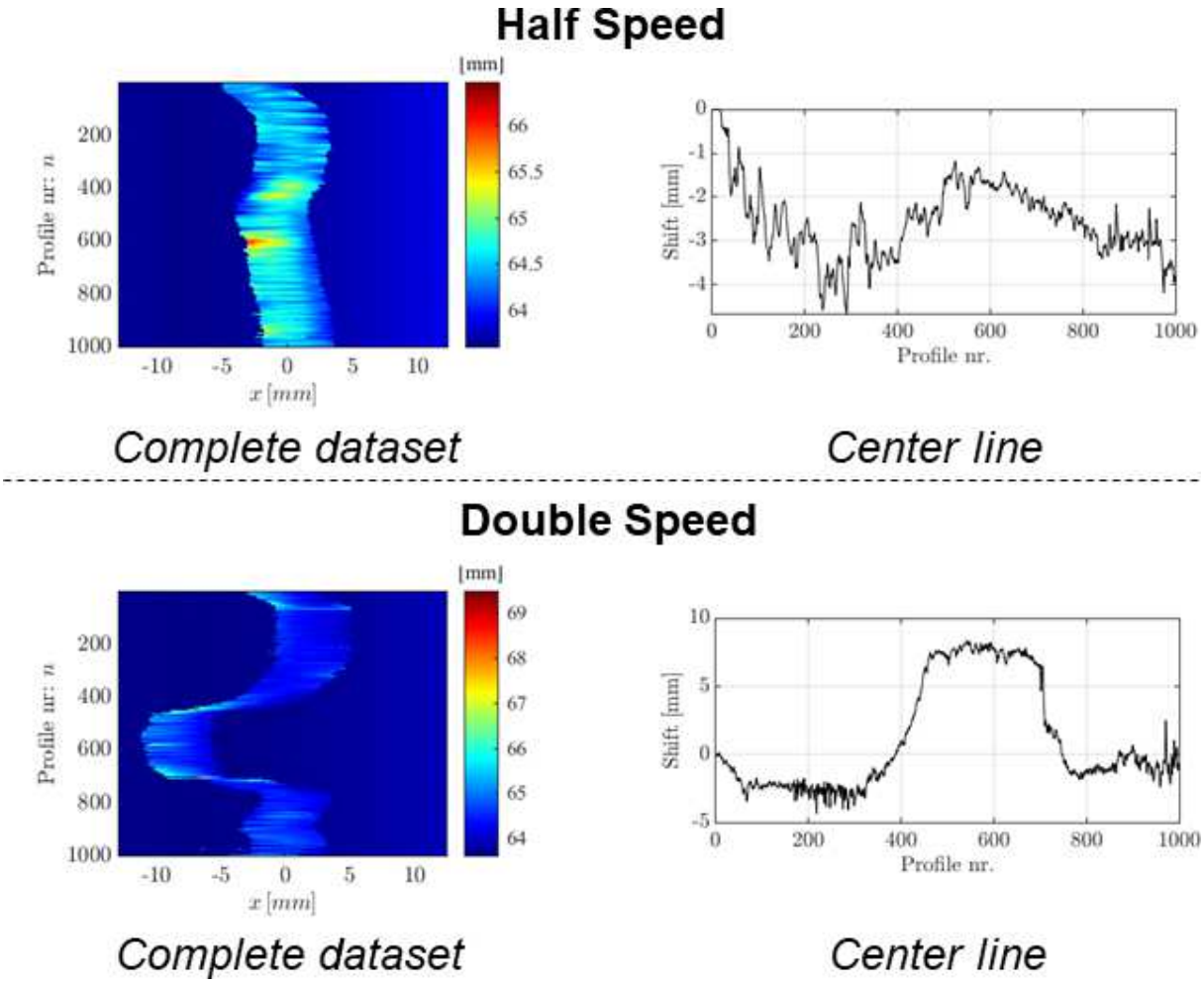

Figure 44: Visualization of dataset and center line shift for experiments with half (top) and double (bottom) speed

The snapping of the roving at higher velocities can be seen in the bottom part of Figure 44. Abrupt changes in the roving's position can be explained by friction or sticking effects which emerge and then resolve suddenly. In general, it must be stated that the fiber guidance has a large influence on acting friction and consequently the maximum velocity. In the experiments performed here, the velocity is rather slow compared to industrial processes and the fiber guidance is rather rudimentary. To improve the manufacturing process, the guidance has to be optimized to be able to run the process at a higher speed, e.g., by the usage of suitable rolls and the avoidance of major redirections. Yet, it could be shown that the velocity can have a considerable influence on the result of the profile or in particular the position measurement.

As mentioned, the tension behavior of the roving is important for the process and its inline measurements. A certain level has to be upheld to avoid sagging of the roving

and to guarantee precise positioning. However, excessive tension must be avoided. For example, this can originate in the fiber guidance elements or in the unwinding around the edges of the roving spool. In the experiments here, an elevated tension is introduced by applying a brake force on the unwinding spool. A bungee cord is wrapped around the cardboard spool of the roving to increase friction. The exact value of tension is not measured as it is aimed to give only a qualitative appraisal.

During the experiments, a high tension leading to twisting and snapping of the roving could be observed when the roving was unwound at the edges of the spool. In Figure 45 such a snapping movement of the roving can be seen in the visualization of the normalized data.

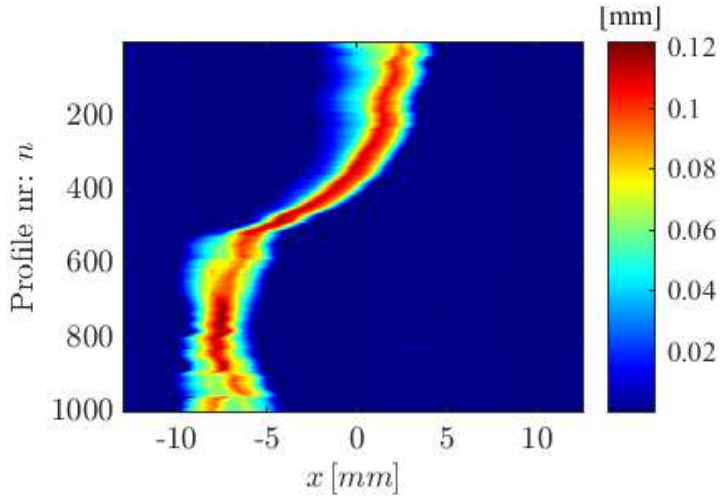

Figure 45: Normalized profile data of a binder roving with a brake on the unwinding axis

The increased tension also became critical for the fiber guidance rolls in the test rig which is another reason to avoid it. Other than the unwanted movements of the roving, no other significant changes in the measurement data could be observed. Even the roving width showed no decrease. This can be explained by the already compacted nature of the presumably pre-tensioned rovings which leave no room for additional cross section tapering. Similar to the experiments on velocity, only an indication of what might happen to the measurement with increased tension should be given here. A filament winding machine used in production is much more complex, and many other friction and tension effects have to be considered. It can be stated that tension can have a strong influence on the result but not on the quality of the measurement.

4.3.4 GEOMETRY CHANGES

In filament winding, changes in the roving geometry are quite common. They may originate in the fiber guidance, defects, or inaccurate placement on the spool. Among them are broken or loose fibers, ruptures, surface alterations, twisting, and splitting. The latter two were investigated in the experiments with the LSS. Often, twisting can occur on the guiding elements, or the roving is already twisted on the roving spool. Splitting can be caused by too high tension or by sharp objects cutting the roving. All those mentioned defects should be detected by an inline monitoring system to be able to perform countermeasures, document them properly, or even stop the process.

In the experiments conducted here, the twisting was introduced manually, and the splitting was provoked with a screwdriver. Figure 46 shows the LSS measurement results of twisting (top) and splitting (bottom). The twist can be seen in the normalized data at around profile 600 in the transition from a broader, lower area to an area that is smaller in width but higher. In the respective Fourier spectrum, a shift to the left can be observed. This indicates that the tension is not distributed symmetrically. This can be an indication of the twisting.

The splitting in the lower part of the figure can also be detected with the LSS and interpreted with the presented algorithm. Two different strands of the roving show less elevation due to the reduced number of filaments. On the right side of the lower half of Figure 46, the baseline compensation is visualized. The split roving can also be recognized and separated from the background. The definition of the object can be controlled with a threshold (transition blue-light blue in the figure). Yet, there is room for improvement, i.e. a flexible definition/recognition of the roving. Machine learning algorithms can be a viable option here. Analogous to the twisting, changes in roving geometry can be detected, and then the severity of the defect can be analyzed.

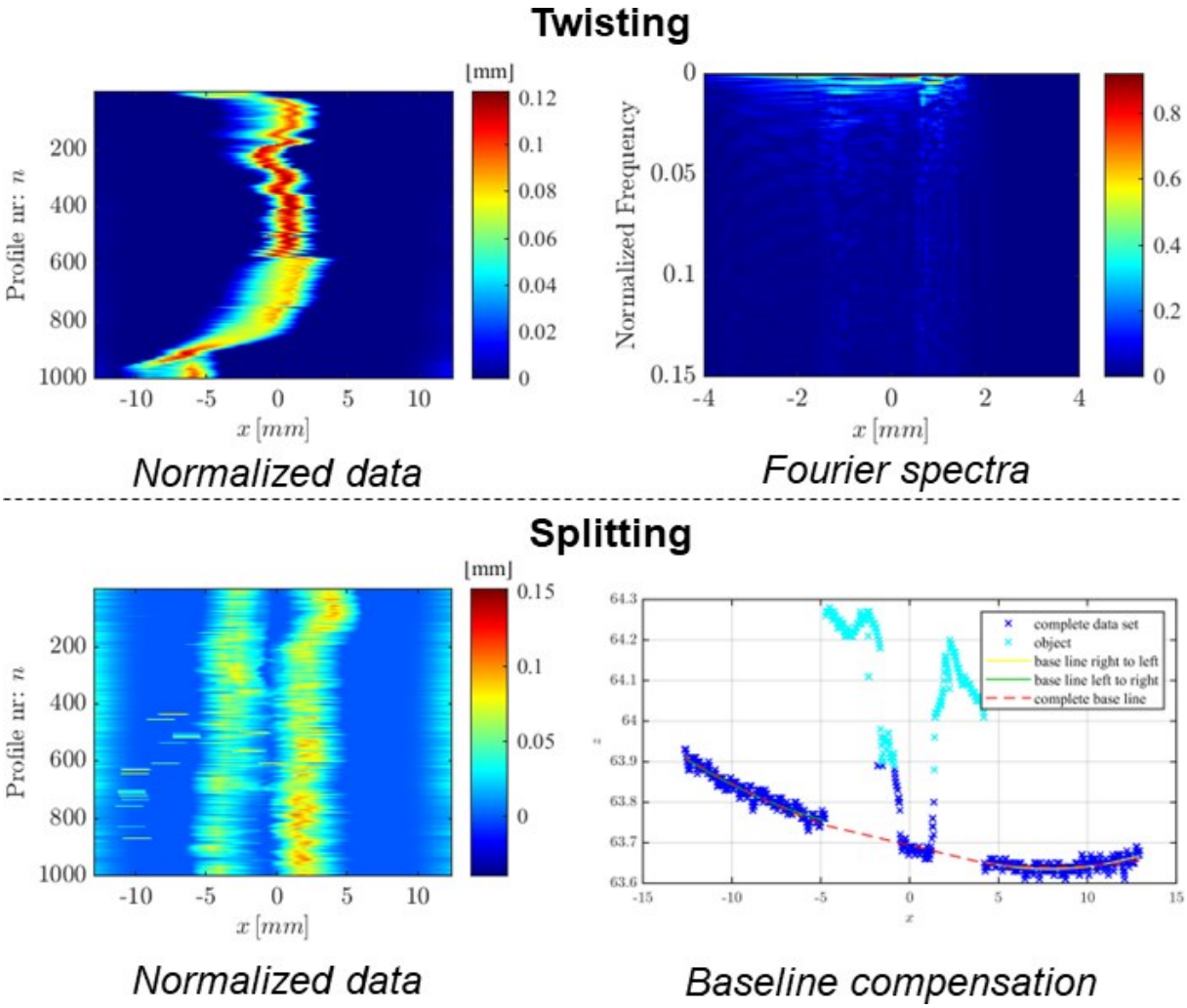

Figure 46: Measurement results after changes in the roving geometry: twisting (top) and splitting (bottom)

4.3.5 BINDER ACTIVATION

The specialty of binder roving is the ability to activate the binder particle to create a different, tackier surface. This also has an immediate effect on the optical properties of the surface. In Figure 55 three different types of surfaces can be observed: the regular, an activated one, and one activated under tension. Depending on the degree of melting and the acting pressure on the binder particles, they distribute more or less on the surface and make it shine blacker. This can lead to unwanted reflections which can make the detection of the LSS more difficult. The activation of the binder is done with four infrared heating lamps. Temperature measurement on the roving surface behind the IR lamps showed around 140 °C, i.e., melting of the binder is secured.

Experimental results show that the LSS measurement works equally well for the activated binder. Figure 47 shows the three-dimensional baseline compensation. The dataset is of good quality and can be processed analogous to the non-activated material before.

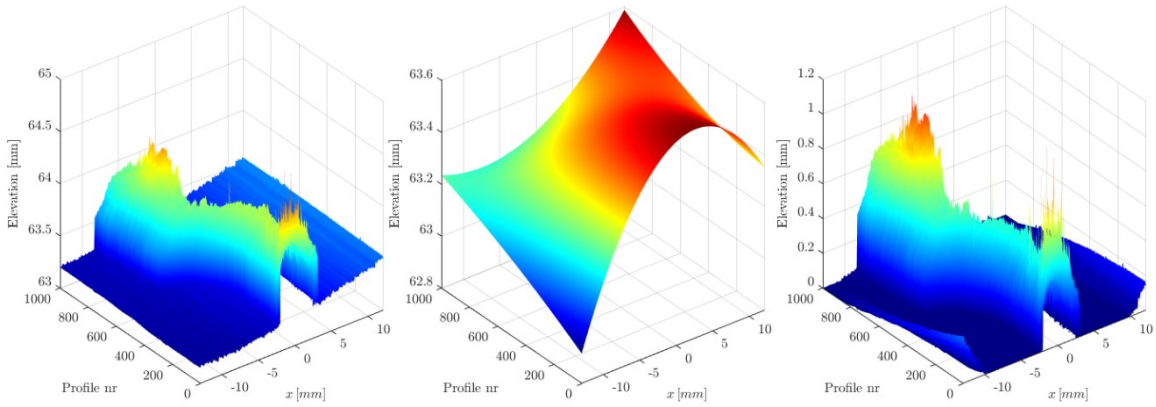

Figure 47: Baseline compensation of a binder roving dataset: Left: Raw data; Center: Tensor polynomial approximation for base values; Right: Data after baseline compensation

4.3.6 SUMMARY: LSS MEASUREMENT OF BINDER ROVINGS

The aim of this chapter was to evaluate the suitability of a laser light sectioning sensor for the measurement of binder rovings and the application of the code developed in the aforementioned publications. Compared to carbon fiber rovings without binder, the measurement results are similar. The black color demands a preferably black, matte background. Exposure time is the most important parameter in the sensor settings to optimize the quality of the measured data. Speed and tension changes as well as defects can be detected and processed in an inline monitoring system accordingly. Activation of the binder does not show a noteworthy influence on the measurement quality.

In general, it must be stated that these experiments were performed on a simplified test rig where many influencing factors of a complex industrial machine do not fall into account. Vibrations, pollution, or simply a more complex machinery can lead to different results. Also, these tests were not in real-time. To do so, the sensor signal has to be linked to the PLC. All the hard- and software components have to be (made) real-time compatible. This also goes for the presented algorithm which surely needs to be adapted to reduce computation time.

5. CAPILLARY FLOW IN BINDERED ROVINGS

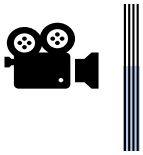

The following chapter is based on the publications [222,223] and may contain some overlaps.

5.1 CAPILLARY RISE EXPERIMENTS

As discussed in Section 2.4, the experimental part of this thesis will cover the capillary flow behavior of bindered rovings. For that purpose, capillary rise experiments have been conducted. In these, the textile is brought into contact with a test liquid so that it will absorb it due to the capillary force between its filaments. Capillary rise test setups are known in many configurations depending on the textile and the respective property that needs to be investigated. The equipment and software used here have been developed by Blößl [24,196] for the testing of flax fiber fabrics. Only a few adjustments were made for the testing of rovings. Most of the experimental parameters were kept upholding comparability.

The focus will be on the influence of different activation temperatures on the capillary flow. Activation duration, the potential influence of tension, and the comparison to virgin rovings will complete the experimental series.

5.1.1 SAMPLE PREPARATION & EXPERIMENTAL SETUP

The preparation of rovings for capillary rise measurements differs slightly from the preparation of a stack of fabrics. Instead of cutting on a CNC machine, the roving is cut from the spool with a scissor. A length of 65 mm is used similar to the fabrics. To reduce the number of experiments and utilize the full cavity space, four rovings are examined in the same experiment.

A polyimide foil is placed on a heating plate (MR 3004 safety, Heidolph Instruments GmbH & Co. KG, Schwabach, Germany) first. After reaching the desired activation temperature, measured by a thermocouple on the foil surface, the cut specimens are placed on the foil. Another polyimide foil is then placed on top of the rovings to reduce

cooling at the surface. This foil is manually pressed on the rovings. Otherwise, it could be observed in pretrials that the binder on the surface would not melt uniformly.

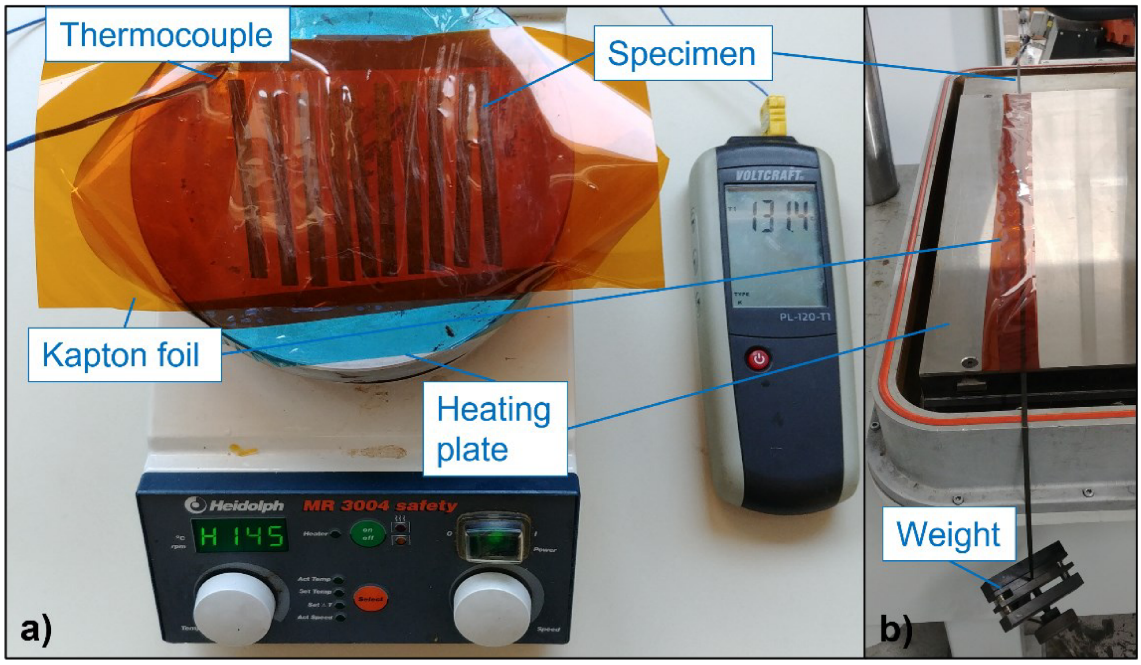

Figure 48: Binder activation for capillary rise experiments: a) regular setup b) under tension influence

Figure 48 shows the sample preparation of the binder rovings. The ‘regular’ setting a) is used for all activation temperatures. The temperature is held for 30 minutes. At 130 °C another set of specimens is prepared with only 30 s activation duration. Also, to test the influence of tension on the capillary flow a roving is placed on foil on a one-meter-long heating plate of a press (WKP 3500 S, Wickert Maschinenbau GmbH, Landau, Germany). The ends are weighted with clamps of ~1 kg. After closing the press, the temperature of 130 °C is held also for 30 minutes. This setup can be seen in Figure 48 b).

As mentioned previously, the focus will lay on the activation temperature. Based on the given temperatures from the datasheet, a range from 100-160 °C every 10 °C is tested and compared to the not-activated specimen at room temperature. A temperature of 130 °C was chosen for the aforementioned preparation modifications because it is well above the recommended activation temperature and should provide a complete melting of the binder. To investigate the general influence of binder material on the flow within a roving, the reference material is tested at room temperature. Here,

the rovings are tested in a straight, flat form directly from the spool and in a twisted, irregular shape similar to the form during processing/ roving guidance. An overview of the tested parameters and the important temperatures is given in Figure 49.

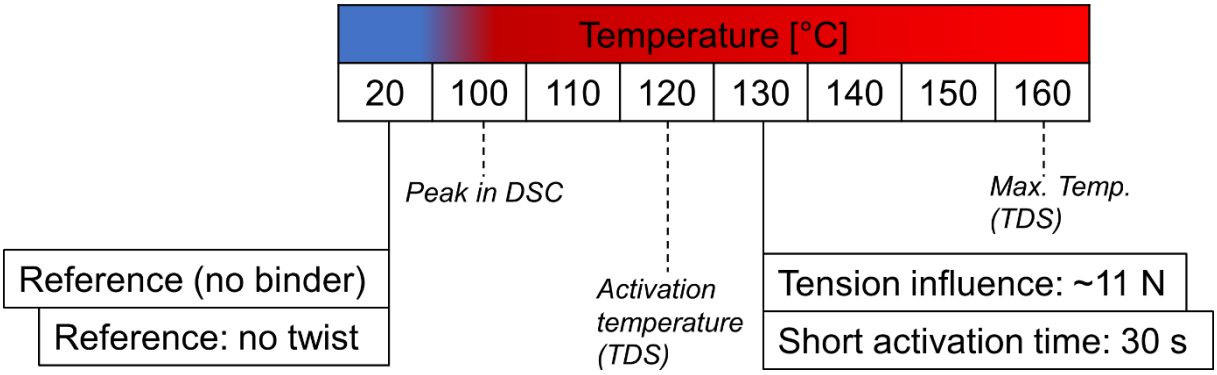

Figure 49: Parameters and characteristic temperatures in the capillary rise experiments

After the activation, the specimens are taken from the heating plate and cooled down for some minutes. Then, they are carefully removed from the foil. Too early removal and a wrong peeling angle can easily lead to a fanning of the roving, leaving the specimen destroyed.

Four specimens are then placed on the lower glass block of the sample holder of the capillary test rig. A distance frame of 0.5 mm is used to provide a suitable cavity. After placing the upper glass plate, the sample holder is tightly closed by eight screws and then transferred to the test rig. After every experiment, the glass is cleaned with isopropanol and dried with precision wipes.

The mounted sample holder inside the test rig is displayed in Figure 50. Starting the experiment, the platform containing the bowl with the test fluid is lifted upon contact with the glass blocks. While the test fluid is absorbed by the specimen due to capillary forces, the fluid weight and the progression of the flow front are recorded. Also, the temperature is tracked to be able to calculate the temperature dependency of several parameters, e.g., viscosity and density.

The capillary rise in unidirectional materials such as rovings is relatively fast, i.e., <30 s. Therefore, the experiments were stopped after 3 minutes. After lowering the platform, the recording is continued so that excess fluid can drip back into the container. Finally, the sampled holder is removed and cleaned.

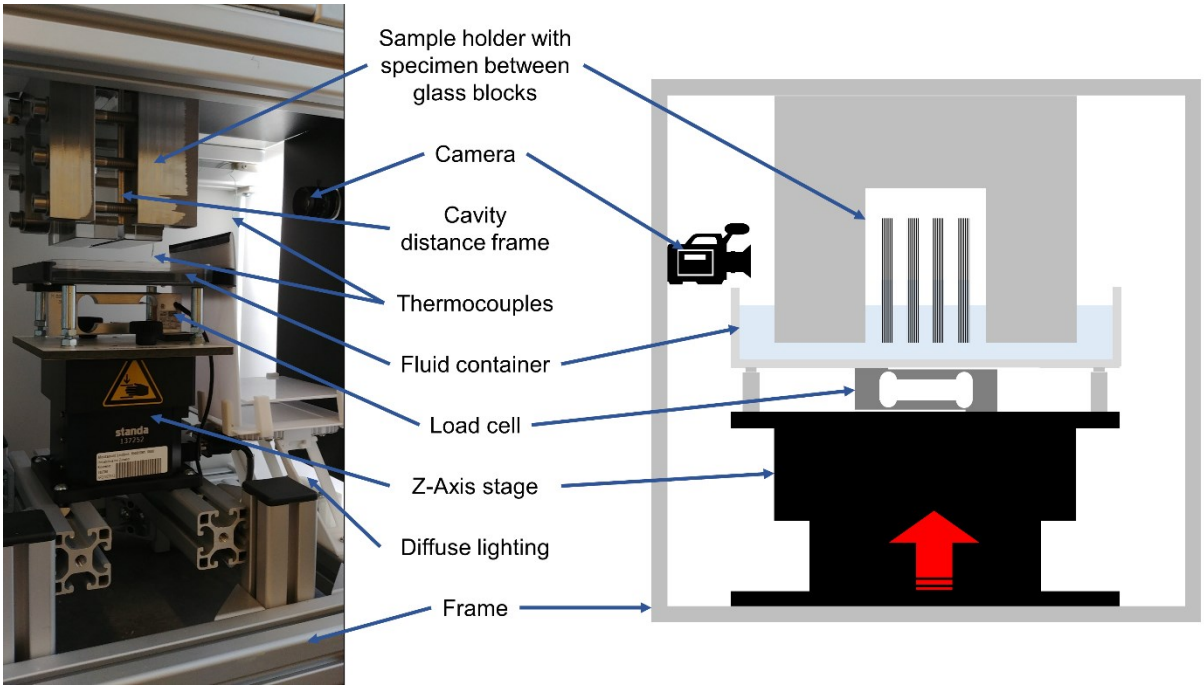

Figure 50: Capillary rise test rig at LVV (adapted from [222])

5.1.2 TEST FLUID

N-decane is chosen as the test fluid in the capillary rise experiments due to its superior wetting behavior [24,224]. In [24] this fluid is chosen because of its non-polarity. Swelling effects of natural fibers can thus be minimized. Moreover, assuming complete wetting (i.e., θ~0°) the calculation of fitting models can be simplified. While in literature n-hexane is commonly used [190,205,225,226], n-decane is favored due to safety aspects.

Here, n-decane is exclusively used as a test fluid to benefit from the full-wetting behavior. Compared to other fluids and resins, it also simplifies the experiments by measuring at room temperature, excluding curing effects, and providing an easy-to-clean surface after each experiment. More application-related measurements with epoxy resin have been made in [24,173]. In those, additional effects such as curing and viscosity change need to be regarded. If an exact study of a certain material combination (fluid and fiber/textile) is wanted, specific contact angle measurements have to be made [190,192]. In the frame of this work, only an overview of the capillary behavior of rovings and a parameter comparison are intended so that these influential fluid parameters are simplified by using a non-polar test fluid and neglecting fluid changes during the experiment.

5.1.3 FLOW FRONT EVALUATION

Both, data acquisition and evaluation on the capillary test rig are performed with MATLAB. Since the amount of imbibed fluid in these experiments is relatively low and hence prone to errors, the focus of the evaluation is on the detection of the flow front. After the platform reaches the upper position the fast image acquisition with a resolution of 1920 x 1200 pixels starts. For the first ten seconds, the acquisition rate is set to twenty frames per second (FPS). After that, one FPS is recorded until the experiment stops. Then, the images are stored in a MATLAB format '.fig' and can additionally be exported as '.png' files.

The evaluation routine starts with the selection of the respective borders of the specimen. In the case of the binder rovings, this has to be done in four different runs.

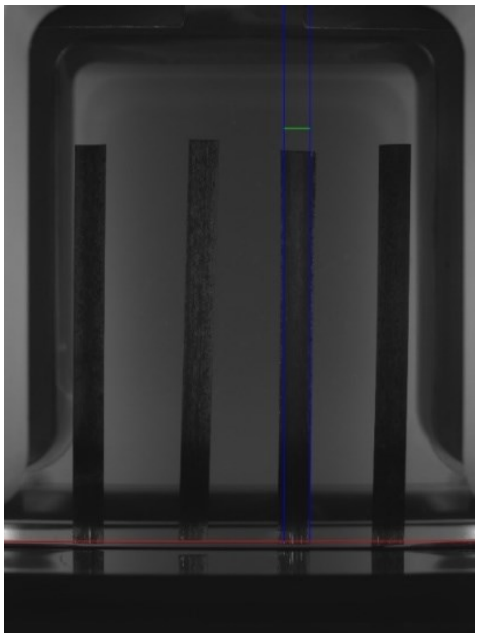

Figure 51: Selection of the evaluation area of a binder roving in capillary rise experiments

Figure 51 shows the selection of the third roving to be evaluated. The red line marks the lower end of the roving to determine where fluid arrives first. The blue lines mark the edges of the roving. They should be selected to provide a good profile of the roving but preferably exclude defects and compensate for possible tilting. In the next step, the parameters to evaluate the flow front on the binary image have to be selected. Figure 52 shows the main window. In the original image on the left side, the borders for the evaluation are marked in green. An evaluation width of 3 mm is selected to compensate

for tilted specimens or stick-out fibers in the edge area. A height of 60 mm is chosen to exclude the edges of the roving.

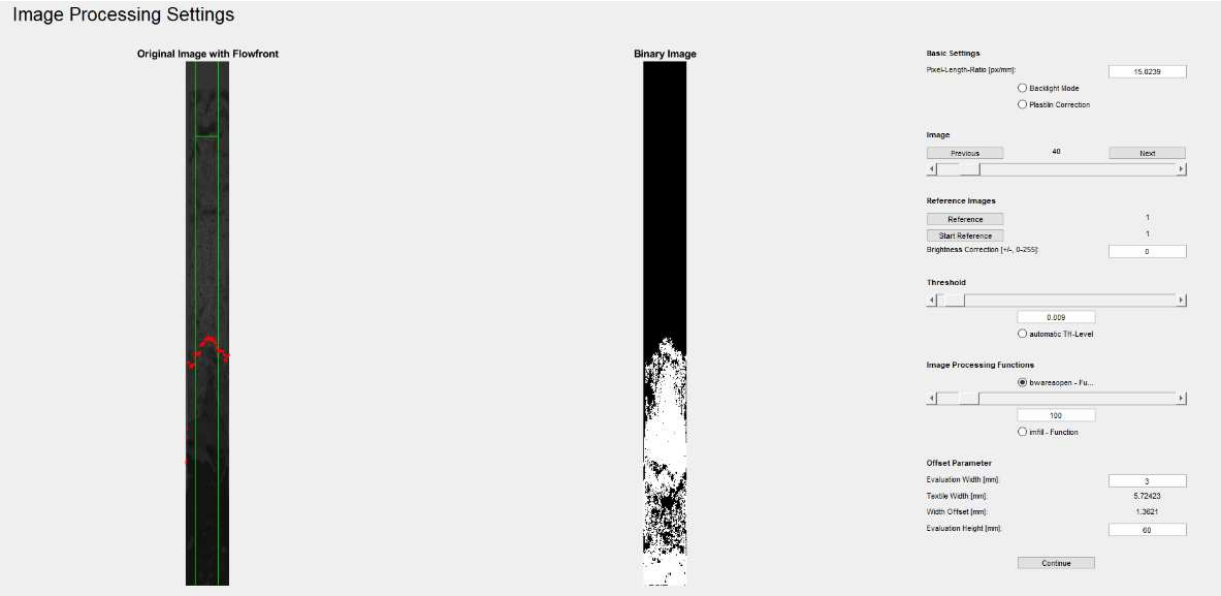

Figure 52: Main evaluation window of capillary rise experiments

In the middle of Figure 52, the binary image is displayed. It is the basis for the flow front detection. On the upper scrollbar, the images can be selected. By scrolling through here, suitable parameters and reference images can be selected. A fixed threshold of 0.009 - 0.012 proved to be a fair value. The function ‘bwarea’ of MATLAB can support the detection by giving a value for the area in a black-and-white image. Values of 100-200 can improve the flow front detection. Also, reference images can be selected to enhance the flow front display. The ‘start reference’ marks the point where the fluid is visible for the first time, while the button ‘reference’ should be selected for an image where the flow front is pronounced.

Yet, there are a couple of reasons why the results of some experiments cannot be deemed valid:

- Camera failure
- Stand-out fibers that falsify the evaluation
- Movement (sinking) of the specimen
- No clear detection of the flow front (shadows, morphology of the roving)
- No fluid uptake

For these reasons, a relatively high number of experiments are performed. Three times four, respective five times four, specimens are evaluated. Also, it must be noted that the handling and even more so the evaluation step itself have a large influence on the outcome of the experiments. Proficient selection of evaluation area and parameters as well as careful handling of the specimens in the sample holder are required.

For a better illustration of the capillary rise curves, the raw data is replaced by a power law fit. A visual inspection of the quality of the fit was executed before the files were stored for further processing.

5.1.4 RESULTS AND VALIDATION

In this section, the results from the capillary rise experiments will be discussed. To emphasize certain observations, additional investigations were performed with a digital microscope (VHX 7000 series, Keyence Corporation, Japan). With these images, binder distribution and degree of melting can be evaluated.

As the most important parameter in the processing of binder rovings, the activation temperature is evaluated first, followed by influence of tension and activation duration. Finally, a comparison is made with rovings without binder.

5.1.4.1 Activation Temperature

Activation temperature describes the temperature where the binder material on the roving is melted so that sufficient adhesion for the processing can be provided. The given values from the manufacturers usually lie slightly above the values generated in measurements of the material. A thorough heating throughout the whole part must be guaranteed.

In the capillary rise experiments, it can be expected that after activation the viscosity rises so that the binder is absorbed by the rovings. With the additional material blocking the capillary tubes, a slower rise of the test fluid is expected.

This behavior can be observed in Figure 53. Curves at room temperature and 100 °C show a significantly faster rise than the others. At temperatures above 110 °C the binder is activated sufficiently, and the capillary rise is hindered. The curve at 140 °C slightly differs. Here, measurement/evaluation inaccuracies could be observed. An

angulated flow within the rovings leads to a faster rise than for the other curves with activated binder.

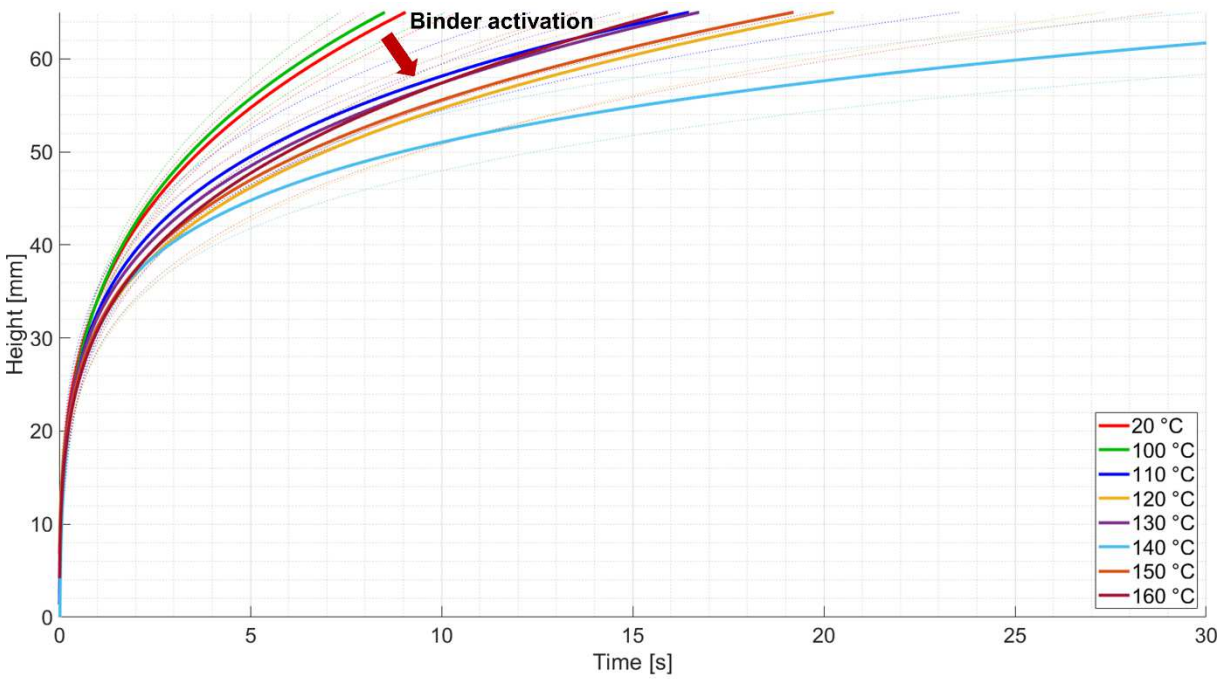

Figure 53: Influence of binder activation on capillary rise (dotted lines: standard deviation)

Since the proposed activation temperature from the data sheet is 10 °C higher than the effect that can be seen in the previous figure, additional microscopy images were recorded. To observe the behavior of the binder on the roving surface under temperature influence the roving was placed on a heating plate under the microscope. Images were recorded every 5 °C between 50-140 °C. Every temperature step was kept for five minutes until the image was taken. Figure 54 shows an overview of these images. For better clarity only steps of 10 °C are shown and temperatures below 70 °C excluded. First, minor changes in the morphology of the drops can observed at 110 °C. Hence, it is in good accordance with the results of the capillary rise experiments. Also, it must be stated that the binder distribution under pressure and for a longer duration will surely accelerate the flow of binder on the surface and then into the roving.

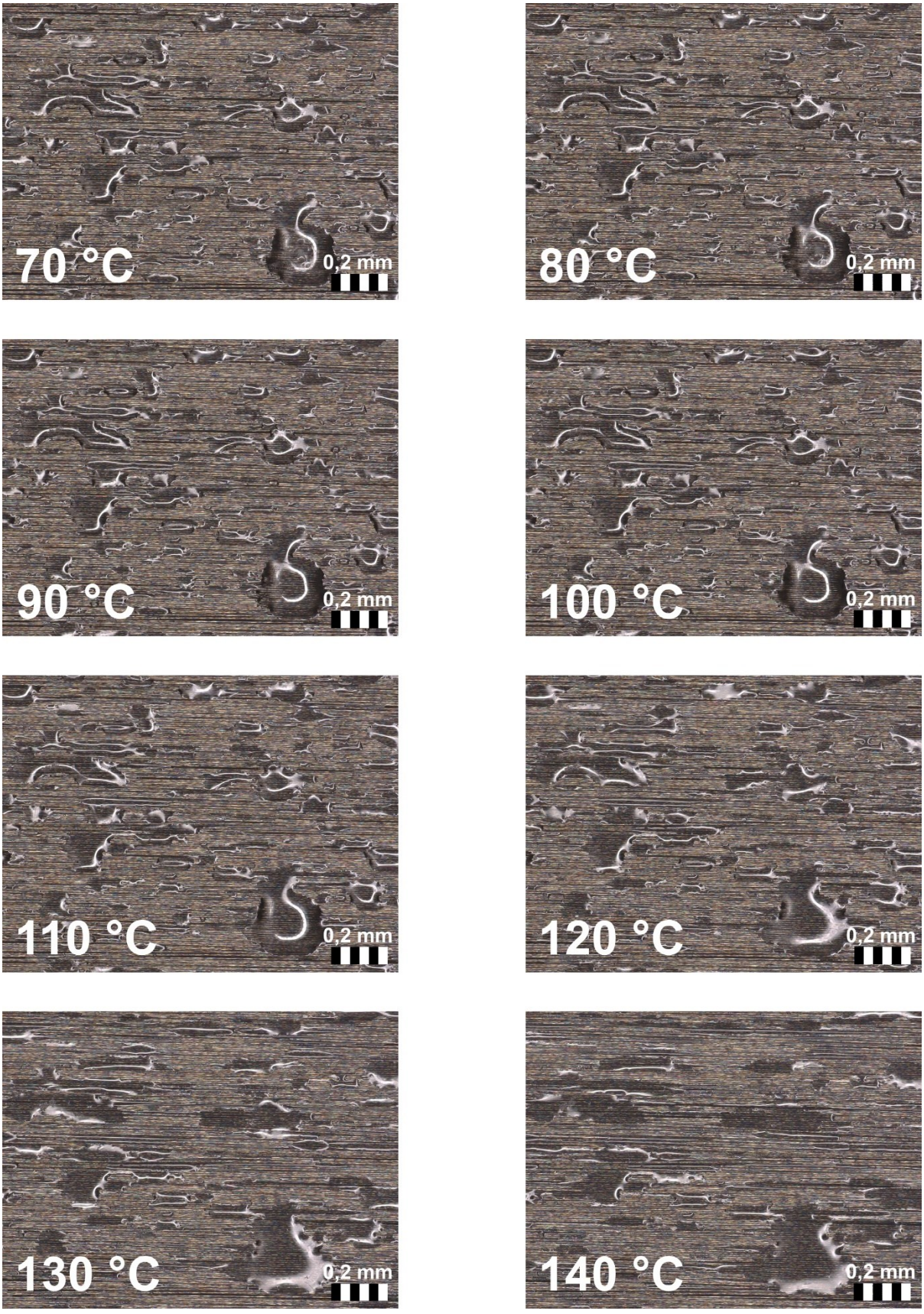

Figure 54: Microscopy images of binder activation on the roving surface

5.1.4.2 Tension and activation duration influence

In the filament winding process, the rovings are placed on the mandrel under a certain tension. Also, as a key benefit of dry winding, a higher process speed impedes a long activation time for the binder material. Consequently, these two factors were also considered in the capillary rise experiments. It must be examined if the measurements on a test rig can be transferred to the real-life process without the consideration of additional parameters.

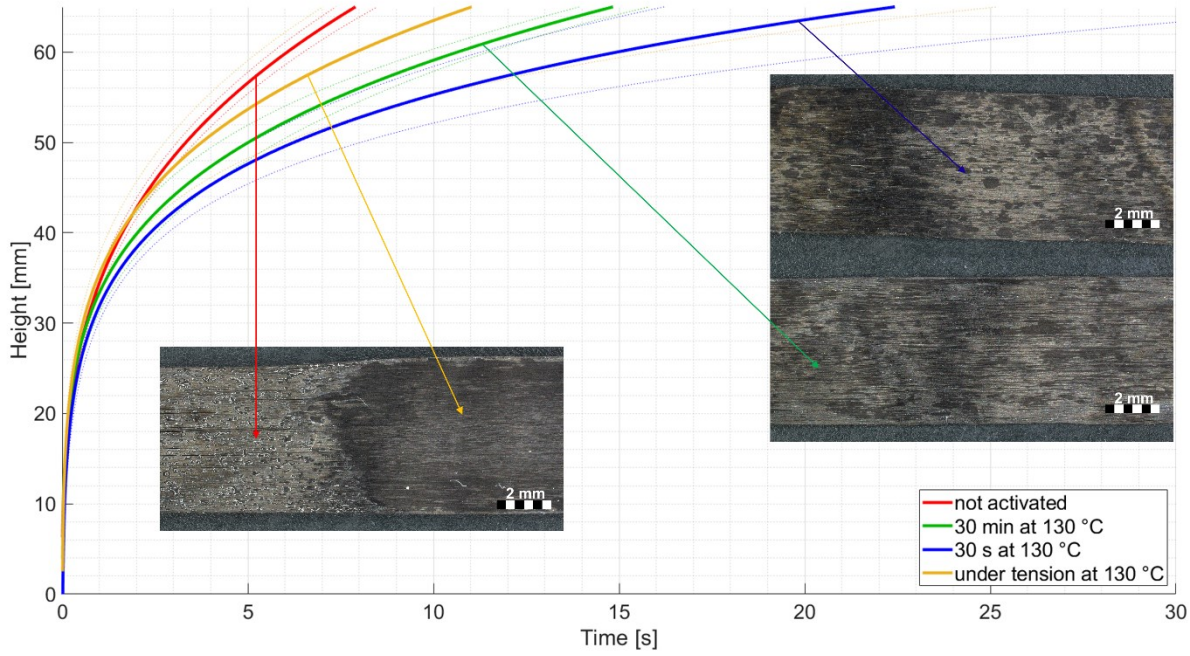

Figure 55: Influence of tension and activation duration on the capillary rise behavior of binder rovings (dotted lines: standard deviation)

Figure 55 shows the capillary rise curves for unbindered material, binder activated for 30 minutes, binder activated for 30 seconds, and binder rovings activated under tension. All specimens with activated binder show a reduced rising velocity as could be expected from the previous results. Yet, the curves differ and show a large standard deviation. Looking at the roving surfaces with 20x magnification different surface structures can be noticed. The not-activated specimen (red) shows the droplets of binder material. After activation on the heating plate (green & blue) these droplets are melted and partially imbibed by the roving. The pattern looks similar and does not depend on the activation duration but on the distribution during the application of the binder. When the binder roving was activated in a heated press (yellow), the roving's

surface looked different. The acting tension leads the binder to spread completely on the roving. The behavior can be seen even better in the images of Figure 56 with a magnification of 200.

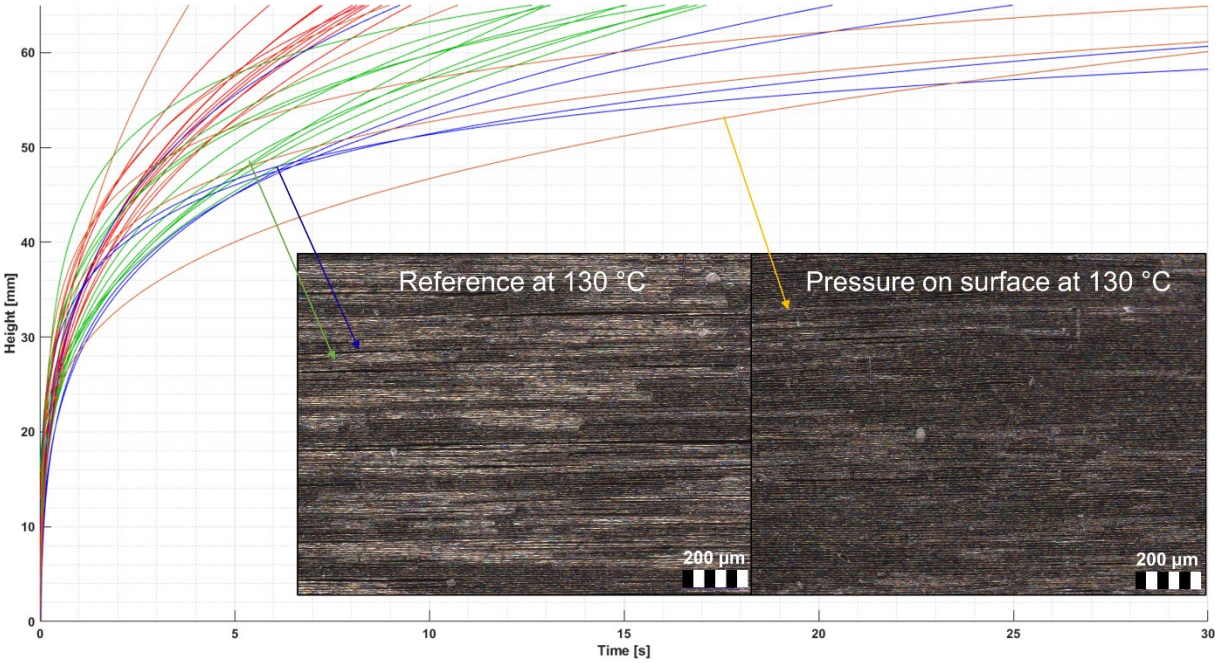

Figure 56: Raw measurement data from Figure 55 with images of the roving surface

Figure 56 also shows that the difference between the single experiments under tension influence (yellow) is rather large. This can be explained by the homogeneous roving surface which makes the determination of the flow front more difficult and vulnerable to higher scatter. Neglecting this (side-) effect, it can be stated that the application of tension to the binder roving has no significant influence on the capillary rise velocity. This result could be expected since the rovings are most likely prestressed by the manufacturer to facilitate the application of the binder material.

Considering the activation time, the results are less clear. Looking at the green and blue curves in the last two figures, it cannot be stated clearly if any effect can be seen or if the curves are within the deviation range. Especially at the beginning, the rise velocity is very much alike. For the specimens activated only for 30 s the curves then drop faster. This could be explained by less time for the binder to flow along the single filaments within the roving and potentially unblocking capillary tubes again.

This behavior should certainly be investigated further when designing the process chain and the respective parameters for dry filament winding.

5.1.4.3 Comparison with virgin roving

Apart from the activation of the binder, the general influence of the preprocessing in the form of binder application needs to be investigated. The surface of the rovings is coated with additional material which might also influence the capillary flow. To examine that, the binder roving was compared with the virgin roving of the same manufacturer, i.e., the sizing should be the same. During processing, it is common for the rovings to twist, especially when they are redirected by eyelets or rollers. This has a significant effect on the geometry of the roving. Consequently, two approaches were chosen before cutting the specimens. On the one hand, despoiling the roving as carefully as possible to conserve the flat, untwisted shape, and on the other hand, handling the roving as it would come off the spool in a regular process. The different roving sections are displayed in the pictures in Figure 57.

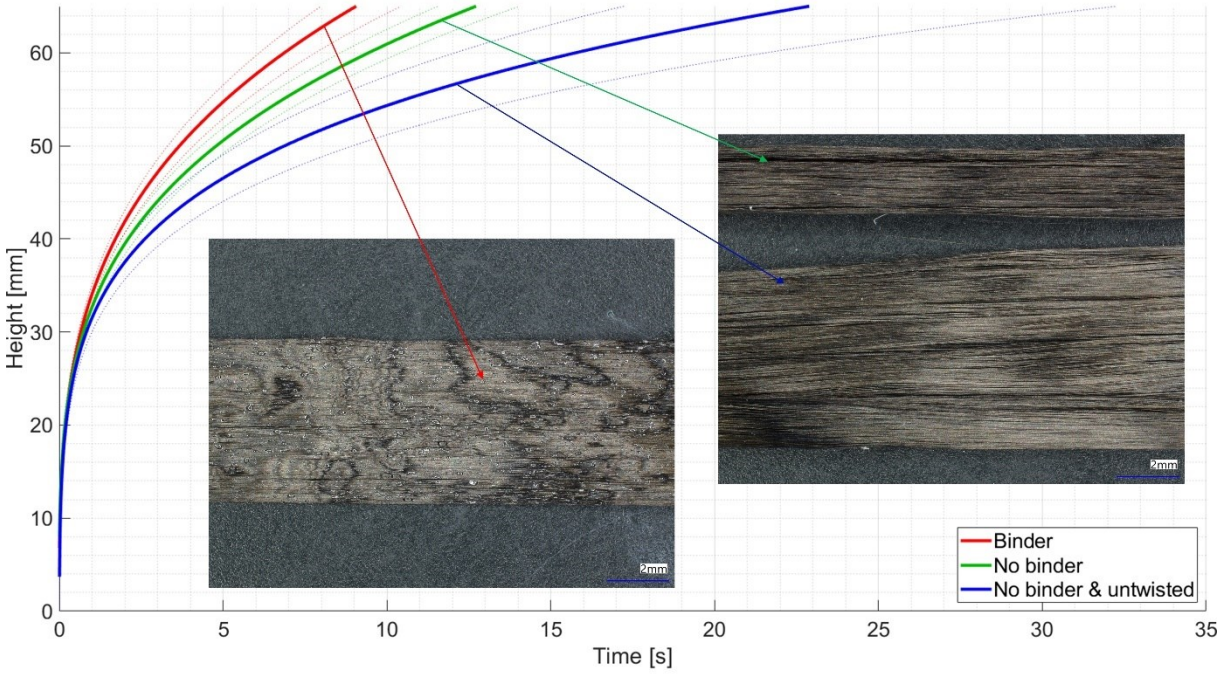

Figure 57: Capillary rise comparison between roving with and without binder (dotted lines: standard deviation)

This figure also shows that both specimens without binder show a slower capillary rise than the bindered specimen. Additionally, it can be observed that the test fluid in the untwisted, flat rovings rises even slower.

This behavior can be explained by the (cross-section) structure of the rovings. Considering the rovings without binder, the untwisted rovings also have a higher width and less height. This means that the capillary tubes are distributed flatter and less excess fluid from a neighboring tube can flow across.

Comparing the binder roving with the other material, the binder material on the outside seems to have no negative effect. Most likely, the preprocessing of these rovings is what makes their capillary flow that much faster. Before application of the binder by the manufacturer, the rovings are spread and brought to a uniform shape (width and height) which is then fixed by the binder. This makes the capillary tubes more straight and less affected by transverse filaments or an uneven distribution of the filaments in general. Figure 58 shows the difference between virgin (a) and binder (b) rovings. Due to the binder on the outside, the rovings on the right side show a more uniform distribution of the filaments. This also shortens the ways for peripheral flow which can accelerate the capillary rise within a roving.

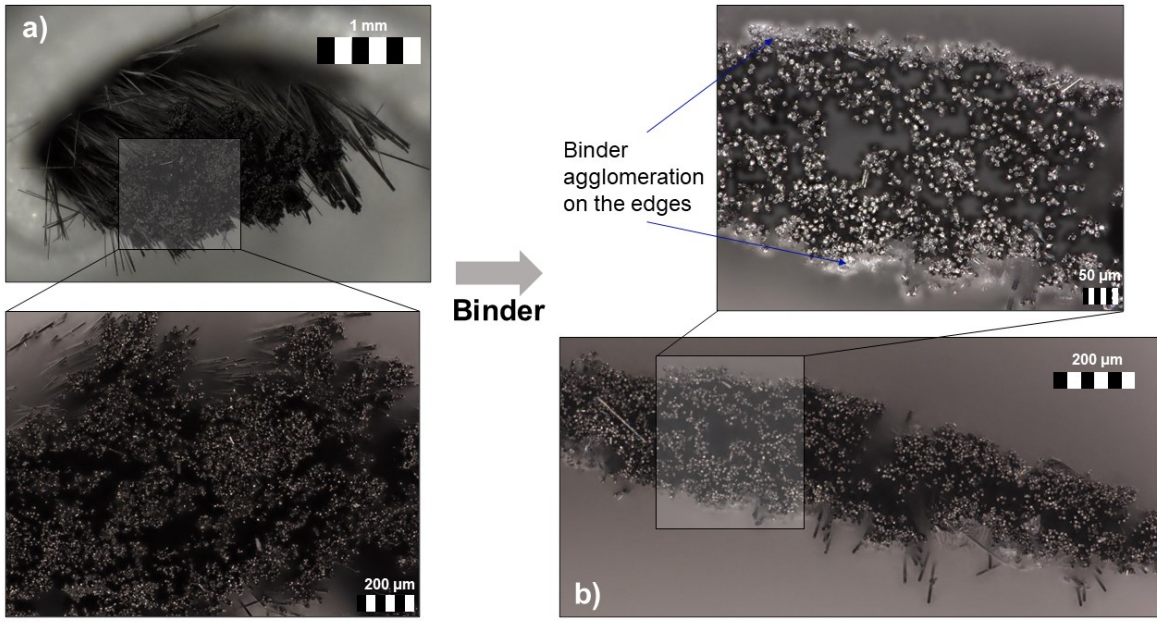

Figure 58: Microscopy comparison of rovings with (b) and without binder (a) and the respective magnifications

5.2 SUMMARY: CAPILLARY RISE

Capillary rise experiments of single-layer rovings were performed. It could be shown that the activation of the binder decelerates the capillary rise velocity due to the absorption of the binder and blocking of flow channels. The influence of tension and activation duration is harder to determine. A tendency for a slower rise after shorter activation can be observed. Yet, these measurements show high scatter and further investigation will be necessary in a process-like environment. Comparing the binder rovings with rovings without binder, a binder influence on the capillarity is not detectable. Nevertheless, the preprocessing has a major influence by straightening and fixing the (capillary) flow channels. It can be expected that properly spread and tensioned rovings without binder would show comparable results (if it would be possible to handle them in the measurement environment).

6. SUMMARY & CONCLUSION

This thesis aims to contribute to the understanding of the dry winding process with (epoxy-)bindered rovings. For that, a literature review was executed and the potential as well as weaknesses of this process were identified. A SWOT analysis (strengths, weaknesses, opportunities, threats) displayed in Figure 59 sums up the main findings. They will be presented shortly hereafter. Moreover, the results and significance of the performed experiments will be classified.

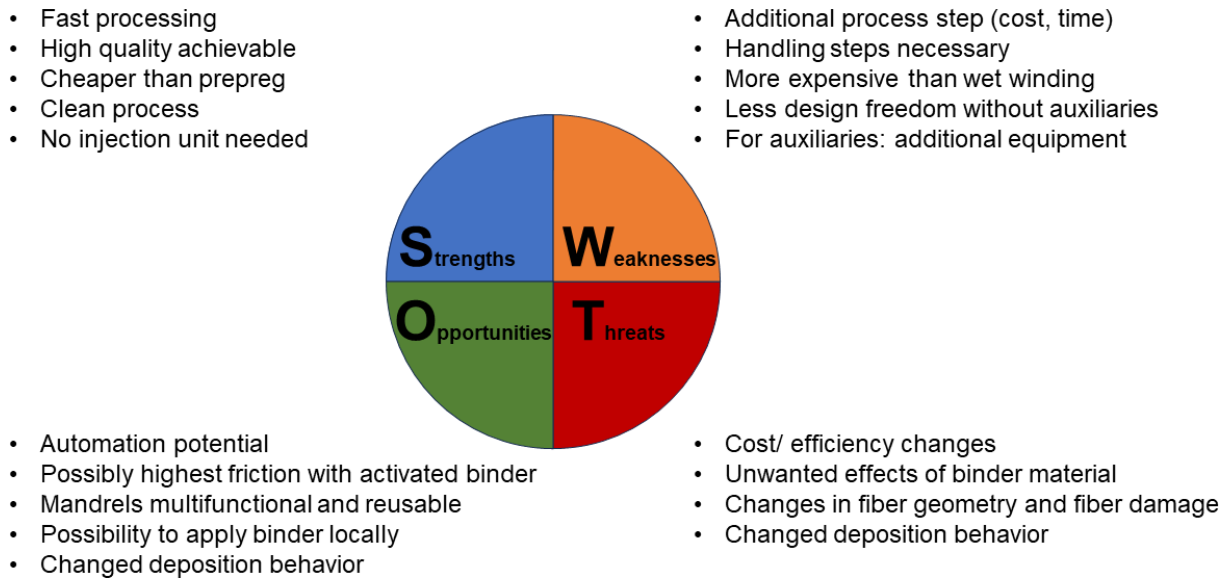

Figure 59: SWOT analysis of establishing a dry fiber winding process

In this SWOT analysis the question of using a dry fiber winding process (with or without) binder is in relation to the usage of a wet or prepreg winding process for a specific winding task. Many factors of this evaluation rely strongly on the considered product to be manufactured and the available infrastructure of the company. This will be elaborated in more detail for the various points. In addition, SWOT is divided into strengths and weaknesses caused by an internal origin and opportunities and threats caused by an external origin. The external origin here, may not strictly be something that comes from the outside world but also circumstances that (could) have not been considered here and might change the evaluation of the process.

The identified benefits of dry fiber winding process are the associated possibility for fast processing and high part quality. With the resin impregnation of the roving being

the main deceleration of a wet winding process, higher process velocities can be chosen for dry and prepreg winding. Without binder or prepreg resin on the roving, even a faster process can be imagined due to less tendency for fiber damage. Part quality of wet wound parts is usually rather mediocre.
A better quality can be achieved with prepreg parts cured in an autoclave, or dry wound parts followed by a convenient LCM process such as RTM. Both, the towpreg material as well as an autoclave curing are yet more expensive than the dry winding/LCM solution. Avoiding viscous resin during the winding process also provides other benefits. Compared with wet winding, an impregnation unit such as a resin bath or a siphon unit is not required which reduces the cost of the equipment. In addition, the process itself is much cleaner without resin being spilled. This minimizes the cleaning effort and raises workplace safety.

Much like in every modern production process, automation plays a key role in modern filament winding processes. As shown in Section 4 with a specific sensor type and a self-developed algorithm, the potential is immense. Light section sensor technology is one available method for optical, non-destructive testing which is essential for accurate inline monitoring. Experiments performed in this work indicate that profile measurement of a roving during processing is a feasible task. Speed, tension, and geometry changes can be detected and do not significantly impair the measurement quality. A good measurement environment has to be established though. Suitable background and fitting recording parameters (e.g. exposure time) have to be set up. The developed algorithm shows the potential for the usage of the profile data. Detection of defects (e.g. splitting, twisting, loose fibers), recording of speed and tension changes, control of the wound pattern, or position control are among the possible applications of this measurement method. Given a perfect measurement environment, even the determination of binder content by evaluating the particles on the surface is thinkable. Yet, there is room for improvement, especially considering the real-time processing of data.

Another aspect of the usage of automation in filament winding is the presented robotic winding setup in Section 3.2. Despite the simple core process, filament winding applications nowadays require various degrees of freedom to wind elaborate forms. Hereby, robotic winding is an open and rather cost-efficient solution given the

development potential of a robotic cell and control unit. Moreover, an open main controller unit allows for individual extensions of the system.

An advantage of using binder rovings can be the possible high friction factor. It is easily above wet and dry rovings and can even exceed prepreg, depending on the specific resin/binder material and the processing conditions (esp. activation temperature). Figure 25 shows that an activated binder roving approximately doubles the friction compared to an unbindered roving. Having a high friction of the roving on the surface enables the designer to choose more elaborate winding patterns which in turn can lead to an increase in mechanical properties of the final part. Another advantage of the usage of binder can be the local friction support, e.g., in turning zones. With less material input a winding pattern needing high adhesion can be realized.

A characteristic of a dry winding process is the two-step processing with winding and infusion. The mandrel now has to fulfill an additional function in terms of supporting the handling of the preform. Ideally, it enables winding, transport, (vacuum) infusion or injection, and can finally be removed and reused.

Depending on the processing parameters and the type of used rovings, the deposition can also change. Here, both improvement and impairment are imaginable. Further studies have to determine if layup quality is better or worse for binder rovings and how the processing influences that.

The major drawback of dry filament winding is the necessity of an additional (LCM-) process and a handling step in between. This means additional cycle time, more effort in handling tasks, and especially more overall cost. It will have to be determined if the possible better part quality or the faster winding process can make up for this additional cost. This will also strongly depend on the existing machinery, knowledge, and experience as well as on the design of the part and the desired output numbers. For high-quality parts, the additional cost of binder roving material and the extra process step must be in relation to the quality improvement of the part, i.e., meeting certain design specifications. Simple, mass-produced parts will most likely still be manufactured with wet winding, since the raw material is cheaper, and the product is directly available. The only option for dry winding (without binder) here is if the process speed increase is significant and a possibility is found to upscale the LCM process.

When planning to wind a part with dry fibers, either the design freedom is limited to a certain extent or auxiliary material has to be used. This can be binder but also mechanical elements such as pins or spikes. The process designer has to decide if a winding path can be realized without having to modify the process and if that path is the best way to meet the design criteria. If that is not possible one has to think about how to modify the process to keep the roving from slipping. This results in additional effort and cost.

The main threat to the cost efficiency of a dry winding process is a (forced) change in the cost structure or in the efficiency of the process. The decision for a dry winding process will likely be a close one. If now, for example, the raw material prices rise or a problem occurs in the LCM process that requires adaptions, it may happen that the overall efficiency is not feasible anymore.

A major concern when processing binder materials is the effect it may have on the LCM process. As a foreign material, it can influence the resin flow between the rovings. Chapter 5 showed that the binder will decelerate the capillary flow through rovings after being activated. When compared to unbindered rovings, the effect of the straightening and pre-tensioning of the rovings for binder application is more pronounced than any possible blockage by binder particles. Yet, it remains to be shown how that effect will play out in a three-dimensional wound structure. Here, the solution of the binder into the resin needs to be considered. Interdependencies with other major influences in LCM processes such as permeability and compaction behavior need to be addressed.

Since not much experience is available with the processing of dry and especially binder rovings in winding, some uncertainties regarding quality aspects may arise. Fiber damage and roving geometry changes during fiber guidance and after deposition may occur. The structure of binder rovings is stiffer and the binder particles on the surface may cause abrasion or unwanted friction. Twisting or breaking of single filaments could be a consequence of this. Moreover, impregnated rovings are lubricated. They can glide into position on the mandrel or back into the guidance on the winding machine. This behavior will be more difficult to enforce in dry winding.

In conclusion, it can be stated that dry fiber filament winding and subsequent LCM can be a viable alternative for winding processes when thoroughly and individually

scrutinized. Especially, the cost aspect has to be regarded given the already available equipment and materials. From a technical side, the process has some minor differences compared to the established wet and prepreg winding. The decision of which process to prefer is highly individual, depending on the part design and specifications as well as on (given) knowledge and equipment.

DECLARATION OF THE USAGE OF ARTIFICIAL INTELLIGENCE

Matter	Share AI [%]	Tool/Version	Notes	Prompts
Spell & grammar check	100	Grammarly Free version, online (30.06.2024 & 10.07.2024)	n/a	n/a

PUBLICATIONS

Research articles:

Neunkirchen, S.; Bender, M.; Schledjewski, R.: Effect of Binder Activation on in-Plane Capillary Flow in Multilayer Stacks of Carbon Fiber Fabrics. In: Appl. Compos. Mater. 31, No. 2 (2024), pp. 709–719.

Neunkirchen, S.; Blößl, Y.; Schledjewski, R.: A porous capillary tube approach for textile saturation. In: Compos. Sci. Technol. 230 (2022), p. 109450.

Neunkirchen, S.; Fauster, E.; Lehner, S.; O'Leary, P.: Instrumentation of an Inspection Test Rig for Geometry Measurement of Fiber Bundles in Automated Composite Manufacturing. In: IEEE Trans. Instrum. Meas. 71 (2022), p. 1–9.

Neunkirchen, S.; Schledjewski, R.: Tack measurement of bindered rovings for the dry fiber winding process. In: Polym. Compos. 42, No. 9 (2021), p. 4607–4616.

Sofi, T.; Neunkirchen, S.; Schledjewski, R.: Path calculation, technology and opportunities in dry fiber winding: a review. In: Adv. Manuf. Polym. Compos. Sci. 4, No. 3 (2018), p. 57–72.

Conference contributions:

Neunkirchen, S.; Schledjewski, R.: Dry fiber filament winding - Fundamentals and challenges. 30th Leoben-conference on polymer engineering & science. Department Polymer Engineering and Science & PCCL GmbH. Leoben, Austria, 15.09.2022.

Neunkirchen, S.; Salzmann, M.; Schledjewski, R.: Spectroscopic monitoring of prepreg properties. International Conference on Manufacturing of Advanced Composites (ICMAC) 2022. The Institute of Materials, Minerals and Mining. Sheffield, UK, 14.09.2022.

Schledjewski, R.; Blößl, Y.; Neunkirchen, S.: Capillary Driven Saturation of Textile Reinforcing Structures Proposal for an Extension of Lucas-Washburn Equation. In: Achievements and Trends in Material Forming- Peer-reviewed extended papers selected from the 25th International Conference on Material Forming, ESAFORM

2022. Vincze, G. & Barlat, F. (eds.). Trans Tech Publications, p. 1372-1378. (Key Engineering Materials; Volume 926 KEM).

Haiden, L., Feuchter, M., Barbezat, M., Pansare, A., Brunner, A. J., Neunkirchen, S. & Pinter, G. G.: Adapting the optical reflectivity of carbon fiber reinforced polymers on the nano-scale: Matrix vs. fiber modification. In: AMCA (ed.): EPF European Polymer Congress. Book of abstracts. 1st ed., Prague, p. 282, 26.06-01.07.2022.

Neunkirchen, S., Blößl, Y. & Schledjewski, R.: Experimental validation of the porous tube model for capillary rise, 23. Symposium Verbundwerkstoffe und Werkstoffverbunde – Abstract Booklet, Leoben, Austria, DGM (ed.), p. 28, 20.06.2022.

Lehner, S., Neunkirchen, S., Fauster, E. & O'Leary, P.: Instrumentation of a Roving Inspection Test Rig with Surface Geometry Measurement of Fiber Bundles. In: 2021 IEEE International Instrumentation and Measurement Technology Conference (I2MTC) Proceedings. IEEE Xplore (online): Institute of Electrical and Electronics Engineers, 29.06.2021.

Neunkirchen, S.; Schledjewski, R.: Determination of the friction coefficient in dry-fiber filament winding. In: European conference on composite materials (ECCM18). ECCM18. Athens, Greece, 22-28.06.2018.

REFERENCES

[1] Shrigandhi, G. D.; Kothavale, B. S.: Biodegradable composites for filament winding process. In: *Mater. Today: Proc.* 42 (2021), pp. 2762–2768.

[2] Hopmann, C.; Magura, N.; Rozo Lopez, N.; Schneider, D.; Fischer, K.: Detection and evaluation of the fibers' deposition parameters during wet filament winding. In: *Polymer Engineering & Sci* 61, No. 5 (2021), pp. 1353–1367.

[3] Munro, M.: Review of manufacturing of fiber composite components by filament winding. In: *Polym. Compos.* 9, No. 5 (1988), pp. 352–359.

[4] Peters, S. T.: Composite filament winding. Materials Park, Ohio: ASM International, 2011.

[5] Neitzel, M.; Mitschang, P.; Breuer, U. (Eds.): Handbuch Verbundwerkstoffe. München: Carl Hanser Verlag GmbH & Co. KG, 2014.

[6] Frketic, J.; Dickens, T.; Ramakrishnan, S.: Automated manufacturing and processing of fiber-reinforced polymer (FRP) composites: An additive review of contemporary and modern techniques for advanced materials manufacturing. In: *Addit. Manuf.* 14 (2017), pp. 69–86.

[7] Skinner, M. L.: Trends, advances and innovations in filament winding. In: *Reinf. Plast.* 50, No. 2 (2006), pp. 28–33.

[8] Vargas-Rojas, E.: Prescriptive comprehensive approach for the engineering of products made with composites centered on the manufacturing process and structured design methods: Review study performed on filament winding. In: *Compos. B. Eng.* 243 (2022), p. 110093.

[9] Andrianov, A.: A simplified analytical method for the computation of machine path in filament winding of axisymmetric structures: a case study on a bell-contoured rocket nozzle extension. In: *J Braz. Soc. Mech. Sci. Eng.* 45, No. 5 (2023).

[10] Air, A.; Shamsuddoha, M.; Gangadhara Prusty, B.: A review of Type V composite pressure vessels and automated fibre placement based manufacturing. In: *Compos. B. Eng.* 253 (2023), p. 110573.

[11] Jiang, W.; Du, F.; Drechsler, K.; Zheng, J.: Combined composites layup architecture and mechanical evaluation of type IV pressure vessels: A novel analytical approach. In: *Int. J. Hydrogen Energy* 48, No. 46 (2023), pp. 17565–17576.

[12] Alves, M. P.; Gul, W.; Cimini Junior, C. A.; Ha, S. K.: A Review on Industrial Perspectives and Challenges on Material, Manufacturing, Design and Development of Compressed Hydrogen Storage Tanks for the Transportation Sector. In: *Energies* 15, No. 14 (2022), p. 5152.

[13] Azeem, M.; Ya, H. H. et al.: Application of Filament Winding Technology in Composite Pressure Vessels and Challenges: A Review. In: *J. Storage Mater.* 49 (2022), p. 103468.

[14] Hopmann, C.; Magura, N.; Müller, R.; Schneider, D.; Fischer, K.: Impact of winding parameters on the fiber bandwidth in the cylindrical area of a hydrogen pressure vessel for generating a digital twin. In: *Polym. Compos.* 43, No. 3 (2022), pp. 1577–1589.

[15] Hübner, F.; Brückner, A. et al.: Low temperature fatigue crack propagation in toughened epoxy resins aimed for filament winding of type V composite pressure vessels. In: *Polym. Test.* 102 (2021), p. 107323.

[16] Zu, L.; Koussios, S.; Beukers, A.: Optimal cross sections of filament-wound toroidal hydrogen storage vessels based on continuum lamination theory. In: *Int. J. Hydrogen Energy* 35, No. 19 (2010), pp. 10419–10429.

[17] Dackweiler, M.: Modellierung des Fügewickelprozesses zur Herstellung von leichten Fachwerkstrukturen. Düren: Shaker, 2020.

[18] Dackweiler, M.; Hagemann, L.; Coutandin, S.; Fleischer, J.: Experimental investigation of frictional behavior in a filament winding process for joining fiber-reinforced profiles. In: *Compos. Struct.* 229 (2019), p. 111436.

[19] Dackweiler, M.; Mayer, T.; Coutandin, S.; Fleischer, J.: Modeling and optimization of winding paths to join lightweight profiles with continuous carbon fibers. In: *Prod. Eng. Res. Devel.* 13, No. 5 (2019), pp. 519–528.

[20] Rimmel, O.; May, D.; Goergen, C.; Poeppel, A.; Mitschang, P.: Development and validation of recycled carbon fiber-based binder tapes for automated tape laying processes. In: *J. Compos. Mater.* 53, No. 23 (2019), pp. 3257–3268.

[21] Koppert, J.; Boer, H. de; Weustink, A.; Beukers, A.; Bersee, H.: Virtual testing of dry filament wound thick walled pressure vessels. In: Kazuro Kageyama, T. Ishikawa, M. Hojo, S. Sugimoto und T. Ogasawara (Eds.): CD-ROM proceedings of the Sixteenth International Conference on Composite Materials. A giant step towards environmental awareness: from Green Composites to Aerospace. The Sixteenth International Conference on Composite Materials (ICCM16). Kyōto, Japan, 2007 Jul 8-13. Kyōto, Japan.

[22] Bader, M. G.: Selection of composite materials and manufacturing routes for cost-effective performance. In: *Compos. A: Appl. Sci. Manuf.* 33, No. 7 (2002), pp. 913–934.

[23] JEC Group: JEC Observer 2024_Overview of the global composites market 2023-2028. In: *JEC Composites Magazine Special Issue* (2024).

[24] Blößl, Y.: Impregnation of natural fiber reinforcements in liquid composite molding processes. dissertation. Montanuniversität Leoben, Leoben, 2021.

[25] Minsch, N.; Herrmann, F. H.; Gereke, T.; Nocke, A.; Cherif, C.: Analysis of Filament Winding Processes and Potential Equipment Technologies. In: *Procedia CIRP* 66 (2017), pp. 125–130.

[26] Shen, F. C.: A filament-wound structure technology overview. In: *Mater. Chem. Phys.* 42, No. 2 (1995), pp. 96–100.

[27] Chan, S.; Munro, M.; Fahim, A.: Accuracy-speed relationships of a robotic filament winding cell. In: *Rob. Comput. Integr. Manuf.* 12, No. 1 (1996), pp. 3–13.

[28] Scholliers, J.; van Brussel, H.: Computer-integrated filament winding. Computer-integrated design, robotic filament winding and robotic quality control. In: *Compos. Manuf.* 5, No. 1 (1994), pp. 15–23.

[29] Akovali, G.: Handbook of composite fabrication. Shawbury, U.K.: Rapra Technology Ltd, 2001.

[30] Paessler, M.; Miaris, A.; Schledjewski, R.; Mitschang, P.: Ring Winding Technology: Increased Process Efficiency and Effects on the Mechanical Properties of Ring Specimens. In: ASME 2011 Pressure Vessels and Piping Conference: Volume 6, Parts A and B. ASME 2011 Pressure Vessels and Piping Conference. Baltimore, Maryland, USA, 2011 Jul 17–21: ASME, pp. 69–77.

[31] Koussios, S.; Bergsma, O. K.; Beukers, A.: Filament winding. Part 2. Generic kinematic model and its solutions. In: *Compos. A: Appl. Sci. Manuf.* 35, No. 2 (2004), pp. 197–212.

[32] Koussios, S.: Filament Winding: a Unified Approach. dissertation. TU Delft, Delft, Netherlands, 2004.

[33] Campbell, F. C.: Manufacturing processes for advanced composites. Oxford: Elsevier, 2004.

[34] Buragohain, M. K.: Composite Structures. Design, Mechanics, Analysis, Manufacturing, and Testing. 1st ed. London: CRC Press, 2017.

[35] Mazumdar, S. K.; Hoa, S. V.: Analytical Models for Low Cost Manufacturing of Composite Components by Filament Winding, Part I. Direct Kinematics. In: *J. Compos. Mater.* 29, No. 11 (1995), pp. 1515–1541.

[36] Arrabiyeh, P. A.; May, D.; Eckrich, M.; Dlugaj, A. M.: An overview on current manufacturing technologies: Processing continuous rovings impregnated with thermoset resin. In: *Polym. Compos.* 42, No. 11 (2021), pp. 5630–5655.

[37] Lossie, M., Van Brussel, H.: Design principles in filament winding. In: *Compos. Manuf.* 5, No. 1 (1994), pp. 5–13.

[38] Peters, S. T.: Handbook of composites. 2. ed. London, UK: Chapman and Hall; Chapman & Hall, 1998.

[39] Gąsior, P.; Wachtarczyk, K. et al.: Validation of Selected Optical Methods for Assessing Polyethylene (PE) Liners Used in High Pressure Vessels for Hydrogen Storage. In: *Appl. Sci.* 11, No. 12 (2021), p. 5667.

[40] Bodea, S.; Zechmeister, C.; Dambrosio, N.; Dörstelmann, M.; Menges, A.: Robotic coreless filament winding for hyperboloid tubular composite components in construction. In: *Autom. Constr.* 126 (2021), p. 103649.

[41] Minsch, N.; Müller, M.; Gereke, T.; Nocke, A.; Cherif, C.: 3D truss structures with coreless 3D filament winding technology. In: *J. Compos. Mater.* 53, No. 15 (2019), pp. 2077–2089.

[42] La Magna, R.; Waimer, F.; Knippers, J.: Coreless Winding and Assembled Core – Novel fabrication approaches for FRP based components in building construction. In: *Constr. Build. Mater.* 127 (2016), pp. 1009–1016.

[43] Zhang, P.; Sun, R.; Huang, T.: A geometric method for computation of geodesic on parametric surfaces. In: *Comput. Aided Geom. Des.* 38 (2015), pp. 24–37.

[44] Eschenburg, J.-H.; Jost, J.: Differentialgeometrie und Minimalflächen. 2. Aufl. Berlin, Heidelberg: Springer-Verlag, 2007.

[45] Oprea, J.: Differential geometry and its applications. 2. ed. Washington DC: Mathematical Association of America, 2007.

[46] Weinstock, R.: Calculus of Variations. Newburyport: Dover Publications, 2012.

[47] Sofi, T.; Neunkirchen, S.; Schledjewski, R.: Path calculation, technology and opportunities in dry fiber winding: a review. In: *Adv. Manuf. Polym. Compos. Sci.* 4, No. 3 (2018), pp. 57–72.

[48] Koussios, S.; Bergsma, O. K.; Beukers, A.: Filament winding. Part 1. Determination of the wound body related parameters. In: *Compos. A: Appl. Sci. Manuf.* 35, No. 2 (2004), pp. 181–195.

[49] Blaga, P. A.: Lectures on the Differential Geometry of Curves and Surfaces. Babeş-Bolyai University. Cluj-Napoca, 2005.

[50] Kreyszig, E.: Differential geometry. New York: Dover Publications, 1991.

[51] Carmo, M. P. d.: Differential geometry of curves and surfaces. [reprint]. Upper Saddle River, NJ: Prentice-Hall, 1976.

[52] Kühnel, W.: Differentialgeometrie. Kurven - Flächen - Mannigfaltigkeiten. 6., akt. Aufl. 2013. Wiesbaden: Springer, 2013.

[53] Patrikalakis, N. M.; Maekawa, T.: Shape Interrogation for Computer Aided Design and Manufacturing. Berlin, Heidelberg: Springer, 2010.

[54] Kasap, E.; Yapici, M.; Akyildiz, F. T.: A numerical study for computation of geodesic curves. In: *Appl. Math. Comput.* 171, No. 2 (2005), pp. 1206–1213.

[55] E. I. Abdel-Galil; Nassar H. Abdel-All: Numerical Treatment of Geodesic Differential Equations on a Surface in R3. In: *Int. Math. Forum* 8, No. 1 (2013), pp. 15–29.

[56] Zhang, P.; Yin, L.; Zhou, Z.; Huang, L.: Solving the Boundary Value Problem of Curves With Prescribed Geodesic Curvature Based on a Cubic B-Spline Element Method. In: *IEEE Access* 9 (2021), pp. 119381–119394.

[57] Zu, L.; Koussios, S.; Beukers, A.: Design of filament-wound circular toroidal hydrogen storage vessels based on non-geodesic fiber trajectories. In: *Int. J. Hydrogen Energy* 35, No. 2 (2010), pp. 660–670.

[58] Li, X.; Lin D.: Non-geodesic winding equations on a general surface of revolution. In: F. L. Matthews (Ed.): ICCM & ECCM. The proceedings of the Sixth International Conference on Composite Materials combined with the Second European Conference on Composite Materials. Imperial College of Science and Technology, London, UK, July 20-24 1987. Imperial College of Science and Technology; International Conference on Composite Materials; European Conference on Composite Materials. London, UK: Elsevier, pp. 1152–1160.

[59] Youdong, L.; Zhenqiang, Z.; Guozhao, W.: An extension of clariaut equation and its application. In: *Appl. Math. Chin. Univ.* 12, No. 1 (1997), pp. 1–14.

[60] Menges, G.; Wodicka, R.; Barking, H. L.: Non-geodesic winding on a surface of revolution. In: Society of the Plastics Industry Reinforced Plastics (Ed.): Proceedings of the 33rd Annual Conference-SPI Reinforced Plastics Composites Institute. Washington, D.C., 1978 Feb 7-10. New York: Society of the Plastics Industry.

[61] Carvalho, J. de; Lossie, M.; Vandepitte, D.; van Brussel, H.: Optimization of filament-wound parts based on non-geodesic winding. In: *Compos. Manuf.* 6, No. 2 (1995), pp. 79–84.

[62] Barking, H. L.: Steuerungskonzepte für das Präzisionswickeln von faserverstärkten Kunststoffen. dissertation. RWTH Aachen, Aachen, Germany. Institut für Kunststoffverarbeitung, 1977.

[63] Liang, Y. D.; Zou, Z. Q.; Zhang, Z. F.: Quasigeodesics - a new class of simple and non-slip trajectories on revolutional surfaces. In: 28th International SAMPE Technical Conference, 1996 Nov 4-7, pp. 1071–1079.

[64] Wells, G. M.; McAnulty, K. F.: Computer aided filament winding using non-geodesic trajectories. In: F. L. Matthews (Ed.): ICCM & ECCM. The proceedings of the Sixth International Conference on Composite Materials combined with the Second European Conference on Composite Materials. Imperial College of Science and Technology, London, UK, July 20-24 1987. Imperial College of Science and Technology; International Conference on Composite Materials; European Conference on Composite Materials. London, UK: Elsevier, pp. 1161–1173.

[65] Koussios, S.; Bergsma, O. K.; Mitchell, G.: Non-geodesic filament winding on generic shells of revolution. In: *Proceedings of the IMechE* 219, No. 1 (2005), pp. 25–35.

[66] DiVita, G.; Marchetti, M.; Moroni, P.; Perugini, P.: Designing complex shape filament-wound structures. In: *Compos. Manuf.* 3, No. 1 (1992), pp. 53–58.

[67] Lossie, M.; Vandepitte, D.: Extending filament winding capabilities towards obstacle integration. In: *WIT Trans. Eng. Sci.* 10 (1996), pp. 243–252.

[68] Park, J.-S.; Hong, C.-S.; Kim, C.-G.; Kim, C.-U.: Analysis of filament wound composite structures considering the change of winding angles through the thickness direction. In: *Compos. Struct.* 55, No. 1 (2002), pp. 63–71.

[69] Kayran, A.; İbrahimoğlu, C. S.: Preliminary study on the applicability of semi-geodesic winding in the design and manufacturing of composite towers. In: *J. Phys.: Conf. Ser.* 555 (2014), p. 12059.

[70] Mazumdar, S. K.; Hoa, S. V.: Algorithm for filament winding of non-axisymmetric tapered composite components having polygonal cross-section on two-axes filament-winding machine. In: *Compos. Eng.* 4, No. 3 (1994), pp. 343–359.

[71] Fu, J. H.; Yun, J. D.; Jung, Y. H.: Winding Trajectory Generation for Composite Products. In: *AMM* 541-542 (2014), pp. 407–411.

[72] Fu, J.; Yun, J.; Jung, Y.; Lee, D.: Generation of filament-winding paths for complex axisymmetric shapes based on the principal stress field. In: *Compos. Struct.* 161 (2017), pp. 330–339.

[73] Fu, J.; Yun, J.; Jung, Y.: Filament winding path generation based on the inverse process of stability analysis for non-axisymmetric mandrels. In: *J. Compos. Mater.* 51, No. 21 (2016), pp. 2989–3002.

[74] Carrino, L.; Polini, W.; Sorrentino, L.: Modular structure of a new feed-deposition head for a robotized filament winding cell. In: *Compos. Sci. Technol.* 63, No. 15 (2003), pp. 2255–2263.

[75] Zu, L.: Stability of fiber trajectories for winding toroidal pressure vessels. In: *Compos. Struct.* 94, No. 5 (2012), pp. 1855–1860.

[76] E. Anamateros; L. Carrino et al.: A solution to manufacture structural parts with concave surfaces by robotized filament winding. In: *National Aerospace Laboratory NLR* 3 (2007), pp. 1339–1348.

[77] Laval, C.: CADWIND 2006 – 20 years of filament winding experience. In: *Reinf. Plast.* 50, No. 2 (2006), pp. 34–37.

[78] Scholliers, J.: Robotic Filament Winding of Asymmetric Composite Parts. dissertation. KU Leuven, Leuven, Belgium, 1992.

[79] TANIQ B.V.: Composite Design Software TaniqWind Pro — TANIQ. https://www.taniq.com/taniqwindpro (27.04.2024).

[80] Crescent Consultants Ltd: Filament Winding Software by Cadfil. https://www.cadfil.com/index.html (27.04.2024).

[81] Johansen, B.; Lystrup, A.; Jensen, M.: CADPATH. A complete program for the CAD-, CAE- and CAM-winding of advanced fibre composites. In: *J. Mater. Process. Technol.* 77, No. 1-3 (1998), pp. 194–200.

[82] Composicad: Home - Composicad. https://www.composicad.com/ (27.04.2024).

[83] Engineering Technology Corporation: Winding Software. https://etcwinders.com/filament-winding-software/ (27.04.2024).

[84] Ahmadi Jebeli, M.; Heidari-Rarani, M.: Development of Abaqus WCM plugin for progressive failure analysis of type IV composite pressure vessels based on Puck failure criterion. In: *Eng. Fail. Anal.* 131 (2022), p. 105851.

[85] MATERIAL SA: CADWIND V9 User Manual. Brussels, Belgium.

[86] Markov, L.; Cheng, R. M.: Conceptual design of robotic filament winding complexes. In: *Mechatronics* 6, No. 8 (1996), pp. 881–896.

[87] Weisberg, A.; Aceves, S. M.: The potential of dry winding for rapid, inexpensive manufacture of composite overwrapped pressure vessels. In: *Int. J. Hydrogen Energy* 40, No. 11 (2015), pp. 4207–4211.

[88] Mertiny, P.; Ellyin, F.: Influence of the filament winding tension on physical and mechanical properties of reinforced composites. In: *Compos. A: Appl. Sci. Manuf.* 33, No. 12 (2002), pp. 1615–1622.

[89] Polini, W.; Sorrentino, L.: Influence of winding speed and winding trajectory on tension in robotized filament winding of full section parts. In: *Compos. Sci. Technol.* 65, No. 10 (2005), pp. 1574–1581.

[90] Polini, W.; Sorrentino, L.: Estimation of the winding tension to manufacture full section parts with robotized filament winding technology. In: *Adv. Compos. Mater* 14, No. 4 (2005), pp. 305–318.

[91] Duvall, F. W.: Cost comparisons of wet filament winding versus prepreg filament winding for Type II and Type IV CNG cylinders. In: Thierry Massard (Ed.): ICCM-12 Europe. 12th International Conference on Composite Materials; Palais des Congrès,Paris. International Conference on Composite Materials; ICCM Europe. Paris.

[92] Miaris, A.; Paessler, M.; Schledjewski, R.; Mitschang, P.: Modeling the Impregnation Process of a Siphon Impregnation System During Filament Winding. In: ASME 2011 Pressure Vessels and Piping Conference: Volume 6, Parts A and B. ASME 2011 Pressure Vessels and Piping Conference. Baltimore, Maryland, USA, 2011 Jul 17–21: ASME, pp. 79–87.

[93] Dalibor, I. H.; Almeida Jr., J.; Costamilan, E.; Shynkarenko, O.; Amico, S. C.: Design of a composite nozzle manufactured by filament winding. In: V. Tita und J. M. Ferreira (Eds.): Meeting on Aeronautical Composite Materials and Structures - MACMS 2015. MACMS 2015. São Carlos, Brazil, 2015 Dec 3-4.

[94] Dalibor, I. H.; Lisbôa, T. V.; Marczak, R. J.; Amico, S. C.: Influence of slippage coefficient on the non-geodesic return trajectory at mandrels extremities in filament winding process. In: Proceedings of the 4th Brazilian Conference on Composite Materials. Brazilian Conference on Composite Materials, 22/07/2018: Pontifícia Universidade Católica do Rio de Janeiro, pp. 717–724.

[95] Lisbôa, T. V.; Almeida, J. H. S. et al.: The role of winding pattern on filament wound composite cylinders under radial compression. In: *Polym. Compos.* 41, No. 6 (2020), pp. 2446–2454.

[96] Howell, D. D.; Roundy, F. E.: Filament Wound Preforms for RTM. In: John E. Green und Society for the Advancement of Material and Process Engineering. Mira Digital Publishing. (Eds.): Advanced materials & processes: preparing for the new millennium: 31st International SAMPE Technical Conference. 31st International SAMPE Technical Conference. McCormick Place, Chicago, Illinois, 1999 Oct 26-30. [Covina Calif.]: Society for the Advancement of Material and Process Engineering.

[97] Andrianov, A.; Tomita, E. K.; Veras, C. A. G.; Telles, B.: A Low-Cost Filament Winding Technology for University Laboratories and Startups. In: *Polymers* 14, No. 5 (2022).

[98] Irfan, M. S.; Machavaram, V. R. et al.: Lateral spreading of a fiber bundle via mechanical means. In: *J. Compos. Mater.* 46, No. 3 (2012), pp. 311–330.

[99] Wang, R.; Jiao, W.; Liu, W.; Yang, F.; He, X.: Slippage coefficient measurement for non-geodesic filament-winding process. In: *Compos. A: Appl. Sci. Manuf.* 42, No. 3 (2011), pp. 303–309.

[100] Koussios, S.; Bergsma, O. K.: Friction Experiments for Filament Winding Applications. In: *J. Thermoplast. Compos. Mater.* 19, No. 1 (2006), pp. 5–34.

[101] Di Vita, G.; Grimaldi, M.; Marchetti, M.; Moroni, P.: The Filament Winding Manufacturing Technique: Studies on the Determination of the Friction Coefficient

and on the Optimization of Feed-Eye Motion. In: Leon D. Michelove und Richard P. Caruso (Eds.): Advanced Materials. Looking ahead to the 21. century. International SAMPE Technical Conference. International SAMPE Technical Conference. Boston, MA, November 6 -8 1990. International SAMPE Technical Conference. Covina, Calif.: Society for Advancement of Material and Process Engineering (International SAMPE Technical Conference, 22).

[102] Neunkirchen, S.; Schledjewski, R.: Determination of the friction coefficient in dry-fiber filament winding. In: European conference on composite materials (ECCM18). ECCM18. Athens, Greece, 22-28.06.2018.

[103] Dalibor, I. H.; Lisbôa, T. V.; Marczak, R. J.; Amico, S. C.: Optimum slippage dependent, non-geodesic fiber path determination for a filament wound composite nozzle. In: *Eur. J. Mech. A. Solids* 82 (2020), p. 103994.

[104] Ufer, J.: Reibverhalten von trockenen Faserstrukturen aus einem direkten Faserablageprozess. In: *Zeitschrift Kunststofftechnik* 1 (2016), pp. 311–337.

[105] Cornelissen, B.; Warnet, L.; Akkerman, R.: Friction measurements on carbon fibre tows. In: *EPJ Web of Conferences* 6 (2010), p. 4004.

[106] Cornelissen, B.; Rietman, B.; Akkerman, R.: Frictional behaviour of high performance fibrous tows: Friction experiments. In: *Compos. A: Appl. Sci. Manuf.* 44 (2013), pp. 95–104.

[107] Cornelissen, B.; Sachs, U.; Rietman, B.; Akkerman, R.: Dry friction characterisation of carbon fibre tow and satin weave fabric for composite applications. In: *Compos. A: Appl. Sci. Manuf.* 56 (2014), pp. 127–135.

[108] Madhavi, M.; Rama Swamy, K.; Rao, K.; Narayana Rao, K.: Experimental Evaluation of Available Surface Friction Factor on a Hoop Substrate for a Filament-wound Composite Pressure Vessel. In: *J. Thermoplast. Compos. Mater.* 24, No. 2 (2010), pp. 279–297.

[109] Brody, J. C.; Gillespie, J. W.: Reactive and non-reactive binders in glass/vinyl ester composites. In: *Polym. Compos.* 26, No. 3 (2005), pp. 377–387.

[110] Terekhov, I. V.; Chistyakov, E. M.: Binders Used for the Manufacturing of Composite Materials by Liquid Composite Molding. In: *Polymers* 14, No. 1 (2021).

[111] Lionetto, F.; Moscatello, A.; Maffezzoli, A.: Effect of binder powders added to carbon fiber reinforcements on the chemoreology of an epoxy resin for composites. In: *Compos. B. Eng.* 112 (2017), pp. 243–250.

[112] Schmidt, S.; Mahrholz, T.; Kühn, A.; Wierach, P.: Powder binders used for the manufacturing of wind turbine rotor blades. Part 1. Characterization of resin-binder interaction and preform properties. In: *Polym. Compos.* 39, No. 3 (2018), pp. 708–717.

[113] Coutandin, S.; Wurba, A. et al.: Mechanical characterisation of the shear, bending and friction behaviour of bindered woven fabrics during the forming process. In: *Materialwiss. Werkstofftech.* 50, No. 12 (2019), pp. 1573–1587.

[114] Dickert, M.: Einfluss von Binder auf die Herstellung von Faserkunststoffverbunden. dissertation. TU Clausthal, Clausthal, 2015.

[115] Dickert, M.; Ziegmann, G.: Influence of binder on the mechanical properties and the permeability of a non-crimp fabric preform. ECCM15. ECCM. Venice, Italy, 24.06.2012.

[116] Mack, J.: Entwicklung eines adaptiven Online-Bebinderungsprozesses für die Preformherstellung. dissertation. TU Kaiserslautern, Kaiserslautern, 2015.

[117] Ivanov, D. S.; White, J. A. P. et al.: Stabilizing textile preforms by means of liquid resin print: a feasibility study. In: *Adv. Manuf. Polym. Compos. Sci.* 1, No. 1 (2015), pp. 26–35.

[118] Möllers, H.; Schmidt, C.; Meiners, D.: Spray binder for automated preforming: Spray process and preform properties. In: *Polym. Compos.* 44, No. 1 (2023), pp. 432–443.

[119] Hillermeier, R. W.; Seferis, J. C.: Interlayer toughening of resin transfer molding composites. In: *Compos. A: Appl. Sci. Manuf.* 32, No. 5 (2001), pp. 721–729.

[120] Veldenz, L.; Di Francesco, M. et al.: Characteristics and Processability of Bindered Dry Fibre Material for Automated Fibre Placement. In: Proceedings of the 17th European Conference on Composite Materials. 17th European Conference on Composite Materials (ECCM17). Munich, Germany, 26-30th June 2016. European

Conference on Composite Materials; European Society for Composite Materials; ECCM. Augsburg: MAI Carbon Cluster Management GmbH.

[121] Tonejc, M.; Ebner, C.; Fauster, E.; Schledjewski, R.: Influence of test fluids on the permeability of epoxy powder bindered non-crimp fabrics. In: *Adv. Manuf. Polym. Compos. Sci.* 40 (2019), pp. 1–12.

[122] Chen, J.; Backes, D.; Jayaraman, K.: Dynamics of binder displacement in liquid molding. In: *Polym. Compos.* 17, No. 1 (1996), pp. 23–33.

[123] Tanoglu, M.; Robert, S. et al.: Effects of thermoplastic preforming binder on the properties of S2-glass fabric reinforced epoxy composites. In: *Int. J. Adhes. Adhes.* 21, No. 3 (2001), pp. 187–195.

[124] Klingele, J.; Greb, C.; Linke, M.; Gries, T.: Auftrag und Aktivierung von Bindern. In: *Lightweight Des.* 4, No. 6 (2011), pp. 54–61.

[125] Mack, J.; Mitschang, P.: Efficient and Flexible Technology for Binder Roving Manufacturing. In: *KMUTNB: IJAST* (2015), pp. 1–8.

[126] Kunz, H.; Löchte, C. et al.: Novel form-flexible handling and joining tool for automated preforming. In: *Science and Engineering of Composite Materials* 22, No. 2 (2015), pp. 199–213.

[127] Rimmel, O.; Becker, D.; Mitschang, P.: Maximizing the out-of-plane-permeability of preforms manufactured by dry fiber placement. In: *Adv. Manuf. Polym. Compos. Sci.* 2, No. 3-4 (2016), pp. 93–102.

[128] Ehsani, F.; Hoa, S. V.; Shadmehri, F.: Effect of gaps on preform and laminate made by automated dry fiber placement and resin infusion. In: *Compos. A: Appl. Sci. Manuf.* 173 (2023), p. 107629.

[129] Veldenz, L.; Di Francesco, M.; Giddings, P.; Kim, B. C.; Potter, K.: Material selection for automated dry fiber placement using the analytical hierarchy process. In: *Adv. Manuf. Polym. Compos. Sci.* 4, No. 4 (2018), pp. 83–96.

[130] Helber, F.; Carosella, S.; Middendorf, P.: Effects of reactive and non-reactive tackifying agents on mechanical neat resin and composite performance for

preforming processes and Liquid Resin Infusion (LRI) techniques. In: *Adv. Manuf. Polym. Compos. Sci.* 9, No. 1 (2023).

[131] Rimmel, O.; Mack, J.; Becker, D.; Mitschang, P.: Automatisierte Faserdirektablage mit Online-Bebinderung. In: *Lightweight Des.* 10, No. 2 (2017), pp. 56–61.

[132] Grohmann, Y.; Stoffers, N.; Kühn, A.; Mahrholz, T.: Development of the Direct Roving Placement Technology (DRP). In: Proceedings of the 17th European Conference on Composite Materials. 17th European Conference on Composite Materials (ECCM17). Munich, Germany, 26-30th June 2016. European Conference on Composite Materials; European Society for Composite Materials; ECCM. Augsburg: MAI Carbon Cluster Management GmbH.

[133] Wu, W.; Jiang, B. et al.: Effect of Compaction and Preforming Parameters on the Compaction Behavior of Bindered Textile Preforms for Automated Composite Manufacturing. In: *Appl. Compos. Mater.* 20, No. 5 (2013), pp. 907–926.

[134] Helber, F.; Szcesny, M.; Carosella, S.; Middendorf, P.: Enhancement on automated preforming for composite structures. ICCM22. Melbourne, 11.08.2019.

[135] ISO 472:2013, 02.2013: Plastics — Vocabulary. Available at: https://www.iso.org/standard/44102.html.

[136] Budelmann, D.; Schmidt, C.; Meiners, D.: Prepreg tack: A review of mechanisms, measurement, and manufacturing implication. In: *Polym. Compos.* 41, No. 9 (2020), pp. 3440–3458.

[137] Neunkirchen, S.; Schledjewski, R.: Tack measurement of bindered rovings for the dry fiber winding process. In: *Polym. Compos.* 42, No. 9 (2021), pp. 4607–4616.

[138] Ladegourdie, M.; Kua, J.: Performance Analysis of OPC UA for Industrial Interoperability towards Industry 4.0. In: *IoT* 3, No. 4 (2022), pp. 507–525.

[139] Parmar, H.; Khan, T.; Tucci, F.; Umer, R.; Carlone, P.: Advanced robotics and additive manufacturing of composites: towards a new era in Industry 4.0. In: *Mater. Manuf. Processes* (2021), pp. 1–35.

[140] Carrino, L.; Polini, W.; Sorrentino, L.: Experimental validation of a new fibre deposition device for a robotized filament winding cell. In: Composites for the future : 10th European Conference on Composite Materials (ECCM-10). ECCM-10. Old st. Jan Conference Centre, Brugge, Belgium, 2002 Jun 3-7. Brugge.

[141] Almeida, J. H. S.; St-Pierre, L. et al.: Design, modeling, optimization, manufacturing and testing of variable-angle filament-wound cylinders. In: *Compos. B. Eng.* 225 (2021), p. 109224.

[142] Polini, W.; Sorrentino, L.: Winding Trajectory and Winding Time in Robotized Filament Winding of Asymmetric Shape Parts. In: *J. Compos. Mater.* 39, No. 15 (2016), pp. 1391–1411.

[143] Finkenwerder, F. A.; Geistbeck, M.; Middendorf, P.: Study on the validation of ring filament winding methods for unidirectional preform ply manufacturing. In: *Adv. Manuf. Polym. Compos. Sci.* 2, No. 3-4 (2016), pp. 103–116.

[144] Sorrentino, L.; Marchetti, M.; Bellini, C.; Delfini, A.; Del Sette, F.: Manufacture of high performance isogrid structure by Robotic Filament Winding. In: *Compos. Struct.* 164 (2017), pp. 43–50.

[145] Romano, D.; Pedone, P.: Economic assessment of Product-Process Innovation in Filament Winding Technology. 9th-QMOD. UK, 9-11/08/2006.

[146] REN, S.; Lu, H.; WANG, Y.; FU, H.: Development of PLC-based Tension Control System. In: *Chin. J. Aeronaut.* 20, No. 3 (2007), pp. 266–271.

[147] Yadav, N.; Schledjewski, R.: Review of in-process defect monitoring for automated tape laying. In: *Compos. A: Appl. Sci. Manuf.* 173 (2023), p. 107654.

[148] Meister, S.; Wermes, M. A. M.; Stüve, J.; Groves, R. M.: Review of image segmentation techniques for layup defect detection in the Automated Fiber Placement process. In: *J Intell Manuf* 32, No. 8 (2021), pp. 2099–2119.

[149] Schlegel, K.: A literature review of quality control for automated lay-up processes. In: *Zeitschrift Kunststofftechnik* 15, No. 6 (2019), pp. 392–436.

[150] Oromiehie, E.; Prusty, B. G.; Compston, P.; Rajan, G.: Automated fibre placement based composite structures: Review on the defects, impacts and inspections techniques. In: *Compos. Struct.* 224 (2019), p. 110987.

[151] Krombholz, C.; Bock, M.; Perner, M.; Röstermundt, D.; Meyer, M.: Online Bahnkorrektur eines Industrieroboters mittels optischer Sensoren für den Einsatz im Fiber-Placement-Prozess. In: 60. Deutscher Luft- und Raumfahrtkongress 2011. 27. - 29. September 2011, Congress Centrum Bremen ; Tagungsband - Manuskripte. Bonn: Deutsche Gesellschaft f. Luft- u. Raumfahrt, pp. 503–513.

[152] Schmitt, R.; Niggemann, C.; Mersmann, C.: Contour scanning of textile preforms using a light-section sensor for the automated manufacturing of fibre-reinforced plastics. In: Francis Berghmans, Anna G. Mignani, Antonello Cutolo, Patrick P. Meyrueis und Thomas P. Pearsall (Eds.): Optical Sensors 2008. Photonics Europe. Strasbourg, France, Monday 7 April 2008: SPIE (SPIE Proceedings), 70031I.

[153] Eitzinger, C.; Zambal, S.: Inline Inspection Technologies for Processing of Dry Fibre Materials. SAMPE Europe Conference 2018 Southampton. SAMPE. Southampton, UK, 2018.

[154] Yadav, N.; Oswald-Tranta, B. et al.: In-line and off-line NDT defect monitoring for thermoplastic automated tape layup. In: *NDT & E International* 137 (2023), p. 102839.

[155] Juarez, P. D.; Cramer, K. E.; Seebo, J. P.: Advances in in situ inspection of automated fiber placement systems. In: Joseph N. Zalameda und Paolo Bison (Eds.): Thermosense: Thermal Infrared Applications XXXVIII. SPIE Commercial + Scientific Sensing and Imaging. Baltimore, Maryland, United States, Sunday 17 April 2016: SPIE (SPIE Proceedings), p. 986109.

[156] Cemenska, J.; Rudberg, T.; Henscheid, M.: Automated In-Process Inspection System for AFP Machines. In: *SAE Int. J. Aerosp.* 8, No. 2 (2015).

[157] Shadmehri, F.; Ioachim, O. et al.: Laser-vision inspection system for automated fiber placement (AFP) process. ICCM20. Copenhagen, 19.07.2015.

[158] Schmitt, R.; Niggemann, C.; Mersmann, C.: Laser light-section sensor automating the production of textile-reinforced composites. In: Francesco Baldini, Jiri Homola und Robert A. Lieberman (Eds.): Optical Sensors 2009. SPIE Europe Optics + Optoelectronics. Prague, Czech Republic, Monday 20 April 2009: SPIE (SPIE Proceedings), 73560P.

[159] Krombholz, C.; Perner, M.; Bock, M.; Röstermundt, D.: Improving the Production Quality of the Automated Fiber Placement Process by Means of Online Path Correction. 28th International Congress of the Aeronautical Science. Brisbane, Australia, 23.09.2012.

[160] Nguyen, C. D.; Krombholz, C.; Röstermundt, D.: Einfluss einer Online Bahnkorrektur auf die Materialeigenschaften von Prepreg Tows im Fiber Placement Prozess. Deutscher Luft- und Raumfahrtkongress. Berlin, 10.09.2012.

[161] Kastanis, D.; Steiner, H.; Fauster, E.; Schledjewski, R.: Compaction behavior of continuous carbon fiber tows: an experimental analysis. In: *Adv. Manuf. Polym. Compos. Sci.* 1, No. 3 (2015), pp. 169–174.

[162] Tonejc, M.; Steiner, H.; Fauster, E.; Konstantopoulos, S.; Schledjewski, R.: A Study on Geometrical Parameters Influencing the Mechanical Spreading of Fibre Bundles. ICCM20. ICCM. Copenhagen, 19.07.2015.

[163] Schuster, A.; Mayer, M.; Willmeroth, M.; Brandt, L.; Kupke, M.: Inline Quality Control for Thermoplastic Automated Fibre Placement. In: *Procedia Manuf.* 51 (2020), pp. 505–511.

[164] Kissinger, C.: Ganzheitliche Betrachtung der Harzinjektionstechnik. Messsystem zur durchgängigen Fertigungskontrolle. dissertation. TU Kaiserslautern, Kaiserslautern, 2001.

[165] Ruiz, E.; Achim, V.; Soukane, S.; Trochu, F.; Bréard, J.: Optimization of injection flow rate to minimize micro/macro-voids formation in resin transfer molded composites. In: *Compos. Sci. Technol.* 66, No. 3-4 (2006), pp. 475–486.

[166] Patel, N.; Lee, L. J.: Modeling of void formation and removal in liquid composite molding. Part I: Wettability analysis. In: *Polym. Compos.* 17, No. 1 (1996), pp. 96–103.

[167] Shih, C.-H.; Lee, L. J.: Tackification of Textile Fiber Preforms in Resin Transfer Molding. In: *J. Compos. Mater.* 35, No. 21 (2001), pp. 1954–1981.

[168] Simacek, P.; Advani, S. G.: A numerical model to predict fiber tow saturation during liquid composite molding. In: *Compos. Sci. Technol.* 63, No. 12 (2003), pp. 1725–1736.

[169] Lawrence, J. M.; Neacsu, V.; Advani, S. G.: Modeling the impact of capillary pressure and air entrapment on fiber tow saturation during resin infusion in LCM. In: *Compos. A: Appl. Sci. Manuf.* 40, No. 8 (2009), pp. 1053–1064.

[170] Zhao, C.; Yang, B. et al.: Three-Dimensional Numerical Simulation of Meso-Scale-Void Formation during the Mold-Filling Process of LCM. In: *Appl. Compos. Mater.* 26, No. 4 (2019), pp. 1121–1137.

[171] LeBel, F.; Ruiz, É.; Trochu, F.: Experimental study of saturation by visible light transmission in dual-scale fibrous reinforcements during composite manufacturing. In: *J. Reinf. Plast. Compos.* 36, No. 23 (2017), pp. 1693–1711.

[172] LeBel, F.; Fanaei, A. E.; Ruiz, É.; Trochu, F.: Prediction of optimal flow front velocity to minimize void formation in dual scale fibrous reinforcements. In: *Int. J. Mater. Form.* 7, No. 1 (2014), pp. 93–116.

[173] Hergan, P.; Fauster, E.; Perkonigg, D.; Pinter, G.; Schledjewski, R.: Flow-speed-controlled quality optimisation for one-shot-hybrid RTM parts. In: *Adv. Manuf. Polym. Compos. Sci.* 6, No. 1 (2020), pp. 29–37.

[174] Patel, N.; Lee, L. J.: Modeling of void formation and removal in liquid composite molding. Part II: Model development and implementation. In: *Polym. Compos.* 17, No. 1 (1996), pp. 104–114.

[175] Ravey, C.; Ruiz, E.; Trochu, F.: Determination of the optimal impregnation velocity in Resin Transfer Molding by capillary rise experiments and infrared thermography. In: *Compos. Sci. Technol.* 99 (2014), pp. 96–102.

[176] Rohatgi, V.; Lee, L. J.: Moldability of Tackified Fiber Preforms in Liquid Composite Molding. In: *J. Compos. Mater.* 31, No. 7 (1997), pp. 720–744.

[177] Darcy, H.: Les fontaines publiques de la ville de Dijon. Paris, 1856.

[178] Lucas, R.: Ueber das Zeitgesetz des kapillaren Aufstiegs von Flüssigkeiten. In: *Kolloid-Zeitschrift* 23, No. 1 (1918), pp. 15–22.

[179] Washburn, E. W.: The Dynamics of Capillary Flow. In: *Phys. Rev.* 17, No. 3 (1921), pp. 273–283.

[180] May, D.; Aktas, A. et al.: In-plane permeability characterization of engineering textiles based on radial flow experiments: A benchmark exercise. In: *Compos. A: Appl. Sci. Manuf.* 121 (2019), pp. 100–114.

[181] Estrada, G.; Vieux-Pernon, C.; Advani, S. G.: Experimental Characterization of the Influence of Tackifier Material on Preform Permeability. In: *J. Compos. Mater.* 36, No. 19 (2002), pp. 2297–2310.

[182] Dickert, M.; Berg, D. C.; Ziegmann, G.: Influence of binder activation and fabric design on the permeability of non-crimp carbon fabrics. In: The Centre for Advanced Composite Materials (Ed.): FPCM-11 Proceedings. Eleventh International Conference on Flow Processes in Composite Materials. Auckland, New Zealand. The Centre for Advanced Composite Materials, pp. 10–17.

[183] Shih, C.-H.; Liu, Q.; Lee, L. J.: Vacuum-assisted resin transfer molding using tackified fiber preforms. In: *Polym. Compos.* 22, No. 6 (2001), pp. 721–729.

[184] Zeng, X.; Brown, L. P.; Endruweit, A.; Matveev, M.; Long, A. C.: Geometrical modelling of 3D woven reinforcements for polymer composites: Prediction of fabric permeability and composite mechanical properties. In: *Compos. A: Appl. Sci. Manuf.* 56 (2014), pp. 150–160.

[185] Teixidó, H.; Staal, J.; Caglar, B.; Michaud, V.: Capillary Effects in Fiber Reinforced Polymer Composite Processing: A Review. In: *Front. Mater.* 9 (2022).

[186] Masoodi, R.; Pillai, K. M.: Wicking in Porous Materials: CRC Press, 2012.

[187] Amico, S. C.; Lekakou, C.: Axial impregnation of a fiber bundle. Part 1: Capillary experiments. In: *Polym. Compos.* 23, No. 2 (2002), pp. 249–263.

[188] Pillai, K. M.; Advani, S. G.: Wicking across a Fiber-Bank. In: *J. Colloid Interface Sci.* 183, No. 1 (1996), pp. 100–110.

[189] van de Velde, K.; Kiekens, P.: Wettability of natural fibres used as reinforcement for composites. In: *Angew. Makromol. Chem.* 272, No. 1 (1999), pp. 87–93.

[190] CR: Washburn measurements on porous solids. KRÜSS Application Note AN245e. Hg. v. Krüss GmbH. Hamburg, DE, 1996 (TN302e).

[191] van de Velde, K.; Kiekens, P.: Wettability and surface analysis of glass fibres. In: *IJFTR (Indian Journal of Fibre & Textile Research)* 25, No. 1 (2000), pp. 8–13.

[192] Bahners, T.: The Do's and Don'ts of Wettability Characterization in Textiles. In: *J. Adhes. Sci. Technol.* 25, No. 16 (2011), pp. 2005–2021.

[193] LeBel, F.; Fanaei, A. E.; Ruiz, É.; Trochu, F.: Experimental Characterization by Fluorescence of Capillary Flows in the Fiber Tows of Engineering Fabrics. In: *OJINM* 02, No. 03 (2012), pp. 25–45.

[194] Pucci, M. F.; Liotier, P.-J.; Drapier, S.: Capillary effects on flax fibers – Modification and characterization of the wetting dynamics. In: *Compos. A: Appl. Sci. Manuf.* 77 (2015), pp. 257–265.

[195] Causse, P.; Ravey, C.; Trochu, F.: Capillary Characterization of Fibrous Reinforcement and Optimization of Injection Strategy in Resin Transfer Molding. In: *J. Compos. Sci.* 2, No. 2 (2018), p. 19.

[196] Blößl, Y.; Schledjewski, R.: Analysis of the capillary driven wetting behaviour in reinforcing textile structures. In: 14th International Conference on Flow Processes in Composite Materials. FCPM 14. Luleå, Sweden, 30.05-01.06.2018.

[197] Blößl, Y.; Schledjewski, R.: Natural Fibre Textile Characterization for Dual-Scale Flow Prediction. In: European conference on composite materials (ECCM18). ECCM18. Athens, Greece, 22-28.06.2018.

[198] Caglar, B.; Tekin, C.; Karasu, F.; Michaud, V.: Assessment of capillary phenomena in liquid composite molding. In: *Compos. A: Appl. Sci. Manuf.* 120 (2019), pp. 73–83.

[199] Usevičiūtė, L.; Baltrėnaitė-Gedienė, E.: Modelling of a Capillary Rise Height of Biochar by Modified Lucas–Washburn Equation. In: *Environ. Model. Assess.* (2021).

[200] Vas, L. M.; Gombos, Z.; Nagy, V.; Halász, M.: Tailored saturation functions and its application to liquid uptake processes in fibrous composite reinforcements. In: *J. Ind. Text.* 52 (2022).

[201] Teixidó, H.; Caglar, B.; Michaud, V.: Effect of wettability and textile architecture on fluid displacement and pore formation during infiltration of carbon fibrous preforms. In: *Compos. A: Appl. Sci. Manuf.* 174 (2023), p. 107733.

[202] LeBel, F.; Fanaei, A. E.; Ruiz, E.; Trochu, F.: Experimental characterization by fluorescence of capillary flows in dual-scale engineering fabrics. In: *Text. Res. J.* 83, No. 15 (2013), pp. 1634–1659.

[203] Verrey, J.; Michaud, V.; Månson, J.-A.: Dynamic capillary effects in liquid composite moulding with non-crimp fabrics. In: *Compos. A: Appl. Sci. Manuf.* 37, No. 1 (2006), pp. 92–102.

[204] Wang, J.; Fuentes, C. A. et al.: Wettability of carbon fibres at micro- and mesoscales. In: *Carbon* 120 (2017), pp. 438–446.

[205] Qiu, S.; Fuentes, C. A.; Zhang, D.; van Vuure, A. W.; Seveno, D.: Wettability of a Single Carbon Fiber. In: *Langmuir* 32, No. 38 (2016), pp. 9697–9705.

[206] Qiu, S.; Fuentes, C. A.; Zhang, D.; van Vuure, A. W.; Seveno, D.: Wettability of a Single Carbon Fiber. ICCM21. International Committee on Composite Materials (ICCM). Xi'an,China, 25.08.2017.

[207] Qiu, S.; Wang, J. et al.: Wetting dynamics and surface energy components of single carbon fibers. In: *J. Colloid Interface Sci.* 557 (2019), pp. 349–356.

[208] Toho Tenax Europe GmbH (Ed.): Tenax HTS40 X030 12K filament yarn. Preliminary Product Data Sheet. 01. edition, 2016.

[209] Baruch, M.; Arbocz, J.; Zhang, G. Q.: Laminated conical shells - Considerations for the variations of the stiffness coefficients. In: 35th AIAA/ASME/ASCE/AHS/ASC Structures, Structural Dynamics, and Materials Conference. A collection of technical papers : Hilton Head, SC, April 18-20, 1994. Washington, DC: American Institute of Aeronautics and Astronautics, pp. 2505–2516.

[210] Grothaus, R.: Verfahren zur Herstellung von kegel- und kegelstumpfförmigen Hohlkörpern und demgemäße Erzeugnisse. DE 10 2010 005 986 B4 (2010).

[211] Grothaus, R.: Verfahren zur Herstellung von Hohlkörpern mit bundförmigen Verstärkungen. DE102010005987B4 (2010).

[212] van Oosterom, S.; Allen, T.; Battley, M.; Bickerton, S.: An objective comparison of common vacuum assisted resin infusion processes. In: *Compos. A: Appl. Sci. Manuf.* 125 (2019), p. 105528.

[213] Neunkirchen, S.; Fauster, E.; Lehner, S.; O'Leary, P.: Instrumentation of an Inspection Test Rig for Geometry Measurement of Fiber Bundles in Automated Composite Manufacturing. In: *IEEE Trans. Instrum. Meas.* 71 (2022), pp. 1–9.

[214] Lehner, S.; Neunkirchen, S.; Fauster, E.; O'Leary, P.: Instrumentation of a Roving Inspection Test Rig with Surface Geometry Measurement of Fiber Bundles. IEEE. In: Institute of Electrical and Electronics Engineers, IEEE Instrumentation and Measurement Society 2021 – To measure is to know, pp. 1–6.

[215] Yadav, N.; Schledjewski, R.: Inline tape width control for thermoplastic automated tape layup. In: *Compos. A: Appl. Sci. Manuf.* 163 (2022), p. 107267.

[216] Belhaj, M.; Deleglise, M. et al.: Dry fiber automated placement of carbon fibrous preforms. In: *Compos. B. Eng.* 50 (2013), pp. 107–111.

[217] info@micro-epsilon.de, M.-E. M.: A comparison of blue and red light sensor technology: which one is best for your application? https://www.micro-epsilon.co.uk/news/2022/2022-01-20-UK-ME401-bylined-article-on-Blue-and-Red-light-sensor-technology/ (22.10.2023).

[218] Mel’nik, A. V.; Seredkin, A. V.; Tokarev, M. P.; Gobyzov, O. A.: Laser line scanning of a shape of moving objects with various degree of transparency. In: *J. Phys.: Conf. Ser.* 1677 (2020), p. 12187.

[219] Barkauskas, D. A.; Rocke, D. M.: A general-purpose baseline estimation algorithm for spectroscopic data. In: *Analytica chimica acta* 657, No. 2 (2010), pp. 191–197.

[220] Bookstein, F. L.: Fitting conic sections to scattered data. In: *Comput. Graphics Image Process.* 9 (1), pp. 56–71.

[221] Ma, T.; Shi, J.; Steurer, D.: Polynomial-Time Tensor Decompositions with Sum-of-Squares. In: 57th Annual IEEE Symposium on Foundations of Computer Science. FOCS 2016 : 9-11 October 2016, New Brunswick, New Jersey, USA : proceedings. 2016 IEEE 57th Annual Symposium on Foundations of Computer Science (FOCS). New Brunswick, NJ, USA, 10/9/2016 - 10/11/2016. Institute of Electrical and Electronics Engineers. Piscataway, NJ: IEEE, pp. 438–446.

[222] Neunkirchen, S.; Blößl, Y.; Schledjewski, R.: A porous capillary tube approach for textile saturation. In: *Compos. Sci. Technol.* 230 (2022), p. 109450.

[223] Neunkirchen, S.; Bender, M.; Schledjewski, R.: Effect of Binder Activation on in-Plane Capillary Flow in Multilayer Stacks of Carbon Fiber Fabrics. In: *Appl. Compos. Mater.* 31, No. 2 (2024), pp. 709–719.

[224] Kim, K.-H.; Kim, Y.-G.; Kwon, Y.: Preparation and characterization of surface energy of BPDA-BAPP polyimide. In: *Macromol. Res.* 17, No. 6 (2009), pp. 388–396.

[225] Garat, W.; Pucci, M. F. et al.: Surface energy determination of fibres for Liquid Composite Moulding processes: Method to estimate equilibrium contact angles from static and quasi-static data. In: *Colloids Surf., A* 611 (2021), p. 125787.

[226] Tran, L.; Fuentes, C. A.; Dupont-Gillain, C.; van Vuure, A. W.; Verpoest, I.: Wetting analysis and surface characterisation of coir fibres used as reinforcement for composites. In: *Colloids Surf., A* 377, No. 1-3 (2011), pp. 251–260.